1-1-2013

Film Cooling with Surface Enhancements

Xavier Chang
Ryerson University

FILM COOLING WITH SURFACE ENHANCEMENTS

By

Xavier Chang, BEng

Aerospace Engineering

Ryerson University, 2011

A report presented to Ryerson University

in partial fulfillment of the requirements for the degree of

Master of Engineering

in the Program of

Aerospace Engineering

Toronto, Ontario, Canada, 2013

Author’s Declaration

AUTHOR'S DECLARATION FOR ELECTRONIC SUBMISSION OF A THESIS

I hereby declare that I am the sole author of this thesis. This is a true copy of the thesis, including any required final revisions, as accepted by my examiners.

I authorize Ryerson University to lend this thesis to other institutions or individuals for the purpose of scholarly research

_____

Xavier Chang

I further authorize Ryerson University to reproduce this thesis by photocopying or by other means, in total or in part, at the request of other institutions or individuals for the purpose of scholarly research.

I understand that my thesis may be made electronically available to the public.

_____

Xavier Chang

Abstract

Film cooling has been studied for many decades but the study of film cooling using surface enhancements is still relatively new. In this project numerical analysis has been carried out to find the film cooling performance of ramp, flow aligned blocker, and trench surface enhancements in comparison to the standard elliptical injection configuration. A comparative study of the effects of the blowing ratio has also been carried out for each surface enhancement configuration. In addition to calculating and discussing the centerline and laterally averaged film cooling effectiveness results, detailed analysis of the flow and temperature field of each configuration is also presented. In the end the laterally averaged film cooling effectiveness results suggested that flow aligned blockers would provide the greatest film cooling improvements with closer hole spacing.

Acknowledgements

I would like to thank my supervisor Dr. Bassam Ali Jubran for his mentorship throughout the course of this project.

I would like to thank my family for their sacrifices and support, without them this would not have been possible.

I would like to thank my friends for their support and encouragement.

Lastly I would like to acknowledge the computational resources provided by HPCVL.

Contents

Nomenclature

D	Diameter of Hole
M	Blowing Ratio
Tc	Temperature of coolant
Tg	Temperature of hot gas
Taw	Adiabatic temperature of the wall
Uc	Velocity of the coolant
Ug	Velocity of the hot gas
$H_{\theta}\_$	Hole injection angle, followed my its injection angle in degrees (eg. $H_{\theta 15}$)
$R_{\theta}\_$	Ramp configuration, followed by its inclination angle in degrees (eg. $R_{\theta 15}$)
$F_{D}\_$	Flow aligned blocker configuration, followed by its height in D (eg. $F_{D0.5}$)
$T_{D}\_$	Trench configuration, followed by its depth in D (eg. $T_{D0.5}$)

Greek

γ	Ratio of Specific Heats
ρ	Density
μ	Dynamic Viscosity
ν	Kinematic Viscosity
τ_w	Wall Shear Stress
η	Effectiveness of film cooling
$\bar{\eta}$	Laterally averaged effectiveness of film cooling

List of Tables

List of Figures

Chapter 1: Introduction to Film Cooling

1.1 Film Cooling

For many decades engineers have tried to improve engine performance by increasing the turbine inlet temperature. Today, the turbine inlet temperatures are higher than material limits which has been made possible through the use of both internal and external cooling. Film cooling is used to protect a surface that is exposed to a high temperature environment by introducing a secondary fluid to serve as a barrier between the surface and the hot gas flow. This secondary fluid, which is either a coolant or injected fluid, can be place at one or more discrete locations along the surface. Not only does film cooling protect the immediate region, but also downstream of the injection site [1]. Figure 1 below illustrates the fundamental film cooling concept.

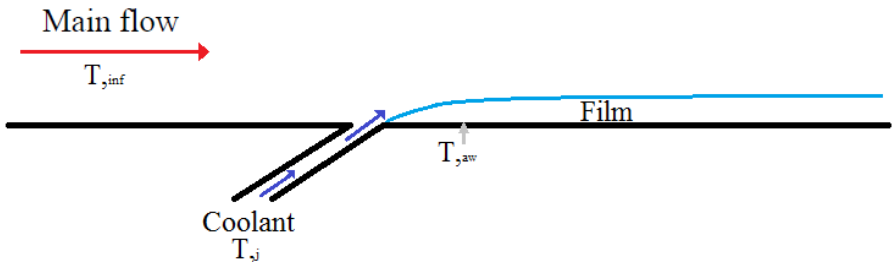

Fig. 1: Basic Film Cooling Design

Goldstein, along with Eckert and Ramsey are considered to be the first to provide a consistent measurement of the film cooling effectiveness from film cooling holes inclined to a surface [2]. Soon after more measurements of which included the variation of compound angle and hole shape followed. A tremendous amount of research has been done on the hole inclination angle, compound angle, spacing, and length to diameter ratio which are commonly regarded as the most relevant film cooling geometric properties [3] [4]. Shaped holes have been shown to provide many advantages over cylindrical holes, however analysis of cylindrical holes is still prevalent today [2]. The main flow and coolant characteristics generally include turbulence intensity, density ratio, blowing ratio, and momentum flux ratio [5]. In 1998 Kercher released a CFD bibliography which includes close to 200 references to papers and dissertations on film cooling, covering years 1971 to 1996 [6]. With the great advancements in computer technology, providing much improved computational power, CFD publications will continue to thrive now and in the future.

Although figure 1 above intuitively looks simple, the interaction between the coolant jet and mainstream create a complex flow structure. The cross flow of the jet interacts with the mainstream flow to produce a pair of counter-rotating vortices. They are often called kidney-shaped vortices due to their shape, and their rotation promotes both jet lift-off and degradation of the film cooling of the surface [7]. This phenomenon is one of the main motivations for film

cooling research, which is to reduce or eliminate the negative effects of kidney vortices on film cooling.

1.2 Surface Enhancement

As previously mentioned, in order to further improve upon the film cooling technique studies have been done to research the effects of changing injection angle, blowing rates, as well as other factors. A more specific area of research in this domain is the effects of surface enhancement or reshaping. Surface enhancement or reshaping refers to modifications that are done to the surface surrounding the film cooling holes. Some examples of these include ramps, flow aligned blockers, and trenches. From a manufacturing standpoint this area of research is very promising, since structures can be manufactured over the layer of thermal baring coating (TBC) provided on the external surface of an airfoil without additional machining work [8].

The addition of a ramp upstream of the film cooling hole has been shown to provide three main changes to the flow structure. The most major change when compared to the standard film cooling set up is that an area of recirculation is created behind the ramp, which acts to lower the momentum of the coolant jet [5]. The area of recirculation and separated shear layer can be seen in figure 2 below. The area of recirculation also acts to pull some of the coolant backwards, which cools the small area behind the film cooling hole [9]. Secondly, the ramp reduces the static pressure of the region in front of the film cooling holes, which allow for the use of higher blowing ratios without as much jet liftoff [9]. This is the result of the ramp deflecting the main stream flow above the injection region. Lastly the ramp allows for better lateral spreading of the film cooling jets. Shih et al. [9] have reported that the laterally averaged adiabatic effectiveness has been show to increase by as much as three times with the addition of a ramp when compared with the standard configuration. Chen et al. [5] have stated that the addition of a ramp has allowed for the use of higher blowing ratios, even those greater than unity, and had film cooling effectiveness increases by as much as 50%.

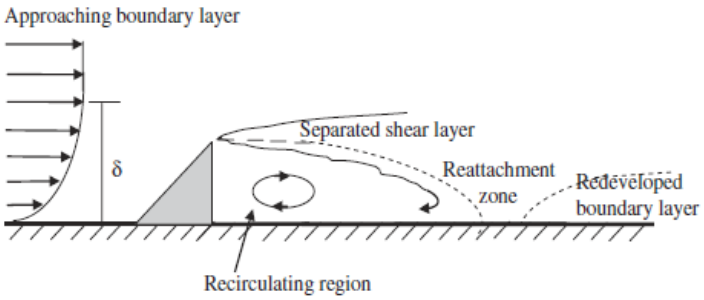

Fig. 2: Flow Structure Behind a Ramp [9]

The addition of a trench, at the film cooling injection location, has been shown to cause lateral spreading of the coolant inside the trench before exiting into the main flow as well as lowering its momentum [10]. This causes the coolant to hug the surface after exiting the trench. For this reason higher blowing ratios can be used since the jet lift-off associated with the standard

configuration does not occur. In general deeper slots increase film cooling effectiveness within the trench but perform poorly far downstream of the trench [10]. A similar trend was found by Baberi et al. [11] who reported that even at a high blowing ratio of 1.25, the jet lift-off had been eliminated almost completely.

Flow aligned blockers have been patented by Shih et al. [12] and are used to increase the adiabatic film cooling effectiveness by minimizing hot-gas entrainment [12]. It does so by simply using a barrier to separate the coolant jet from the main flow in the stream wise direction. In 2008 Chen experimented with various heights, spacing, and widths of flow aligned blocker to see their effects on film cooling effectiveness. He found that the addition of flow aligned blockers increased the centerline film cooling effectiveness by as much as 60% [8]. They also were shown to greatly increase the film cooling effectiveness laterally in between the flow aligned blocker, as well as extend the cooling performance far downstream.

1.3 CFD Considerations

In CFD analysis great importance is placed on the cooling hole and its inflow region. The reason for this is that it affects the characteristics of the counter-rotating vortices that are created by the turning and acceleration of the flow at the hole inlet [2]. As stated earlier the length to diameter ratio is an important geometric parameter that affects the jet flow, as well as the plenum geometry's inflow direction. Changing the length to diameter ratio as well as the inflow directions produces changes in the inhole flow characteristics. The turning of the flow from the plenum into the coolant hole creates a boundary layer which changes the velocity profile in the hole region. This may enhance or decrease film cooling performance as seen in Peterson et al.'s [13] study of short-hole jets in crossflow velocity fields. The focus of this project is to study the effects of surface enhancements on the cylindrical hole's film cooling performance in terms of the flow and temperature fields. Therefore it was decided not to use a plenum and instead introduce a jet coolant with a uniform velocity field. By eliminating the use of the plenum and boundary layer development flow intricacies, it is easier to see the effects that the surface enhancements have on the coolant flow since all configurations start with the same starting uniform velocity profile. However, the results of not using a plenum were still validated by using experimental data.

Many literature agree that Reynolds-Averaged Navier Stokes (RANS) based K-epsilon (K-ε) turbulence model under predicts lateral spreading of film cooling jets, leading to over predictions of centerline film cooling effectiveness. Some of these include CFD analysis on cylindrical film cooling holes done by Volker et al [2] and El-Gabry et al [14]. However, when comparing laterally averaged values of film cooling effectiveness Volker at al. [2] found that the CFD predictions can deliver reasonable results. They also found that qualitatively the comparison of stream wise velocities showed very good agreement. Surveying literature it is believed that using a realizable K-ε model will provide good results, as shown by a computational study of gas turbine blade film cooling by Vickery et al [15]. Numerous experiments also include the use of

an enhanced wall function for even greater accuracy. Although the realizable k-e model was found to be the most used, others have been used and compared to ensure it is the most accurate turbulence model for this project.

1.4 Project Setup

In this project surface enhancement is analyzed using three different geometries as well as a baseline with no modifications made to the surface. The three modifications that were studied are the use of a ramp, flow aligned blockers, and a trench. These surface enhancements are analyzed using Fluent Computational Fluid Dynamics (CFD) software, and the results are compared to various experiments [16]. One goal of this project is to compare the predicted film cooling effectiveness results of using Fluent CFD software to the results of the previously done experiments in order to determine how well the software matches up to real world experiments. The main goal of this project is to be able to provide a detailed analysis and breakdown of the flow and temperature field of the three different surface enhancements mentioned earlier, since it is very difficult to do so with real world experiments. By accomplishing both goals this project can provide a strong baseline of surface enhancement results, upon which can be used for surface enhancement optimization in the future.

One of the best ways to measure the performance of different surface enhancement configurations is to use film cooling effectiveness, given by the formula below.

$$\eta = \frac{(T_{aw} - T_\infty)}{(T_j - T_\infty)} \qquad (1)$$

Referring back to Fig. 1 T_{aw} is the adiabatic wall temperature, T_∞ is the mainstream temperature, and T_j is the jet coolant temperature. Essentially this value relates the temperature difference between a cooled and an uncooled wall. The higher the film cooling effectiveness, the better the jet is cooling. The cooling effectiveness is adequately used to determine the performance of the surface enhancements.

Chapter 2: Numerical Model

2.1 Geometry of Experiments

This models used in this project were created mostly based on the experiment carried out by Sinha [16], Bogard, and Crawford. The experimental test section was scaled down to produce the numerical model geometry as well as using only three holes, to reduce the computational cost and time. The model used in this project has a height of 4 cm, versus a height of 60 cm in the Sinha experiment. Also, the width of the cross section is 9 cm, versus a width of 60 cm for the experiment. Further, the injection hole length used in this 5 D while it is 3.5 D in the Sinha experiment.

Table 1: Geometrical Similarities and Differences

	Cross Section Height	Cross Section Width	Lead up Length	Film Cooling Injection Angle	Film Cooling Hole Length	Ramp Angle	Hole Spacing	Number of Holes
Current Model	4 cm	9 cm	19D	15°,25°,35°,45°	5D	5°,15°,25°	3D	3
Sinha	60 cm	60 cm	19D	35°	3.5D	N/A	3D	>3 (Not Specified)

2.2 Surface Enhancement Geometry

Figures 3 through 6 below illustrate the geometry of the different surface enhancements used in this project:

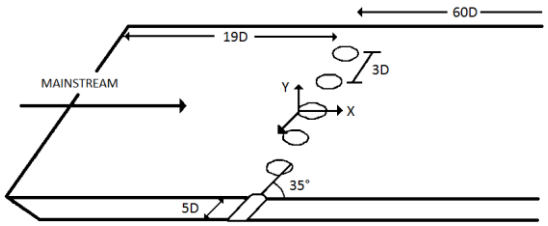

Fig. 3: Baseline Geometry

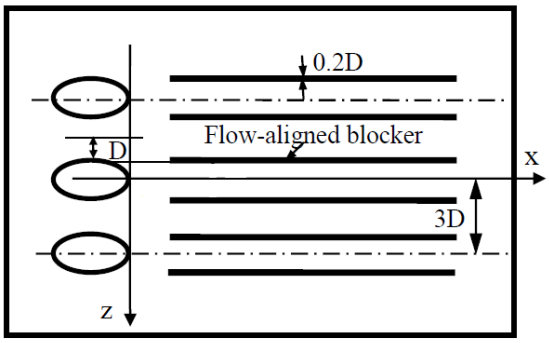

Fig. 4: Flow Aligned Blockers Geometry

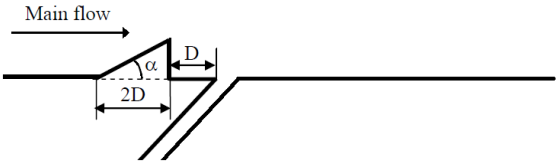

Fig. 5: Ramp Geometry

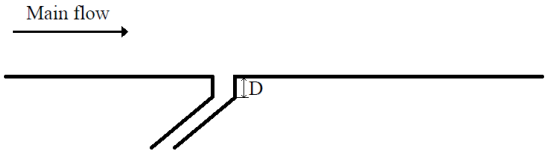

Fig. 6: Trench Geometry

As seen above in figure 3, the baseline geometry has a lead length of 19 diameters and a test surface length of 60 diameters (D) after the film cooling holes. The film cooling injection holes are 5 D in length, and the holes are spaced 3 D across measured from their centers. For the purposes of this project a diameter of 1 cm is used. Figure 4 shows the geometry used for the flow aligned blockers. The blockers used are placed directly in line with the edges of the film cooling holes, and are 0.2 D wide. The heights of the blockers used in this experiment are 0.5 D and 1 D. These blockers run the full length of 59 D across the test surface, which start 1 D behind the film cooling holes. Figure 5 shows the geometry of the ramp. The ramp is placed 1 D in front of the film cooling holes. The ramps have a length of 2 D, and have varying angles (α) of 5°, 15°, and 25° degrees. Figure 6 shows the geometry of the trenches, which have depths of 0.5 D and 1 D. All of these configurations use injection holes that vary in inclination at 15°, 25°, 35°, and 45° angles. The following page contains figures of the CAD models based upon these configurations which were made in Catia and meshed in Gambit.

2.3 CAD Models

The CAD models used in this project are illustrated in the figures below:

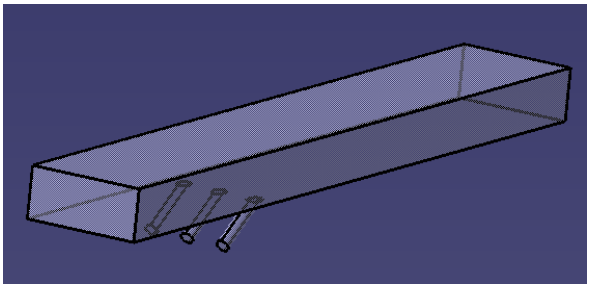

Fig. 7: Computational Domain - Baseline

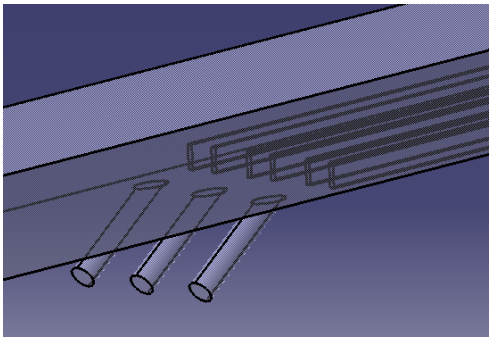

Fig. 8: Computational Domain - Flow Aligned Blockers

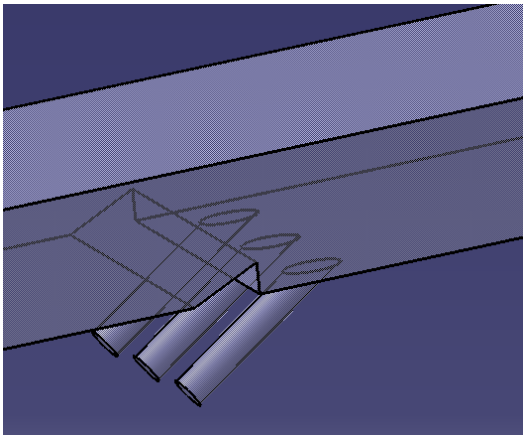

Fig. 9: Computational Domain - Ramp

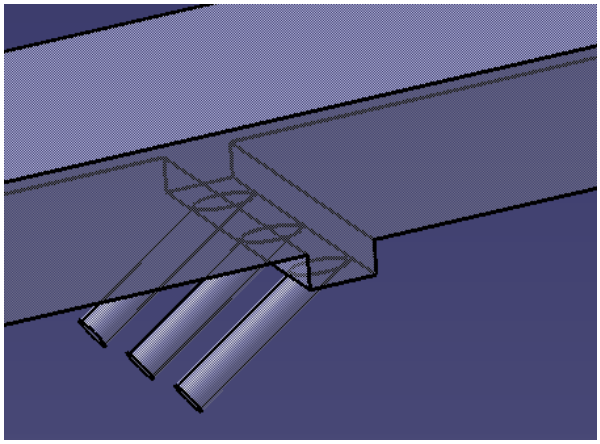

Fig. 10: Computational Domain - Trench

As seen in the figures 7 to 10 above, a set of 3 film cooling injection holes was chosen, along with a cross section that is 9 cm wide and 4 cm tall. This was done to reduce the overall volume of the model in order to effectively reduce the number of overall elements needed for an accurate solution. Because of this, there are some geometrical differences between this project and the two experiments mentioned in the introduction which will be discussed in the next section.

2.4 Numerical Model Configuration

2.4.1 Gambit

By exporting the CAD models from Catia as .stp files, it was then imported into Gambit where it was meshed using hex elements. The results of the hex meshing lead to approximately 1 million elements, after carrying out grid convergence testing that will be shown later. Also within Gambit the walls, inlets, jet inlets, and outlet was defined on their respective surfaces. It is important to note that the side walls were set as symmetry, which effectively simulates and endless row of hole injection sites.

2.4.2 ANSYS Fluent

The solver settings that were used are Pressure Based for the Type, Absolute for the Velocity Formation, and Steady for the Time. The turbulence model that was used is the Realizable K-ε model with the Enhanced Wall Function and Thermal Effects. Also Energy Effects was enabled. Other models such as the Standard K-ε, K-ω, and Shear Stress Transport (SST) were considered, but the Realizable K-ε model provided the best convergence and will be discussed in the model validation.

The boundary conditions for the two different cases that are analyzed in this project exactly the same except for a slight variation. For both cases the mainstream inlet velocity was set to 20 m/s, with a temperature of 300k and a turbulence intensity of 0.20%. The coolant was kept at a temperature of 250k. The only difference between the two cases is that the velocity ratio is 0.208 in the first, and 0.83 in the second. Although these values were made to closely match the Sinha parameters, there are still some differences between this project and his experiment. Therefore a table is shown below illustrating the differences and similarities of the boundary conditions used for analysis.

Table 2: Flow and Boundary Conditions

	Mainstream Velocity	Mainstream Temperature	Case 1 Coolant Velocity Ratio	Case 2 Coolant Velocity Ratio	Coolant Temperature	Turbulence Intensity
Current Model	20 m/s	300k	0.208	0.83	250k	0.20%
Sinha	20 m/s	300k	0.208	0.83	250k	0.25%

2.4 Convergence

2.4.1 Solution Convergence

In order to determine when the numerical model had converged several factors were monitored. First of all the residuals were monitored to be sure they went on the order of $1e^{-6}$. In every model all of the residuals reached this value except for continuity which would fall very slowly on the order of $1e^{-5}$. Instead of dramatically increasing the number of iterations and therefore using valuable computational time, another factor was taken into account. The sum of surface temperature at the centerline of the middle hole location was monitored to see when this value flat lined. This means that the surface temperature is no longer changing and the solution has converged. This occurred at about 800 iterations. As previously stated these solutions were calculated under steady state conditions, however to further ensure that this model was correct this solution was also computed using transient settings. After many adjustments to the time steps, and other settings, the solution that was obtained exactly matched the solution found from steady state conditions. By taking all of these factors into account one can conclude that the resulting model is correct.

2.4.2 Elemental Grid Independence Study

In order to determine the number of elements to use in this numerical study a grid convergence test was carried out. The figure below shows the results.

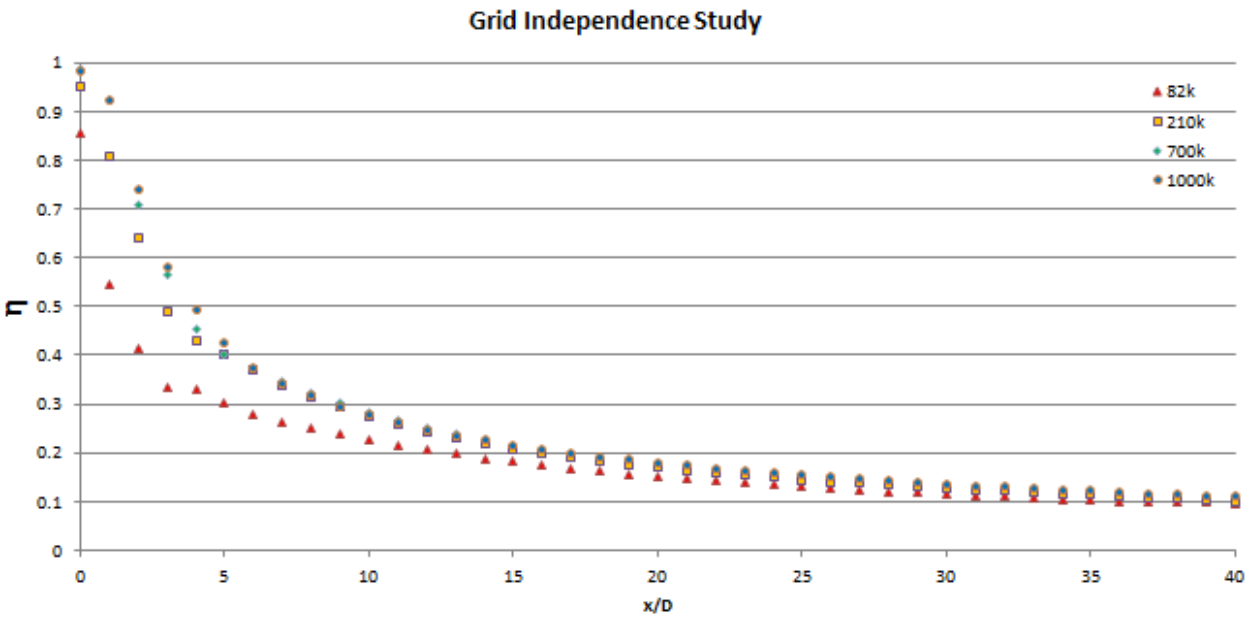

Fig. 11: Grid Independence Study Results

As shown above in order to develop a more accurate model more elements were needed in the near hole location from x/D values from 0 to 15. It was found that moving from a grid of 700,000 elements to 1,000,000 elements yielded very small changes in the near hole location.

Therefore it was deemed that the elemental grid has converged, and a 1 million element grid would be used for all of the models in this study.

2.5 Numerical Model Validation

2.5.1 Turbulence Model Selection

The results of this numerical model were validated by comparing them to an experiment carried about by Sinha and others. Below is figure 12 showing the results of the comparison.

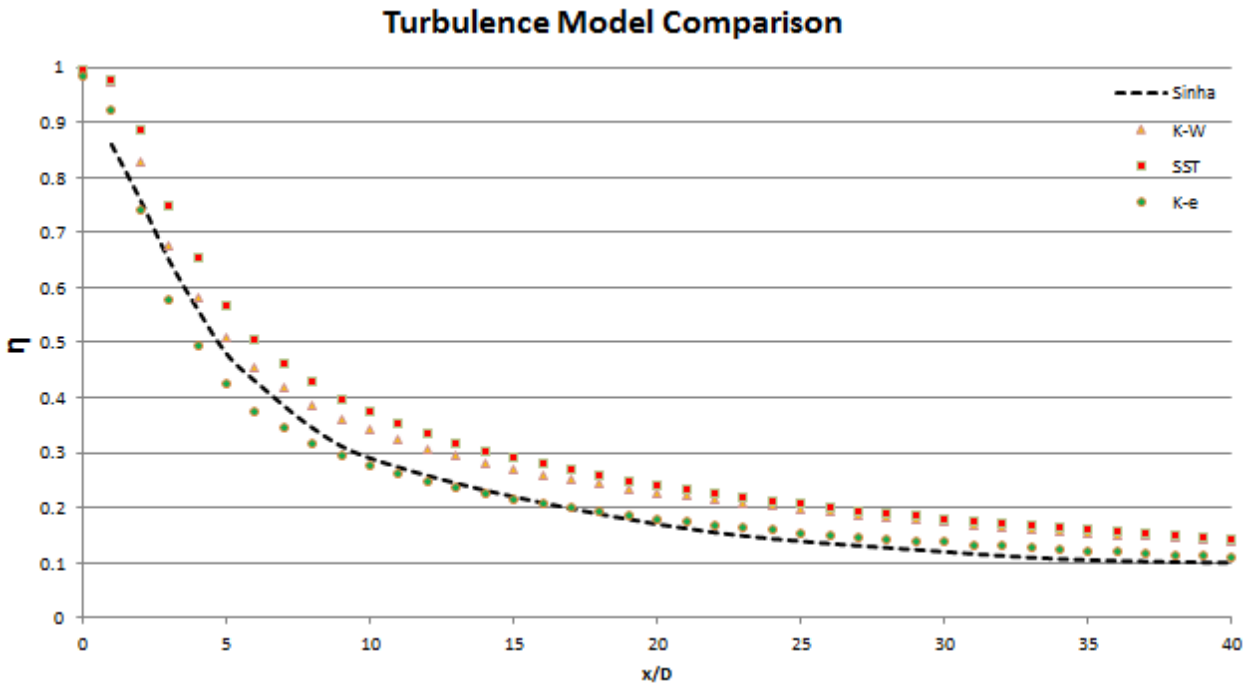

Fig. 12: Turbulence Model Comparison with Sinha Experiment

Figure 12 above contains the center line temperature results from K-ε, K-ω, and SST turbulence models. Examining the K-ω model it appears to provide great results from 2.5 < x/D < 5, but starts to diverge and overestimate film cooling effectiveness further downstream. The SST model is over slightly worse than the K-ω turbulence model and over predicts film cooling effectiveness across the range of values. The realizable K-ε model does not provide as good results from the 2.5 < x/D < 5 locations, but it is very close and under predicts the film cooling effectiveness slightly. However, for x/D > 5 it provides the best film cooling effectiveness predictions. It follows very closely with the experiment from 8 < x/D < 20, and slightly over predicts across the remainder of the surfaces. Although not perfect, the realizable K-ε model provides the best results of this bunch. It follows the experimental results the best and does not over predict film cooling effectiveness as greatly as the others. For safety reasons it is always better to use a model that under predicts, rather than over predicting.

2.5.2 Comparison with Sinha Experiment

The centerline film cooling effectiveness as well as the laterally averaged film cooling results of this project will be compared to the experimental results found by Sinha. Below is a graph of both the high and low blowing ratio cases of the baseline configuration.

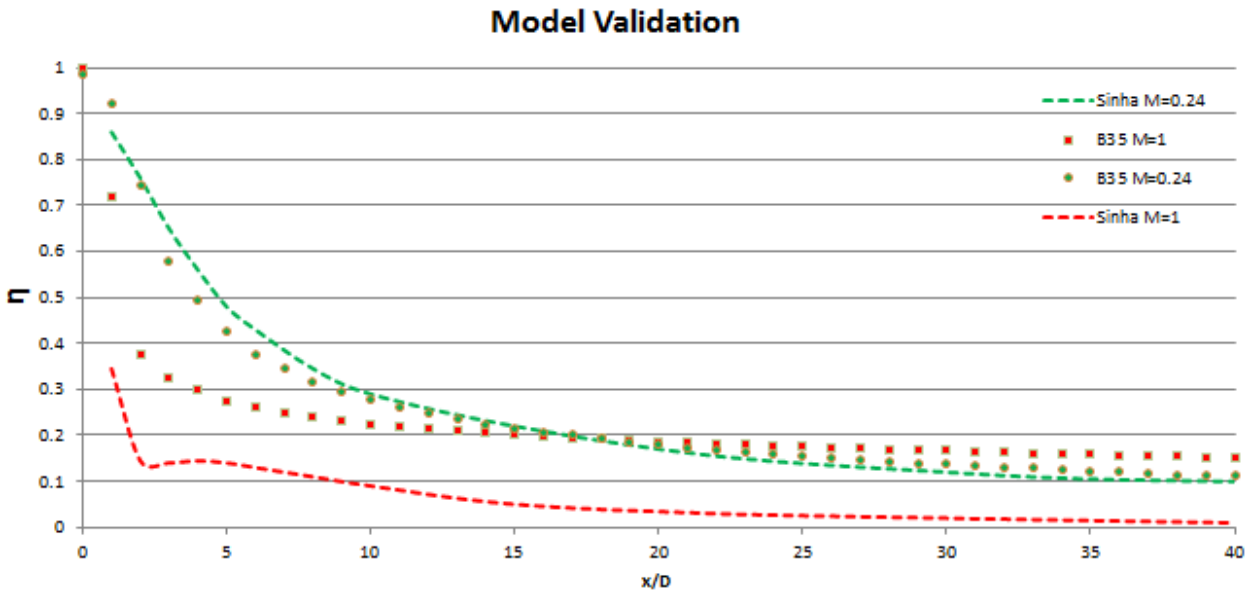

Fig. 13: Prediction of Centerline Film Cooling Effectiveness for Different Blowing Rates

When comparing the baseline case with a blowing ratio of 0.24 the results are very close in both the magnitude and trend. Both curves start at a film cooling effectiveness near 1, and gradually decline along the length of the plate to a value of 0.11 and the end. This shows that the model performs very well at low speeds.

When comparing the baseline case with a blowing ratio of 1 shows a similar trend in which the film cooling effectiveness is high at the beginning, and then drastically drops, thereafter it slowly declines. However, the magnitudes of these values are different which suggests Sinha's experiment saw more jet penetration and stronger kidney vortices which quickly lifted the jet off of the surface, resulting is very low values. The higher blowing ratio creates a complex flow structure which is very hard for the turbulence model to predict with such high accuracy. As a result it over predicts the film cooling effectiveness.

Below is a graph of the comparison of Laterally Averaged Film Effectiveness for the low velocity ratio case of the baseline configuration. Unfortunately there is no plot for the blowing ratio of 1 at the correct 250K coolant temperature in Sinha's study.

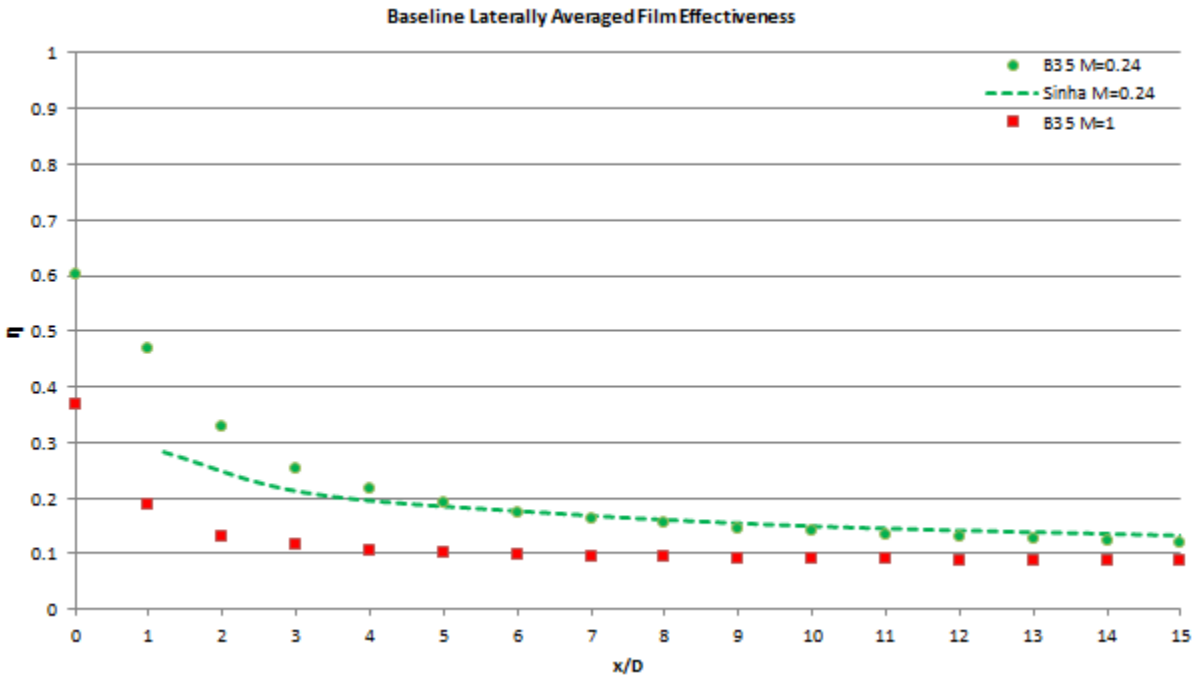

Fig. 14: Comparison of Sinha's Laterally Averaged Film Effectiveness Values for M=0.24

Comparing the predicted values to the results of Sinha's experiment, from x/D < 5 downstream the values do not match very well. However, for x/D > 5 the values match very well. This suggests that there is jet more jet liftoff at injection site in Sinha's experiment. The injection hole length used in this project is longer than the length used in Sinha's experiment by 1.5 D. According to Sinha, shorter holes have a higher effective injection angle which may be the cause for more jet liftoff and the lower values seen above [16].

Chapter 3: Comparative Study of Baseline Configuration

3.1 Baseline Configuration

3.1.1 Centerline Film Cooling Effectiveness

Please observe the centerline film cooling effectiveness results below for the baseline configuration.

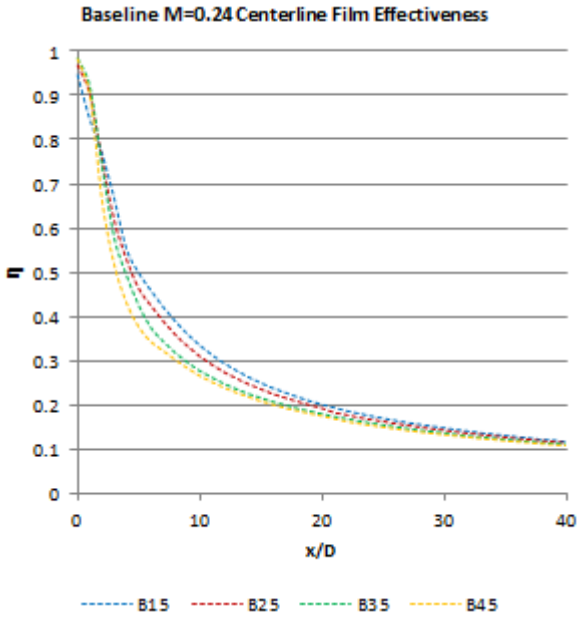

Fig. 15: Centerline Film Effectiveness B_{035} M=0.24

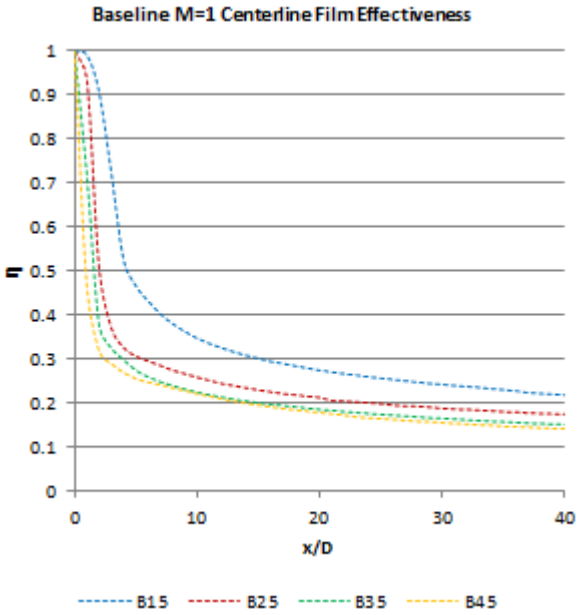

Fig. 16: Centerline Film Effectiveness B_{035} M=1

By looking at figure 15 above, one can see that the film cooling effectiveness starts very high at the hole location and quickly lowers. Initially it starts as high as 1, indicating mostly coolant is at the surface, and drops to a value of 0.1 at x/D = 40. From comparing the different injection angles it is seen that at this low blowing ratio of 0.24 they do not have a great effect on increasing the film cooling effectiveness. The best performing injection angle is at 15°, and each 10° increase lowers the film cooling slightly in the when $5 < x/D < 25$. Outside of this range the values are very similar.

By looking at figure 16 above, once again the film cooling effectiveness is very high at the hole location but more steeply drops off immediately after. The reason for this is that the higher blowing ratio causes the coolant jet to penetrate into the main flow, separating it from the surface briefly before it reattaches. The 15° injection angle is a special case in the fact that even with the higher blowing ratio the coolant jet was able to stay attached to the surface. In general the low blowing ratio performs better while $x/D < 20$, and worse while $x/D > 20$ versus the higher blowing ratio case. The 15° injection angle provides the best results as in with the previous case. To better understand the characteristics of these graphs one must look at the velocity contours,

velocity vectors, temperature contours, as well as the formation of kidney vortices in the following figures.

3.1.2 Velocity Contours and Vectors

Please observe the velocity contours and vectors below.

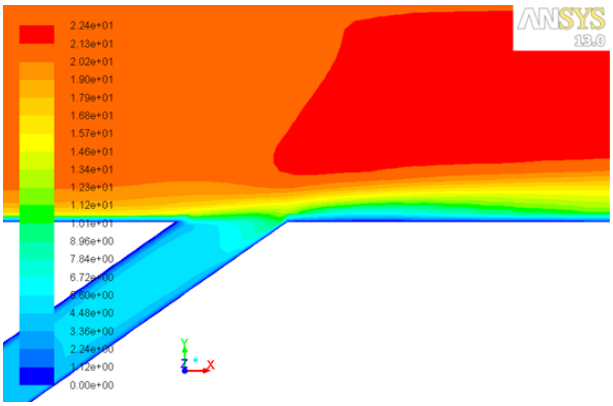

Fig. 17: Velocity Contours B_{035} M=0.24

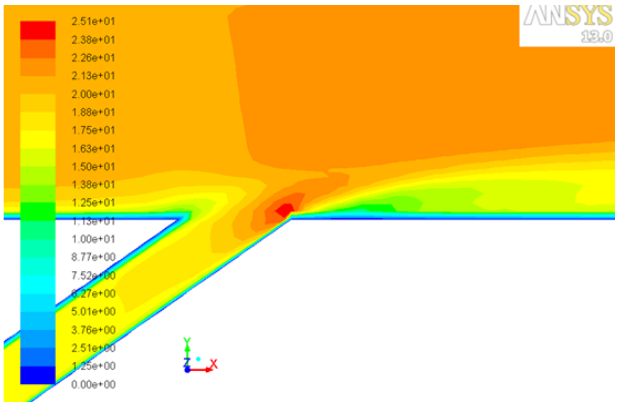

Fig. 18: Velocity Contours B_{035} M=1

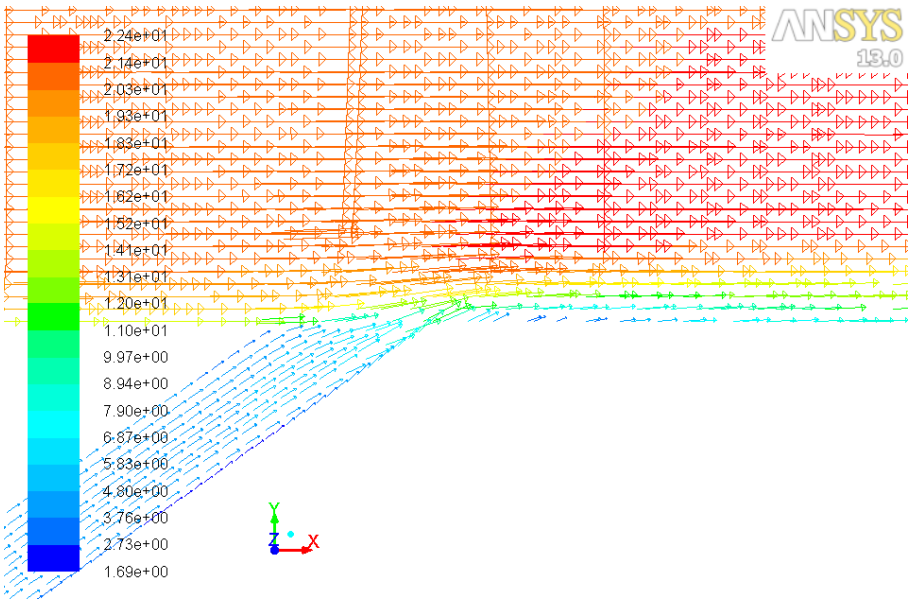

Fig. 19: Velocity Vectors B_{035} M=0.24

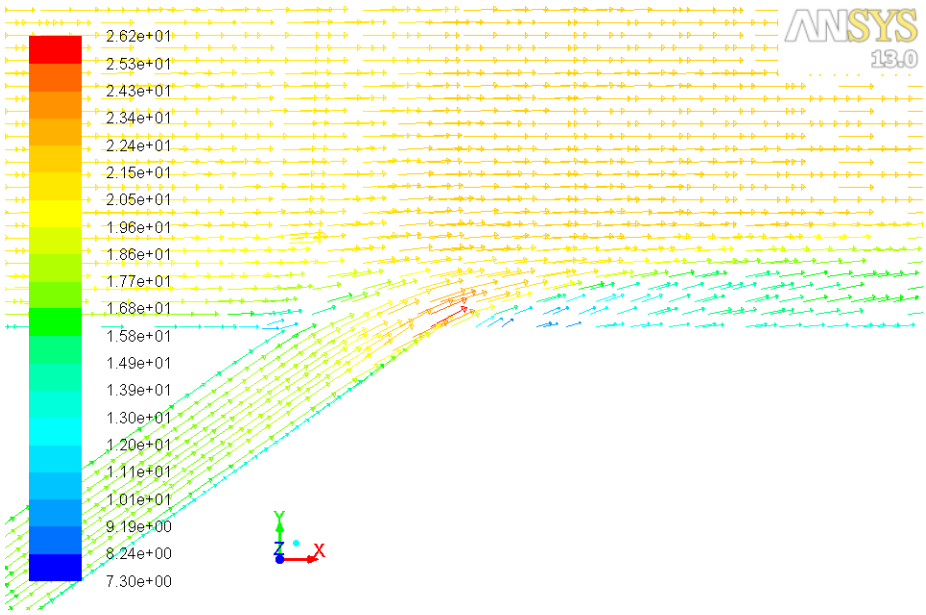

Fig. 20: Velocity Vectors B_{035} M=1

By comparing figures 19 and 20 above, it is seen that in the low blowing ratio case the coolant adheres to the surface downstream of the hole as opposed to the higher blowing ratio case in which the coolant penetrates deeper into the mainstream flow. This is more clearly shown when observing the velocity vectors. This is the reason why the lower blowing ratio performs better while x/D < 20. This is further illustrated by observing the temperature contours, figures 21 and 22.

3.1.3 Temperature Contours

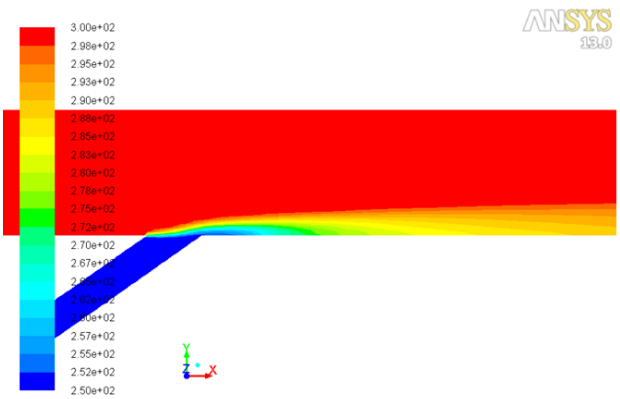

Fig. 21: Temperature Contours $B_{\theta 35}$ M=0.24

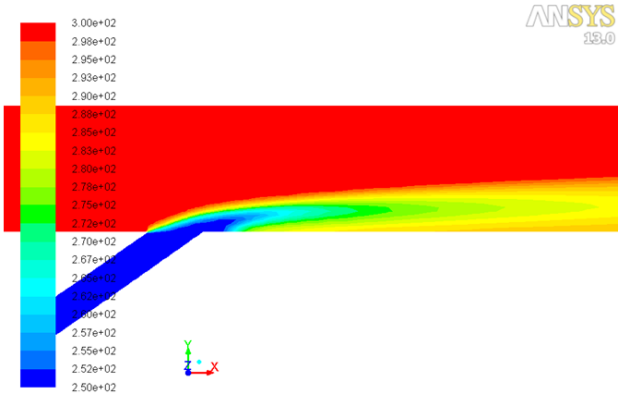

Fig. 22: Temperature Contours $B_{\theta 35}$ M=1

As shown by the figures 21 and 22, the coolant better attaches to the surfaces in the low blowing ratio case resulting in a lower surface temperature for x/D < 20. The reason why the higher blowing ratio case performs better for x/D > 20 is simply because there is more coolant injected into the mainstream which is better able to combat the high temperatures of the main flow further downstream.

3.1.4 Laterally Averaged Film Cooling Effectiveness

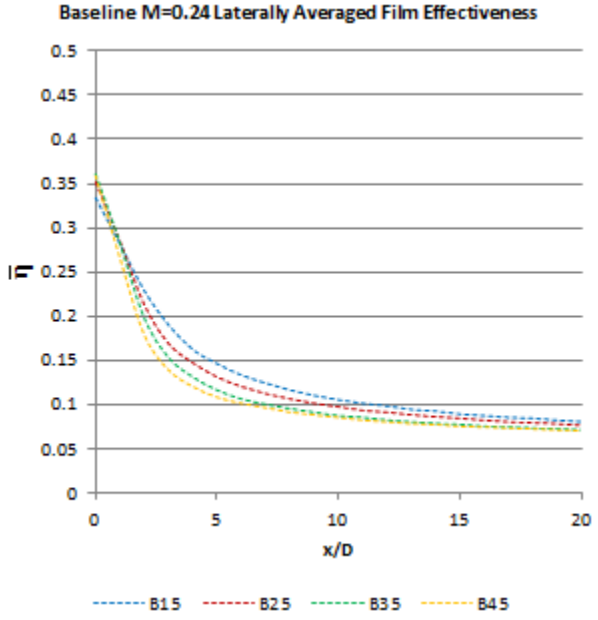

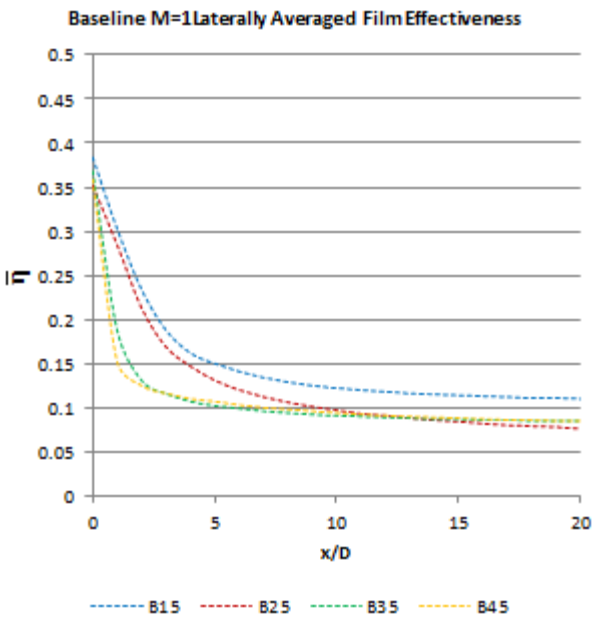

Fig. 23: Laterally Averaged Film Effectiveness $B_{\theta 3}$ M=0.24 Fig. 24: Laterally Averaged Film Effectiveness $B_{\theta 3}$ M=1

The laterally averaged film cooling effectiveness values show similar trends to the centerline film cooling effectiveness values in both the low and high blowing ratio cases. Once again the 15° injection angle provides the best results, and increasing the injection angle lowers the laterally averaged film cooling effectiveness.

3.1.5 Surface Temperature Contours

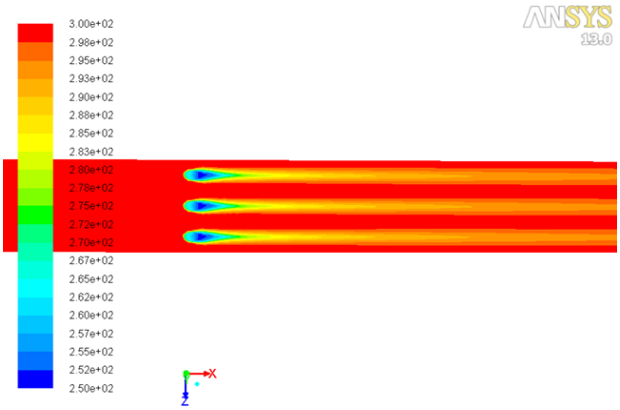

Fig. 25: Surface Temperature Contours B_{035} M=0.24

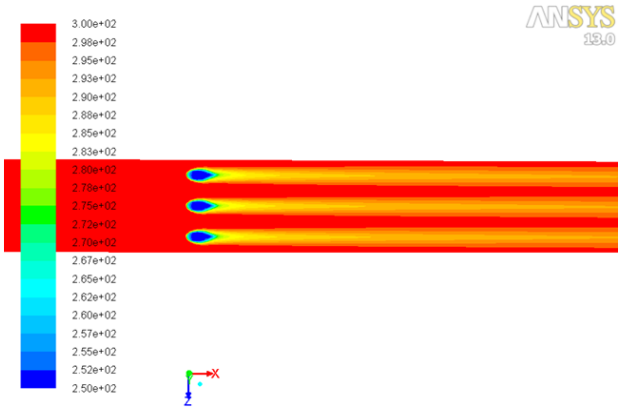

Fig. 26: Surface Temperature Contours B_{035} M=1

Figure 25 above illustrates the better attachment of the coolant in the low blowing ratio case, resulting in lower surface temperatures immediately downstream of the injection site. Figure 26 shows the consequence from jet penetration in the high blowing ratio case, but also the slightly better surface temperatures further downstream of the injection site. To better understand the decay in the performance of the film cooling, one must look at the 3D nature of the problem having to deal with kidney vortices.

3.1.6 Kidney Vortices

The figures below illustrate the kidney vortices that occur due to the injection of the coolant into the mainstream flow.

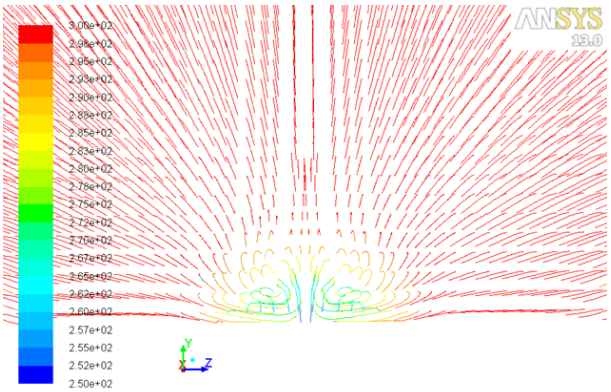

Fig. 27: Kidney Vortices B_{035} M=0.24

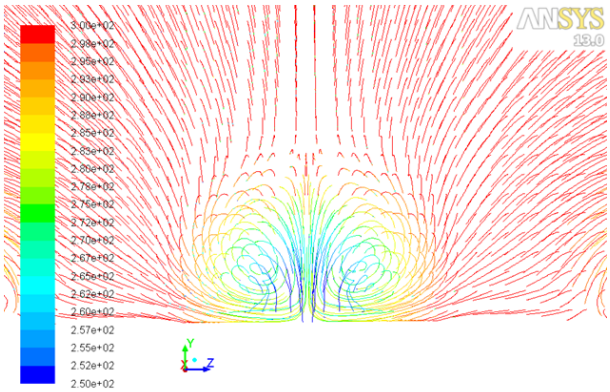

Fig. 28: Kidney Vortices B_{035} M=1

Figure 27 shows almost the lack of kidney vortex formation due to the low momentum of the injected coolant into the mainstream. The low velocity coolant is effectively pushed forward and the kidney vortices that are created are not very strong. In the higher blowing ratio case the coolant has more momentum penetrating into the main flow. This allows the coolant to better interact with the main flow creating stronger kidney vortices. These vortices pull surrounding warm air from the mainstream underneath the stream of coolant which not only rapidly decreases the temperature of the coolant, but also helps to lift the coolant jet off of the surface. As the

coolant stream continues downstream, more warm air mixes in and the jet continues of lift off causing the film cooling effectiveness to drop. To better visualize this progression observe the figures below.

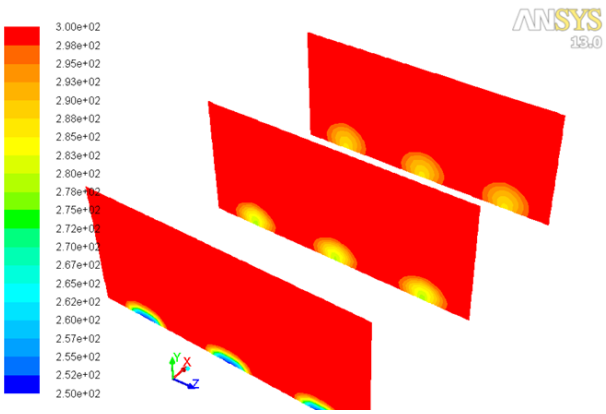

Fig. 29: Temperature Progression $B_{\theta 35}$ M=0.24

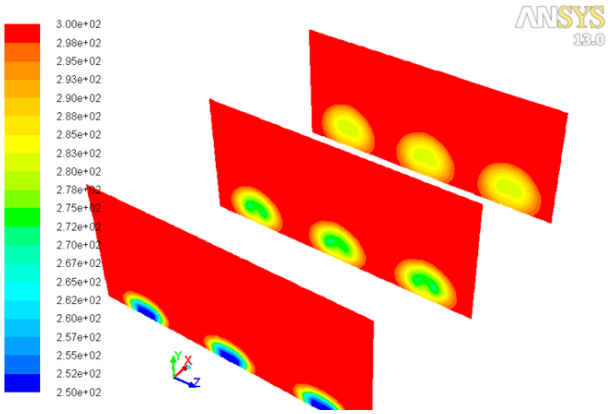

Fig. 30: Temperature Progression $B_{\theta 35}$ M=1

It is clearly seen that the kidney vortices lift the coolant jet off of the surface more in the higher blowing case. It is also easily seen that with the higher blowing ratio the coolant retains a larger, cooler stream when compared with the lower blowing ratio case.

Chapter 4: Comparative Study of Ramp Surface Enhancements

4.1 Ramp Inclined at 5°

4.1.1 Centerline Film Cooling Effectiveness

Please observe the centerline film cooling effectiveness results below for the ramp configurations.

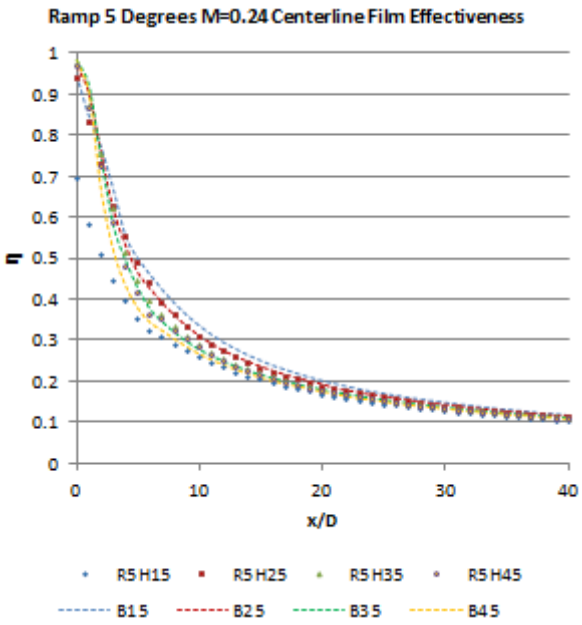

Fig. 31: Centerline Film Effectiveness $R_{05}h_{035}$ M=0.24

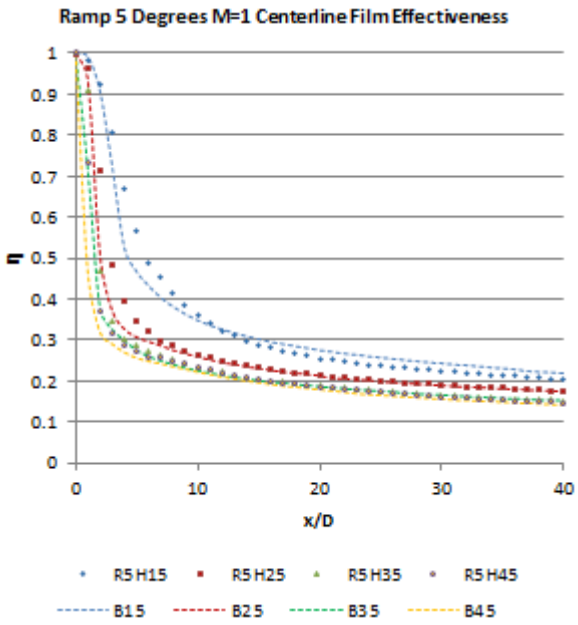

Fig. 32: Centerline Film Effectiveness $R_{05}h_{035}$ M=1

From figure 31, one can see that the addition of a 5° ramp decreases the centerline film cooling effectiveness when compared to the baseline configuration. However, it is important to note that the 45° injection angle provides the best results. Every 10° decrease in injection angle causes poorer film cooling performance, as opposed to the baseline configuration. The reason for lower performance is the fact that lower pressure region is created behind the ramp which decreases the momentum in the already low velocity coolant jet. This is easier to understand when looking at the visual representations of the velocity vectors and contours.

Figure 32 shows that the higher blowing ratio increases the centerline film cooling effectiveness slightly while x/D < 10. Beyond that it remains equivalent with the baseline configuration except for the 15° injection angle. The reason for this is that the higher blowing ratio gives the coolant more momentum to withstand the recirculation effects created by the ramp. Even though the jet still penetrates into the main flow, the ramp creates more protection of the surface by deflecting the hot main flow away from the coolant. This is what allows the 5° ramp surface enhancement to perform better than the baseline configuration at the higher blowing ratio.

4.1.2 Velocity Contours and Vectors

Please observe the velocity contours and vectors below.

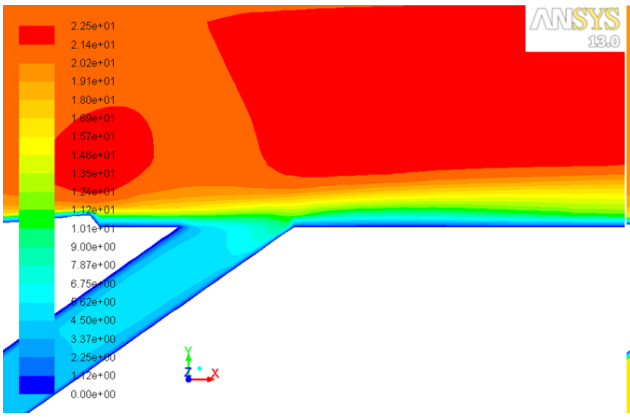

Fig. 33: Velocity Contours $R_{05}H_{035}$ M=0.24

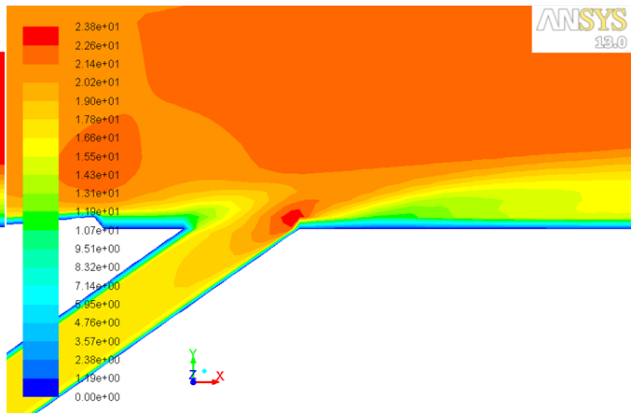

Fig. 34: Velocity Contours $R_{05}H_{035}$ M=1

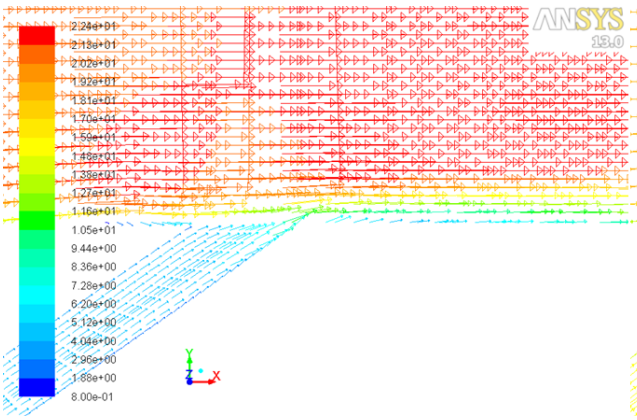

Fig. 35: Velocity Contours $R_{05}H_{035}$ M=0.24

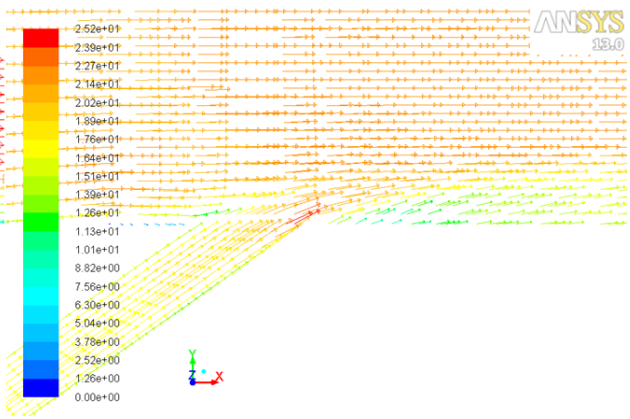

Fig. 36: Velocity Contours $R_{05}H_{035}$ M=1

By comparing figures 33 and 34, it is seen that in the low blowing ratio case the coolant adheres to the surface downstream of the hole as opposed to the higher blowing ratio case in which the coolant penetrates deeper into the mainstream flow. In the higher blowing ratio case the point of highest velocity occurs right at the exit of the injection site. This is the result of slow moving, higher pressure area after the jet exit that is created from both the ramp's protection that causes greater jet penetration. This allows for better film cooling performance while x/D < 10 after the injection site when compared with the baseline configuration. However, the lower blowing ratio continues to perform better than the higher blowing ratio case in general.

4.1.3 Temperature Contours

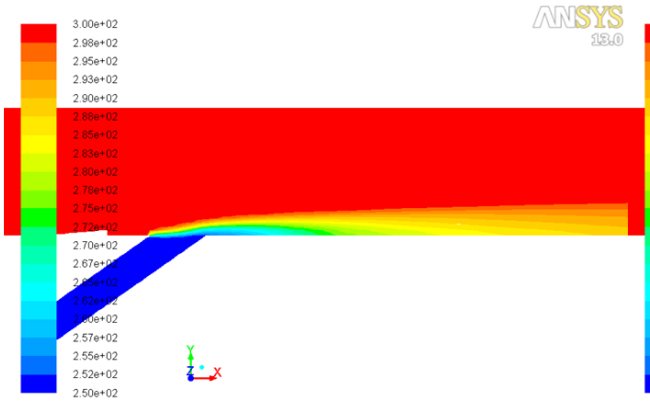

Fig. 37: Temperature Contours $R_{05}H_{035}$ M=0.24

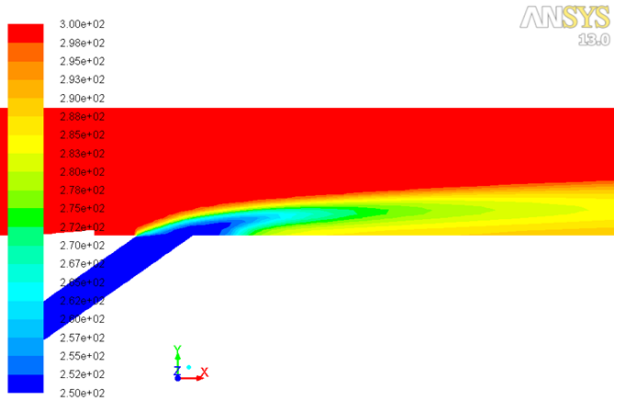

Fig. 38: Temperature Contours $R_{05}H_{035}$ M=1

As shown by the figures 37 and 38, the coolant better attaches to the surfaces in the low blowing ratio case resulting in lower surface temperatures across the length of the surface. Although there is initially better film cooling effectiveness in the near injection hole region, the ramp causes greater jet penetration which leads to the coolant jet detaches from the surfaces slightly quicker than the baseline configuration. It is the protection that the ramp creates which allows the film cooling performance to remain approximately the same further downstream.

It is important to note that the lower the injection angle, the greater is the opening of the of the injection elliptical hole. By increasing the width of the elliptical hole, the flow's velocity decreases as well as its momentum. Below are figures which show why in the case of lower blowing ratio the lower injection angle causes too much momentum loss, which results in not enough momentum to combat the main flow and therefore decreases the center line film cooling effectiveness.

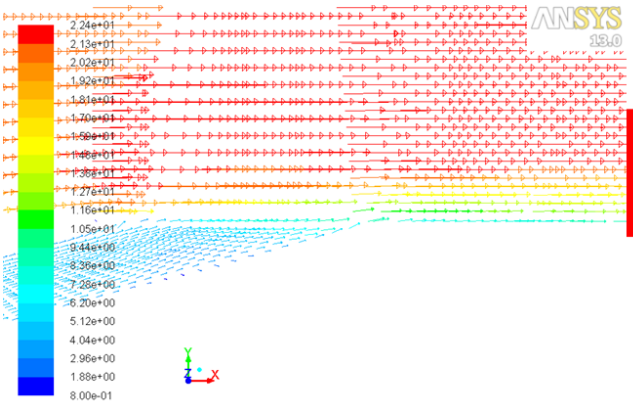

Fig. 39: Velocity Vectors $R_{05}H_{015}$ M=0.24

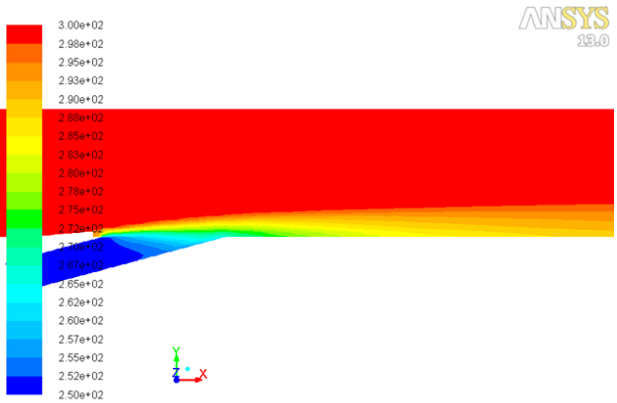

Fig. 40: Temperature Contours $R_{05}H_{035}$ M=1

4.1.4 Laterally Averaged Film Cooling Effectiveness

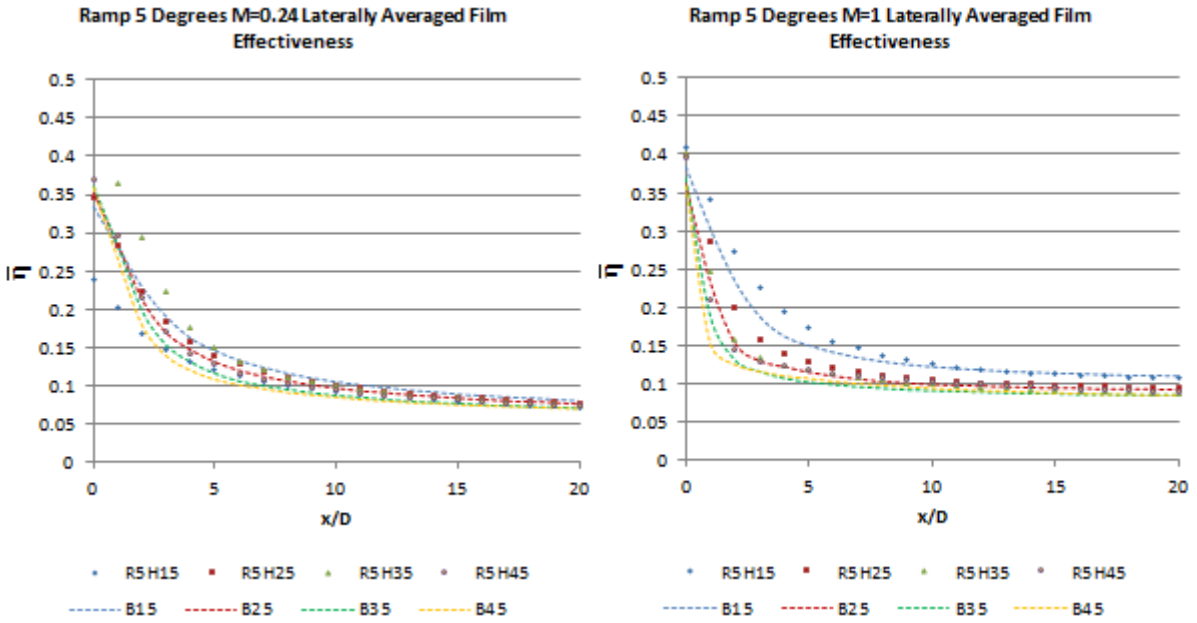

Fig. 41: Laterally Averaged Film Effectiveness $R_{05}H_{035}$ M=0.24 Fig. 42: Laterally Averaged Film Effectiveness $R_{05}H_{035}$ M=1

In the case of lower blowing ratio the laterally averaged film cooling effectiveness values increase with increasing injection angle from 15° to 35°, but decreases when going from 35° to 45°. This is believed due to finding the balance between having not enough, or too much, momentum when combating the main flow. The 15° injection angle performed worse that its baseline counterpart, while the rest saw increased performance. In the case of higher blowing ratio all injection angles performed better than their baseline counterparts since they had enough momentum to combat the main flow. The lowest injection angle performed the best since it had the least jet penetration.

4.1.5 Surface Temperature Contours

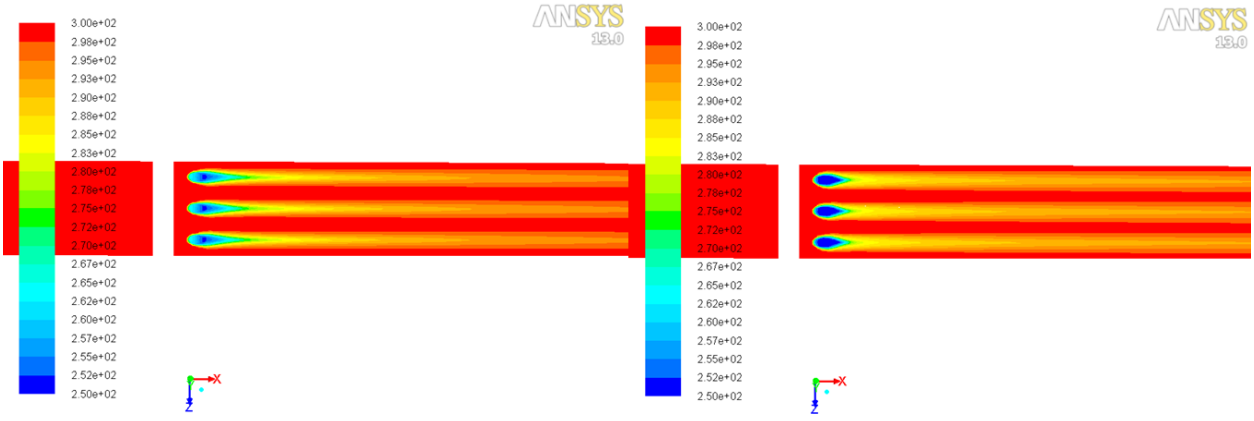

Fig. 43: Surface Temperature Contours $R_{05}H_{035}$ M=1 Fig. 44: Surface Temperature Contours $R_{05}H_{035}$ M=1

Figure 43 illustrates the better attachment of the coolant in the low blowing ratio case, resulting in lower surface temperatures immediately downstream of the injection site. Figure 44 shows the consequence from jet penetration in the high blowing ratio case, but also the slightly better surface temperatures further downstream of the injection site due to the protection provided by the ramp. To better understand the decay in the performance of the film cooling, one must look at the 3D nature of the problem having to deal with kidney vortices.

4.1.6 Kidney Vortices

The figures below illustrate the kidney vortices that occur due to the injection of the coolant into the mainstream flow.

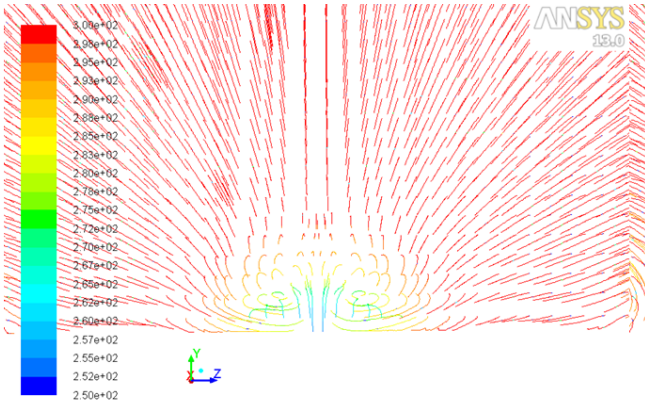

Fig. 45: Kidney Vortices $R_{05}H_{035}$ M=0.24

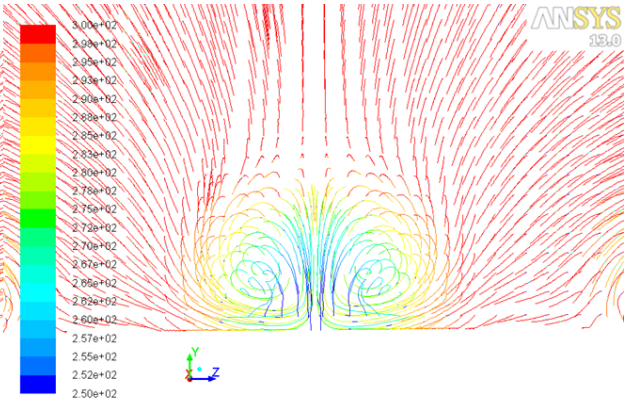

Fig. 46: Kidney Vortices $R_{05}H_{035}$ M=1

Figure 45 shows almost the lack of kidney vortex formation due to the low momentum of the injected coolant into the mainstream. In the higher blowing ratio case the coolant has more momentum penetrating into the main flow which allows the coolant to better interact with the main flow creating stronger kidney vortices. The ramp does provide slightly better protection from the mainstream flow when compared to the baseline case. This allows for a slightly better reduction of jet lift off and attachment of the coolant jet. To better visualize this progression observe figures 47 and 48 below.

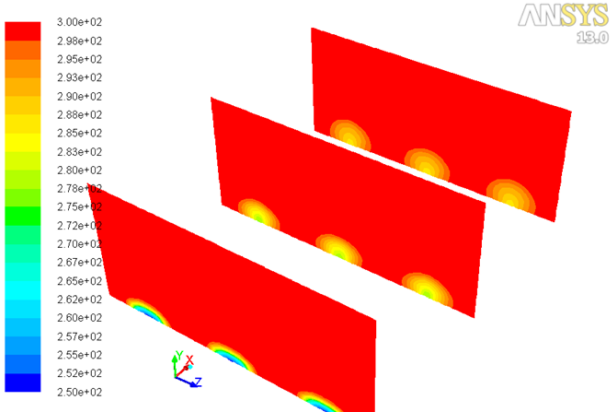

Fig. 47: Temperature Progression $R_{05}H_{035}$ M=0.24

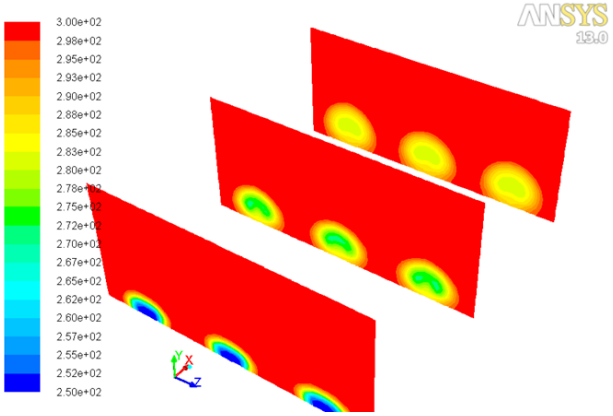

Fig. 48: Temperature Progression $R_{05}H_{035}$ M=1

It is clearly seen that the kidney vortices lift the coolant jet off of the surface more in the higher blowing ratio case.

4.2 Ramp Inclined at 15°

4.2.1 Centerline Film Cooling Effectiveness

Please observe the centerline film cooling effectiveness results below for the ramp configurations.

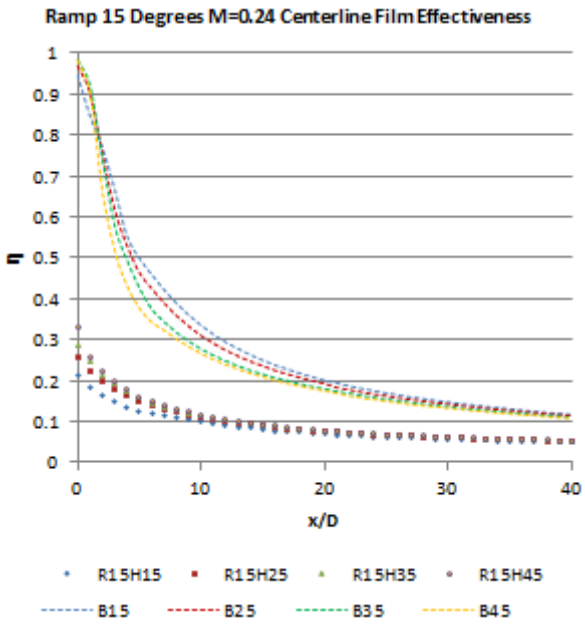

Fig. 49: Centerline Film Effectiveness $R_{\theta 15}H_{\theta 35}$ M=0.24

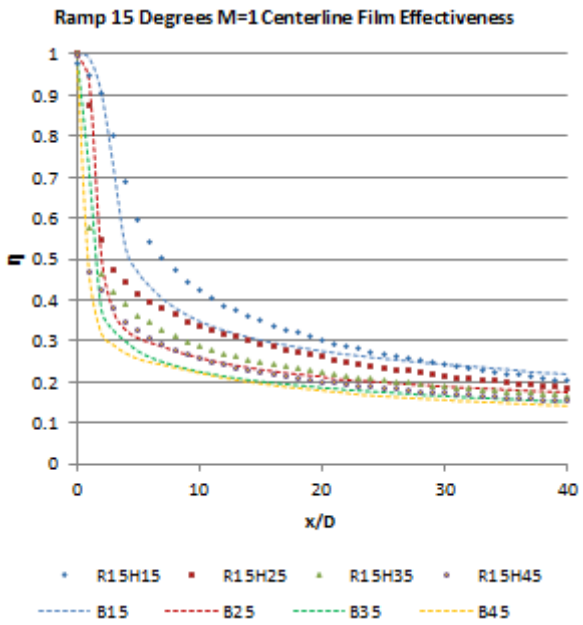

Fig. 50: Centerline Film Effectiveness $R_{\theta 15}H_{\theta 35}$ M=1

By looking at figure 49 above, it is seen that the centerline film cooling effectiveness has dropped significantly compared to the baseline configuration. The steeper ramp angle of 15° deflects the mainstream flow much more than the 5° ramp, which now creates an area of recirculation behind the ramp. Not only does this area of recirculation lower the momentum of the injected coolant, but it also pulls some of it backwards. From comparing the results different injection angles it is seen that this low blowing ratio case is completely dominated by this recirculation effect.

Figure 50 indicates that, the higher blowing ratio greatly increases the centerline film cooling effectiveness in this 15° ramp configuration. The reason for this is that while the ramp deflects the main flow away from the injected coolant, the jet has enough momentum to better overcome the recirculation effects, thereby allowing it to fully utilize the protection provided by the ramp. Three dimensional effects also account for the greater centerline film cooling effectiveness, since the lower pressure area created behind the ramp allows the injected coolant to expand in the lateral direction, which will be shown later. To better understand the characteristics of these graphs one must view the recirculation areas by viewing the velocity contours and velocity vectors. Also, the span wise expansion of the coolant helps to hinder the detrimental effects of kidney vortices pulling in surrounding warmer air.

4.2.2 Velocity Contours and Vectors

Please observe the velocity contours and vectors below.

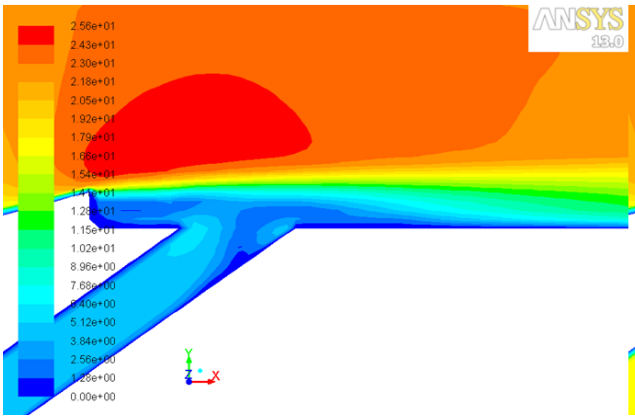

Fig. 51: Velocity Contours $R_{\theta 15}H_{035}$ M=0.24

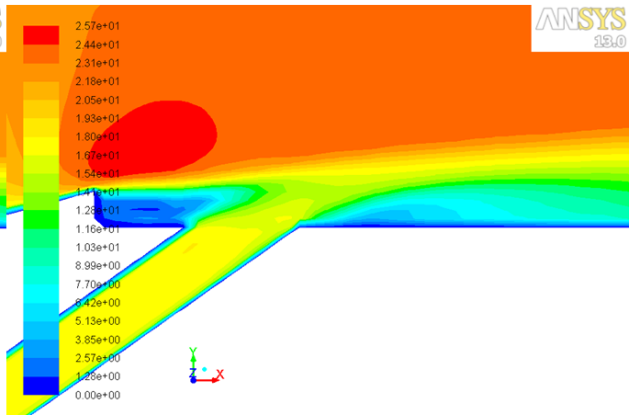

Fig. 52: Velocity Contours $R_{\theta 15}H_{035}$ M=1

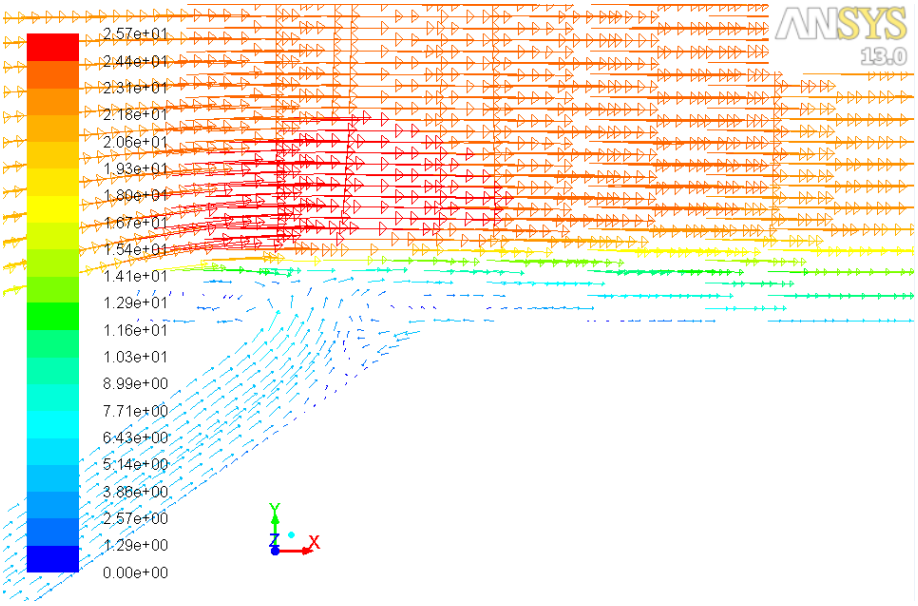

Fig. 53: Velocity Vectors $R_{\theta 15}H_{035}$ M=0.24

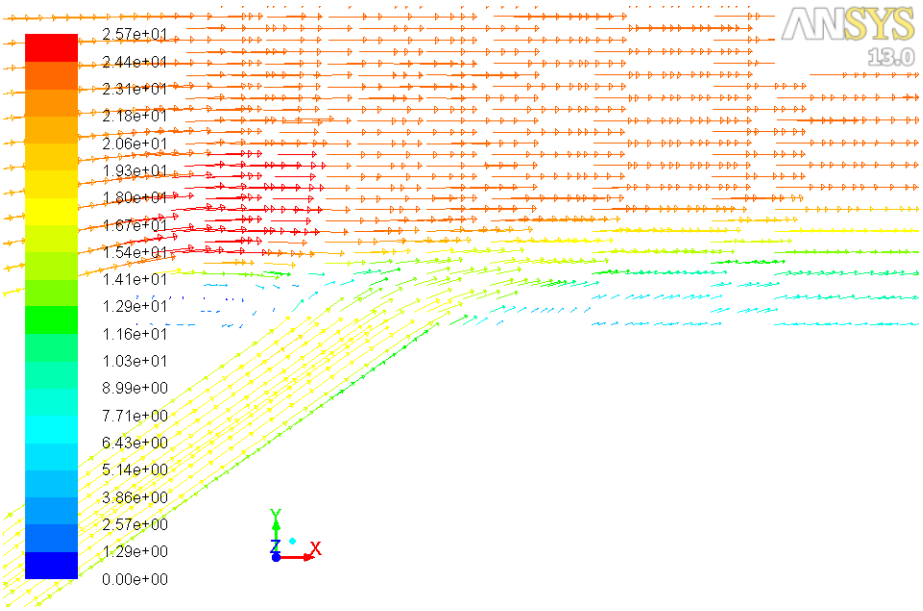

Fig. 54: Velocity Vectors $R_{\theta 15}H_{\theta 35}$ M=1

By comparing figures 51 and 52 above, it is seen that in the low blowing ratio case does not have enough momentum to overcome the recirculation region created by the ramp. Examining figure 53 more closely, one can see that there are actually two recirculation regions, the second being located at the edge where the film cooling hole meets the cooled surface. This is very bad for film cooling as this turbulent recirculation mixes the main stream in with the coolant causing greatly lowered performance. The higher blowing ratio case does not have this problem as the injected coolant clearly has enough momentum to overcome the recirculation region. The following page further illustrates this by observing the temperature contours.

4.2.3 Temperature Contours

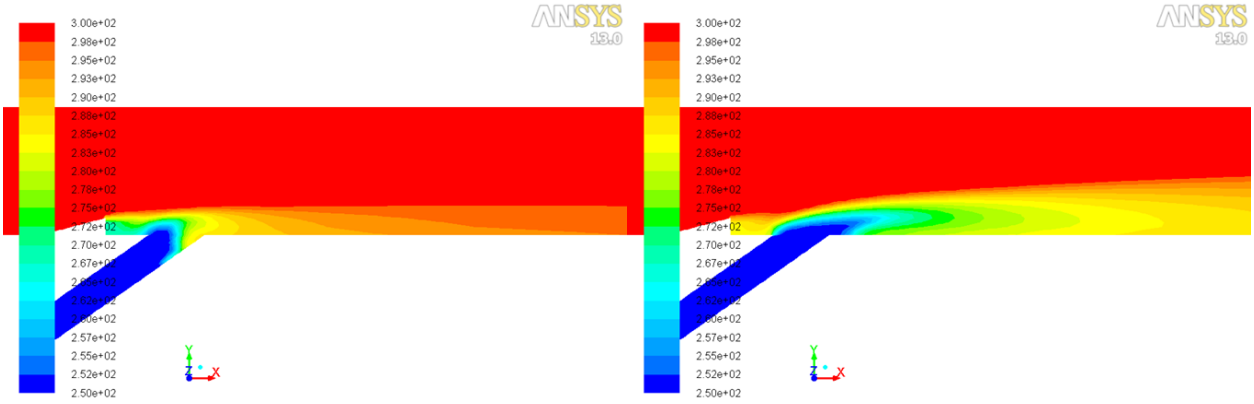

Fig. 55: Temperature Contours $R_{\theta 15}H_{035}$ M=0.24 Fig. 56: Temperature Contours $R_{\theta 15}H_{035}$ M=1

As shown by the low blowing ratio case above, some of the coolant is pulled backwards towards the ramp. The second recirculation site causes mixing great enough to cause an increase in temperature within the film cooling hole. Although some of the coolant in the higher blowing ratio case is pulled backwards towards the ramp, the majority of it has enough momentum to continue downstream along the surface. The 15° ramp deflects the mainstream flow away from the injected coolant, unlike the 5° ramp which deflected the mainstream flow only slightly, providing much greater film cooling performance.

4.2.4 Laterally Averaged Film Cooling Effectiveness

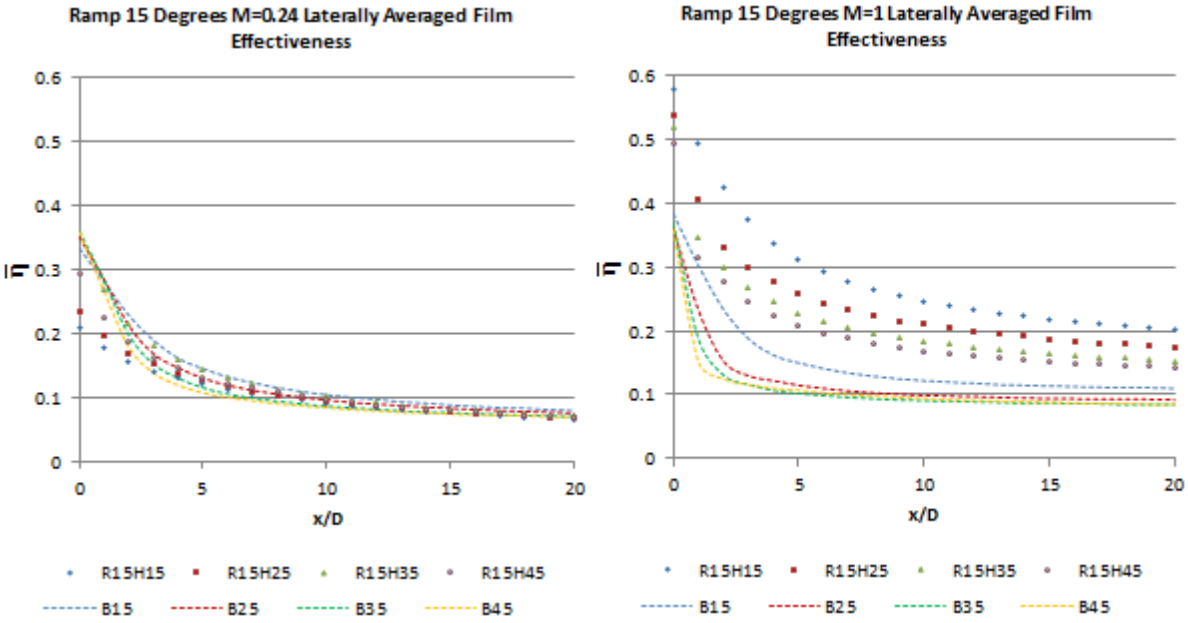

Fig. 57: Laterally Averaged Film Effectiveness $R_{\theta 15}H_{035}$ M=0.24 Fig. 58: Laterally Averaged Film Effectiveness $R_{\theta 15}H_{035}$ M=1

The laterally averaged film cooling effectiveness values are lower than the baseline configuration, as expected from looking at the recirculation effects. The higher blowing ratio case performs much better than the baseline configuration. The figures below show the typical

surface temperature contours of this baseline configuration, which explain the laterally averaged film cooling effectiveness results.

4.2.5 Surface Temperature Contours

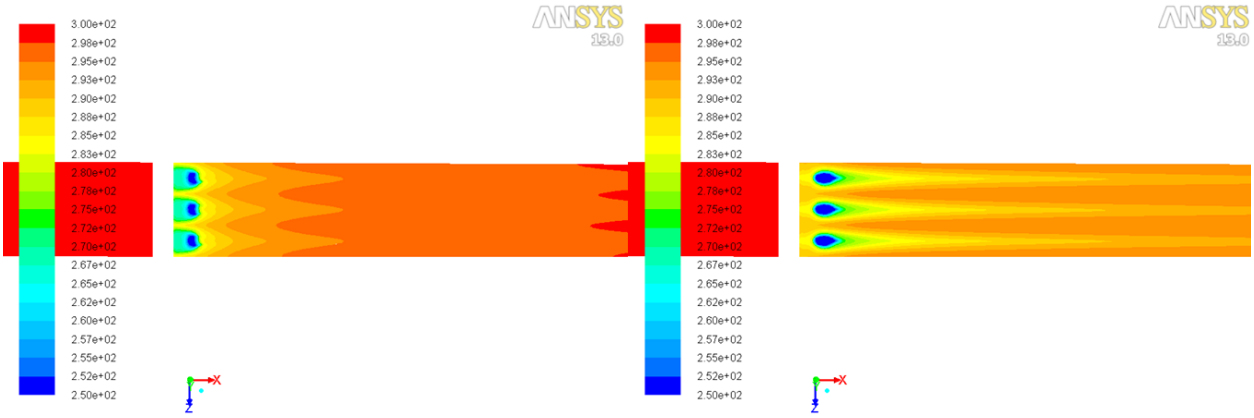

Fig. 59: Surface Temperature Contours $R_{\theta 15}H_{\theta 35}$ M=0.24

Fig. 60: Surface Temperature Contours $R_{\theta 15}H_{\theta 35}$ M=1

Figure 59 above illustrates the recirculation problem, as the coolant is shown to be moving backwards, instead of providing better cooling performance downstream of the injection site. Although the ramp allows the coolant jets to spread laterally, there simply isn't enough momentum in the jets to make use of the lateral spreading effectively. Figure 60 shows that the coolant is able to spread laterally and has enough momentum to cool the surface downstream of the injection site. This shows that with the correct flow conditions, the ramp can provide benefits to the film cooling effectiveness in both the downstream and lateral directions. However, even with the lateral spreading the coolant jets still suffer decay in the performance from kidney vortices.

4.2.6 Kidney Vortices

The figures below illustrate the kidney vortices that occur due to the injection of the coolant into the mainstream flow.

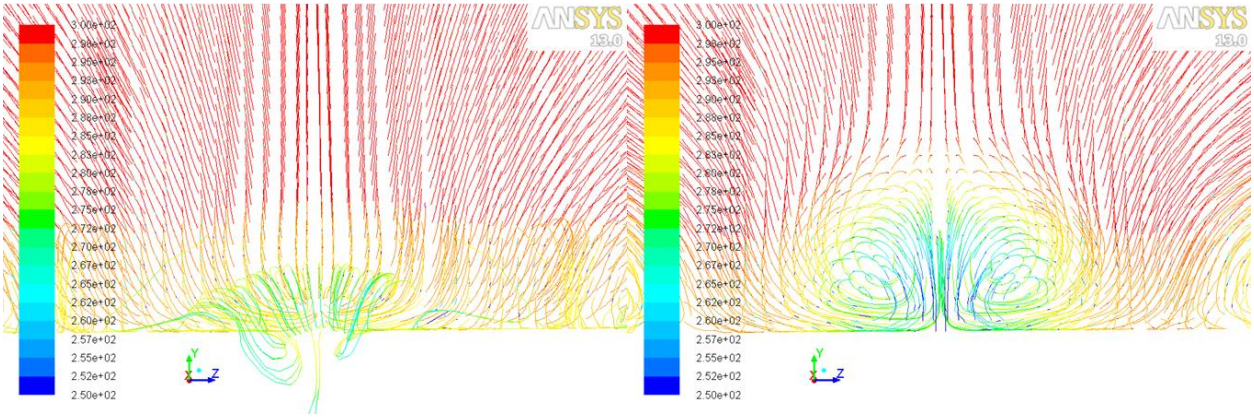

Fig. 61: Kidney Vortices $R_{\theta 15}H_{\theta 35}$ M=0.24

Fig. 62: Kidney Vortices $R_{\theta 15}H_{\theta 35}$ with M=1

Figure 61 shows almost the lack of kidney vortex formation due to the low momentum of the injected coolant into the mainstream, as well as the lateral spreading. In the higher blowing ratio case the coolant much larger kidney vortices are formed compared to those seen in the previous configurations due to the lateral spreading. One can also see that the lateral spreading allows these vortices to pull in air that is cooler than the mainstream. As a result the film cooling performance decays slower than in the previous configurations. This is clearly visible when observing the figures below.

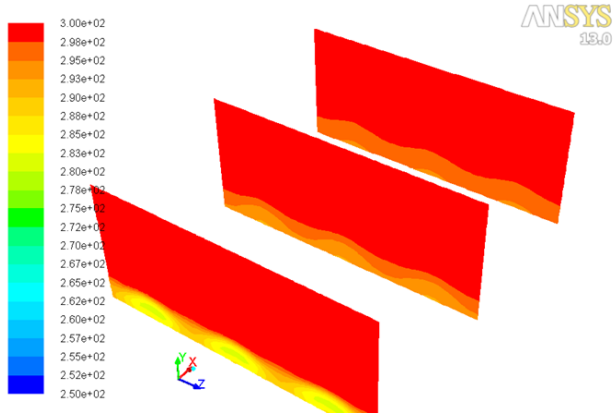

Fig. 63: Temperature Progression $R_{\theta 15}H_{\theta 35}$ M=0.24

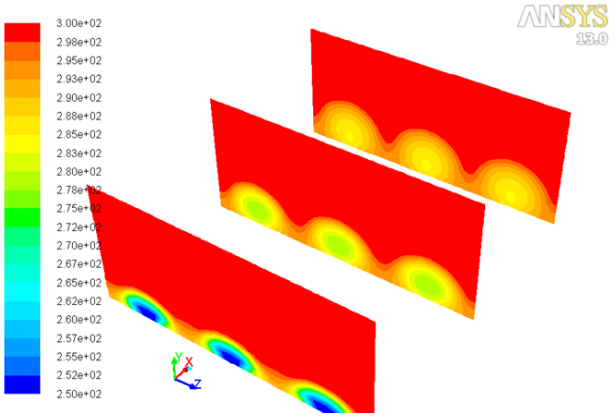

Fig. 64: Temperature Progression $R_{\theta 15}H_{\theta 35}$ M=1

4.3 Ramp Inclined at 25°

4.3.1 Centerline Film Cooling Effectiveness

Please observe the centerline film cooling effectiveness results below for the ramp configurations.

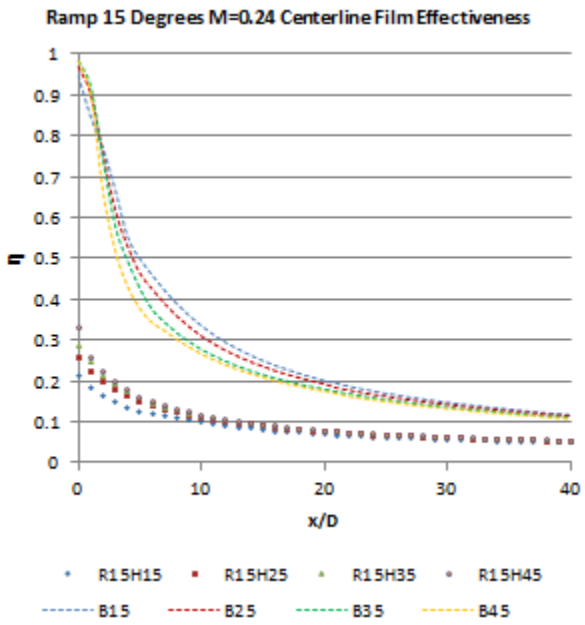

Fig. 65: Centerline Film Effectiveness $R_{025}H_{035}$ M=0.24

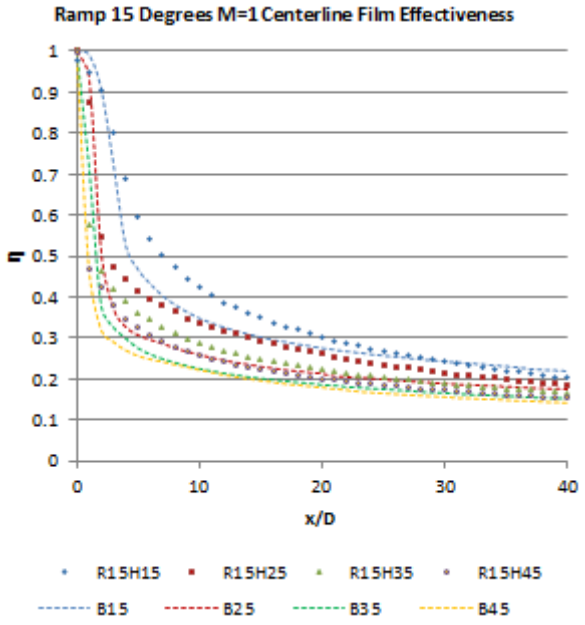

Fig. 66: Centerline Film Effectiveness $R_{025}H_{035}$ M=1

By looking at figure 65 above, one can see that the centerline film cooling effectiveness results are independent of the injection angle, as was found to be the case of the 15° ramp. However, in general it does provide better performance while x/D < 20. Although recirculation plays a role in pulling the coolant backwards, the angle to ramp is steep enough to vault the mainstream flow far above and over the first 20 diameters after the injection site.

By looking at figure 66 above, the higher blowing ratio provides significantly higher centerline film cooling effectiveness when compared to the baseline. In this case the injection angle only slightly affects the film cooling performance. The reason for this is that the ramp appears to deflect the mainstream flow away from the coolant jets entirely. The steeper ramp allows the coolant jets to spread laterally more effectively than in the previous 15° ramp configuration. To better understand the characteristics of these graphs the velocity contours and velocity vectors will be examined on the following page.

4.3.2 Velocity Contours and Vectors

Please observe the velocity contours and vectors below.

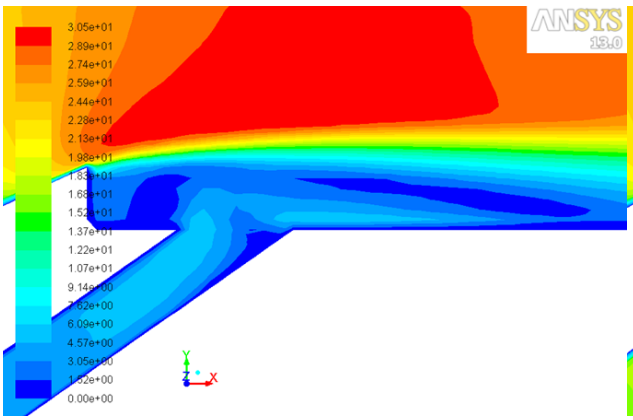

Fig. 67: Velocity Contours $R_{025}H_{035}$ M=0.24

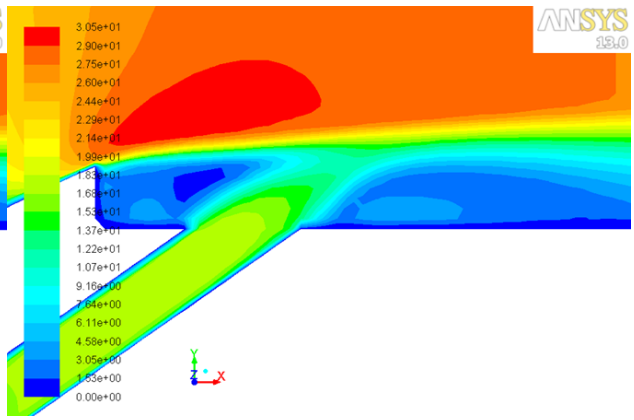

Fig. 68: Velocity Contours $R_{025}H_{035}$ M=1

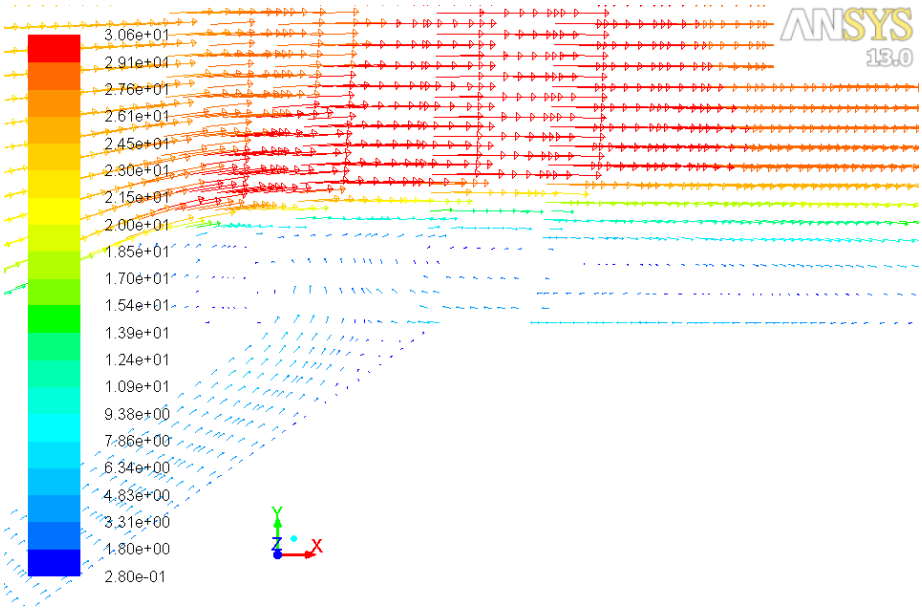

Fig. 69: Velocity Vectors $R_{025}H_{035}$ M=0.24

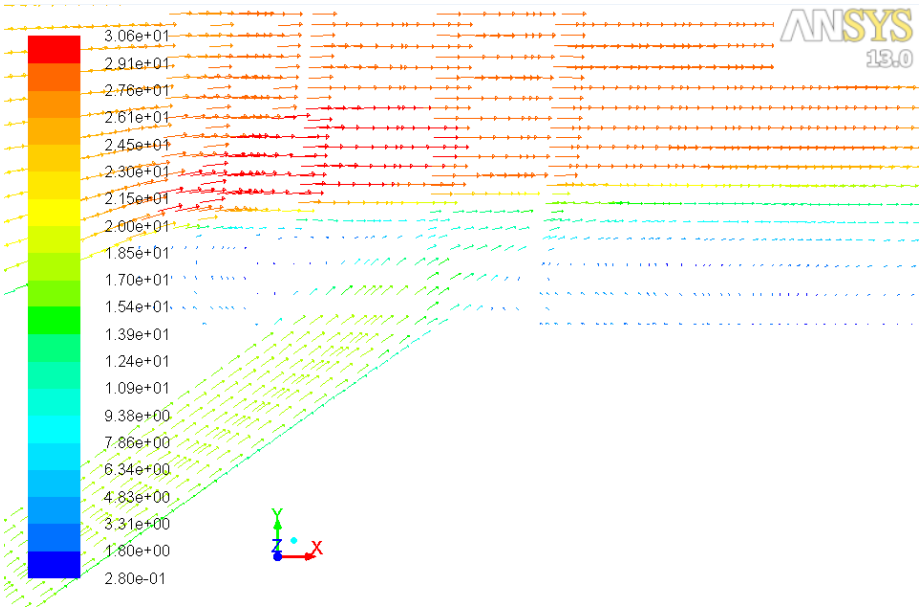

Fig. 70: Velocity Vectors $R_{025}H_{035}$ M=1

By looking at figures 67 and 68 above, it is seen that in the low blowing ratio case the mainstream flow is vaulted up over in injection site and seems to reattach much further downstream when compared to the 15° ramp configuration. Even with the greater recirculation effects seen above, better film cooling effectiveness is still achieved on the surface close to the injection site. Figure 69 shows the recirculation regions, but also the momentum of the jet which allows it to combat the main flow, helping to keep it away from the surface. This is what allows this configuration to perform much better than the baseline, which is illustrated by the temperature contours on the next page.

4.3.3 Temperature Contours

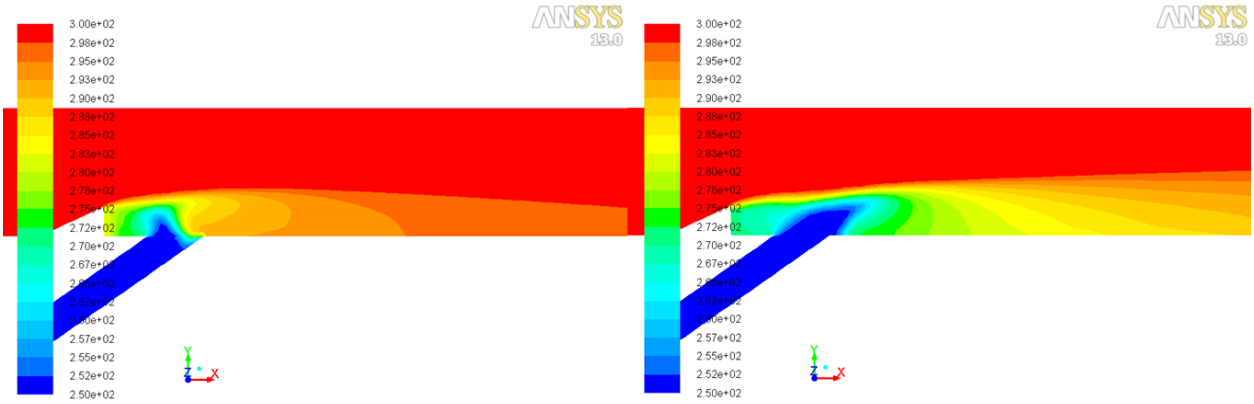

Fig. 71: Temperature Contours $R_{025}H_{035}$ M=0.24

Fig. 72: Temperature Contours $R_{025}H_{035}$ M=1

As shown by figures 71 and 72, the low blowing ratio case is dominated by recirculation effects while the higher blowing ratio case sees much better temperatures along the surface. Once again, the mixing causes lower coolant temperatures inside the film cooling hole in the low blowing ratio case while the higher blowing ratio case appears to be unaffected.

4.3.4 Laterally Averaged Film Cooling Effectiveness

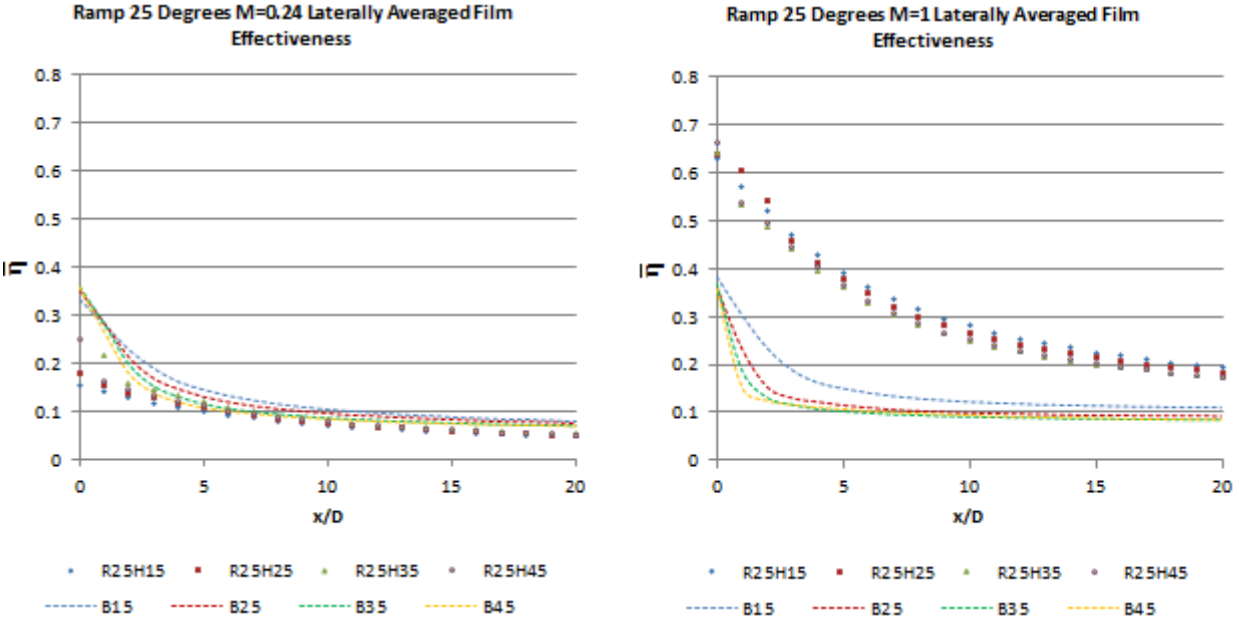

Fig. 73: Laterally Averaged Film Effectiveness $R_{025}H_{035}$ M=0.24

Fig. 74: Laterally Averaged Film Effectiveness $R_{025}H_{035}$ M=1

As in the 15° ramp configuration, at a low blowing ratio this configuration performs very poorly in terms of laterally averaged film cooling effectiveness. Although the mainstream flow is vaulted over the injection site, it is apparent that there is little to no film cooling protection far downstream. The high blowing ratio case produces tremendous results, showing great film cooling coverage across the entire surface as seen in the figures below.

4.3.5 Surface Temperature Contours

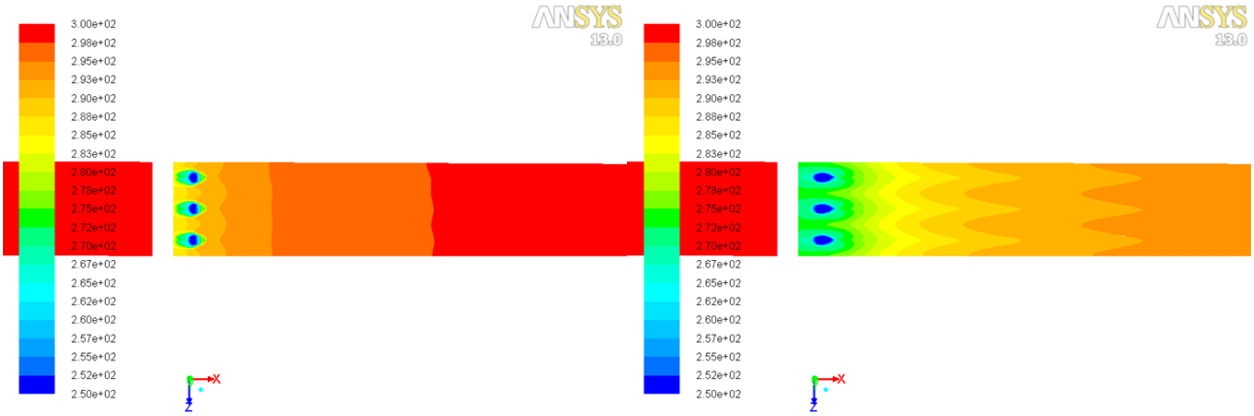

Fig. 75: Surface Temperature Contours $R_{025}H_{035}$ M=0.24

Fig. 76: Surface Temperature Contours $R_{025}H_{035}$ M=1

Figure 75 above illustrates the same problems as seen with the 15° ramp configuration. Figure 76 shows improved performance over the 15° ramp configuration. In particular the lateral spreading of the coolant jets is significantly enhanced, whereas the 15° ramp configuration still shows streaks of where the jets are cooling the surface. The decay in the performance of the film cooling is drastically reduced as a result. The reason for this is shown below in the figures of the kidney vortices.

4.3.6 Kidney Vortices

The figures below illustrate the kidney vortices that occur due to the injection of the coolant into the mainstream flow.

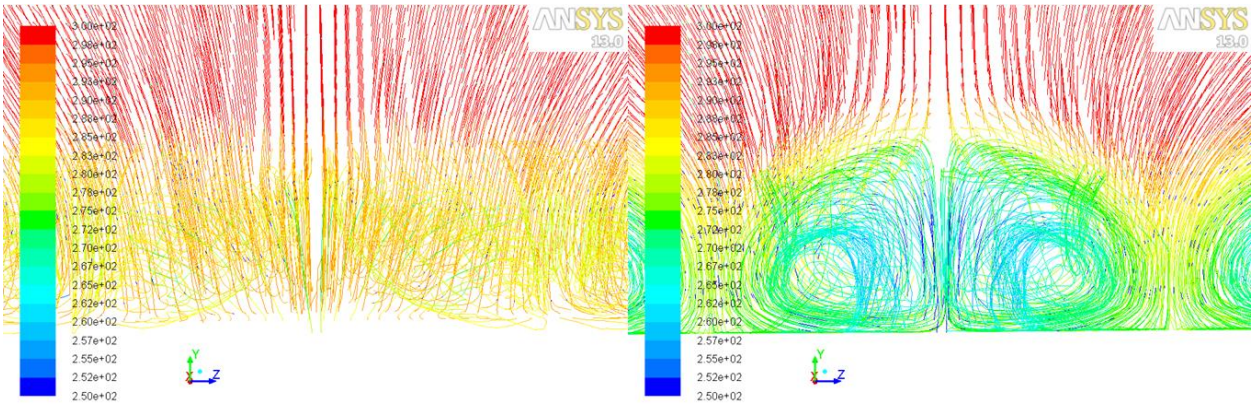

Fig. 77: Kidney Vortices $R_{025}H_{035}$ M=0.24

Fig. 78: Kidney Vortices $R_{025}H_{035}$ M=1

Figure 77 shows almost the lack of kidney vortex formation due to the low momentum of the injected coolant into the mainstream, as well as the lateral spread of the coolant jets. In the higher blowing ratio case the coolant has more momentum and creates even bigger kidney vortices than in the 15° ramp configuration. As shown in figure 78 above, these kidney vortices are so large that they touch those created from the neighboring injection sites. As a result the kidney vortices recirculate air that is much cooler than the mainstream flow, allowing the surface

to be greater protected much further downstream. This progression is illustrated in the figures below.

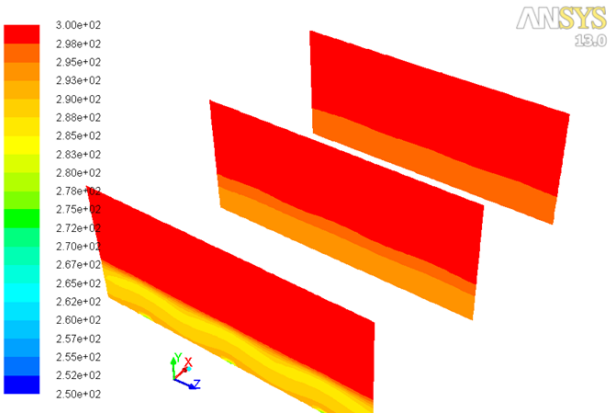

Fig. 79: Temperature Progression $R_{025}H_{035}$ M=0.24

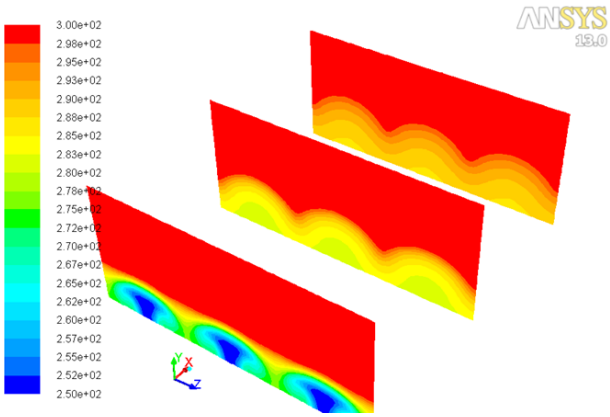

Fig. 80: Temperature Progression $R_{025}H_{035}$ M=1

4.4 Comparison of all Ramp Configurations

The graph below shows the laterally averaged film cooling effectiveness performance gains and losses for the ramp surface enhancements for x/D < 20.

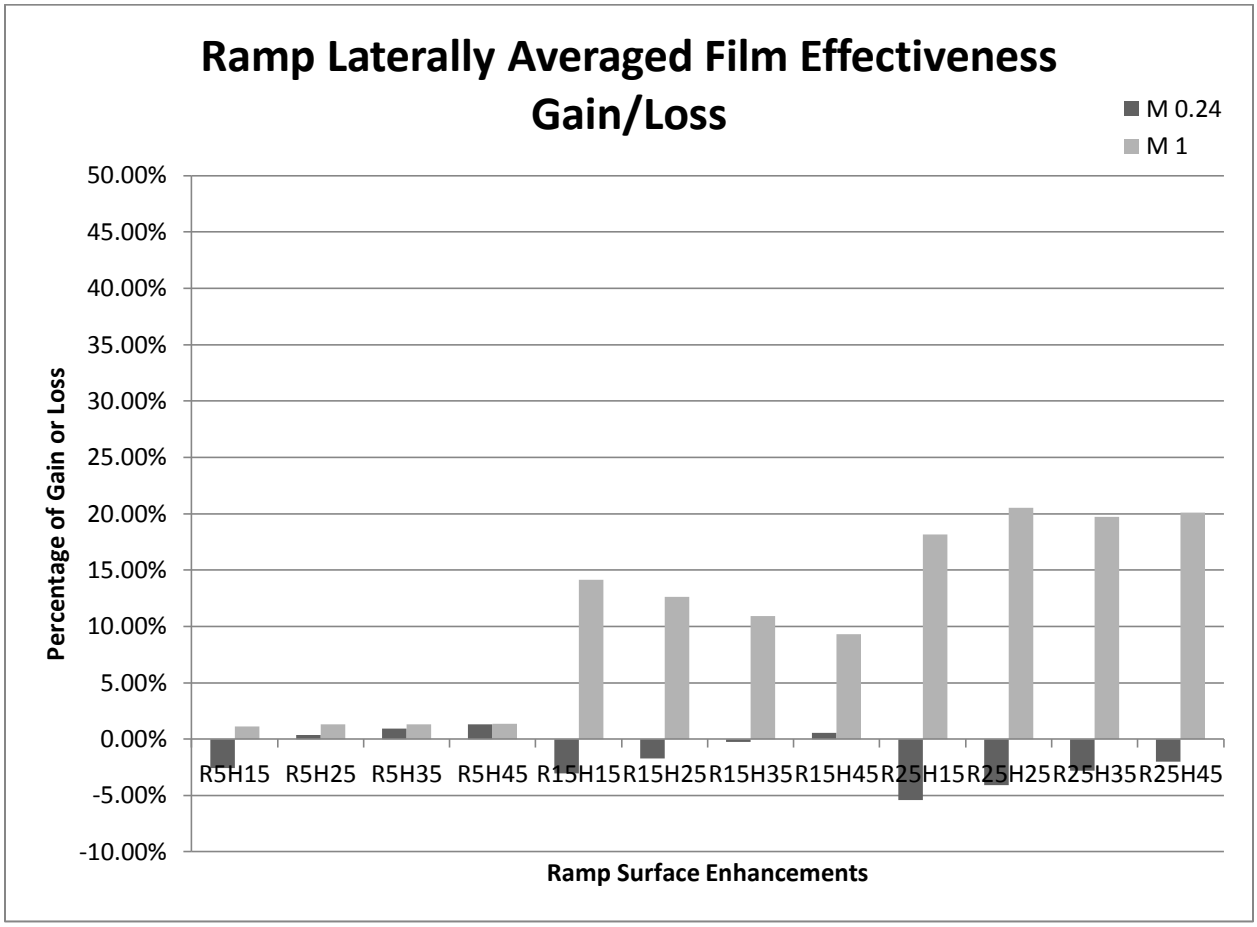

Fig. 81: Laterally Averaged Film Effectiveness Performance Gains or Losses for Ramps

Examining the figures above, the 5° ramp configuration shows negligible gains in laterally averaged film cooling effectiveness performance for both the low and high blowing ratio cases. When looking at the results of the 15° ramp configuration it is seen that at the low blowing ratio of 0.24, this surface enhancement decreases the film cooling performance compared to the baseline. However, the high blowing ratio of 1 saw increases of performance up to 14% with the 15° injection angle which fell to 9% with the 45° injection angle. The steeper ramp of 25° saw even worse performance for the lower blowing ratio, and higher performance gains for the higher blowing ratio when compared to the 15° ramp configuration. The results were inconclusive of determining where a lower, or steeper, injection angle is preferred and the performance gains range from as high as 20.5% down to 18%.

Looking at the ramp surface enhancements laterally averaged film cooling performance as a whole, two conclusions can be drawn. Firstly, ramps do not perform well using low blowing ratios. Secondly, increasing the angle of the ramp, at the high blowing ratio, increases the film cooling performance. However, it is important to keep in mind the significant deflection of that main flow that is caused by the steeper angled ramps. Depending on the surface that needs to be cooled, this may eliminate this configuration from being a possible solution to a cooling problem.

Chapter 5: Comparison Study of Flow Aligned Blocker Surface Enhancements

5.1 Flow Aligned Blocker with 0.5D Height

5.1.1 Centerline Film Cooling Effectiveness

Please observe the centerline film cooling effectiveness results below for the ramp configurations.

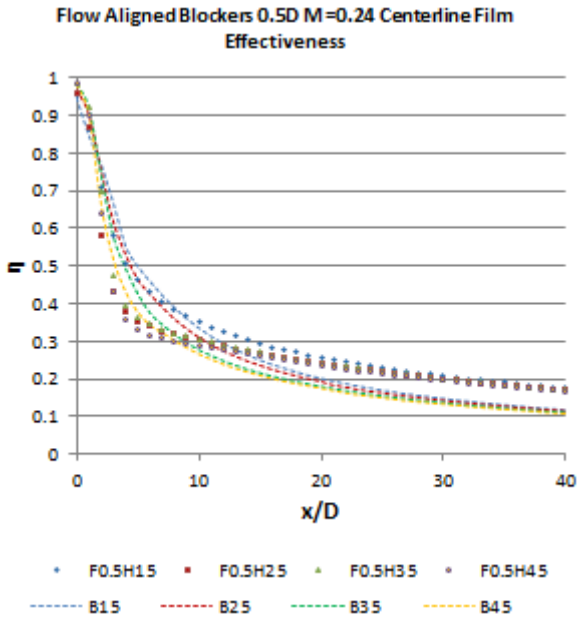

Fig. 82: Centerline Film Effectiveness for $F_{D0.5}H_{035}$ M=0.24

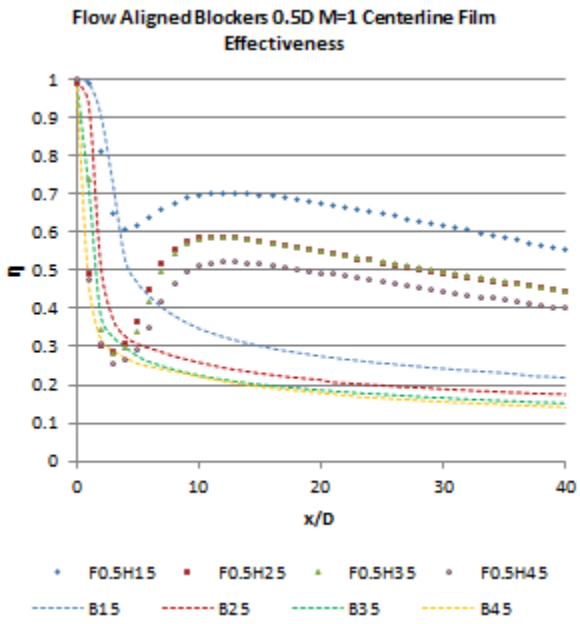

Fig. 83: Centerline Film Effectiveness for $F_{D0.5}H_{035}$ M=1

By looking at figure 82 above, one can see that although the centerline film cooling effectiveness falls lower than the baseline configuration in the first 15 diameters, after that the centerline film cooling effectiveness decays at a slower rate and maintains a slightly higher magnitude. The flow aligned blockers are designed to separate the kidney vortices from the flow of the mainstream, which is why it shows greater performance far downstream from the injection site. Comparing the different injection angles it appears that they do not play a big factor at low blowing ratios.

By looking at figure 83 above, there is an initial drop in centerline film cooling effectiveness at approximately the x/D = 3.5. After that there is a steep rise which peaks and the performance decays slowly. By looking at the injection angles it would appear as though the coolant jet is penetrating into the main flow and reattaching later to the surface is the reasoning for this steep initial drop. However, other factors may need to be taken into account such as lateral spreading, and the effects of the front of the flow aligned blockers. To better understand the characteristics of these graphs one must look at the velocity contours, velocity vectors, temperature contours, as well as the formation of kidney vortices in the following figures.

5.1.2 Velocity Contours and Vectors

Please observe the velocity contours and vectors below.

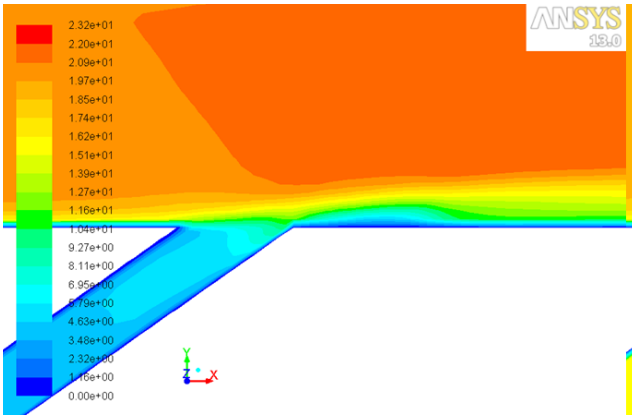

Fig. 84: Velocity Contours for $F_{D0.5}H_{035}$ M=0.24

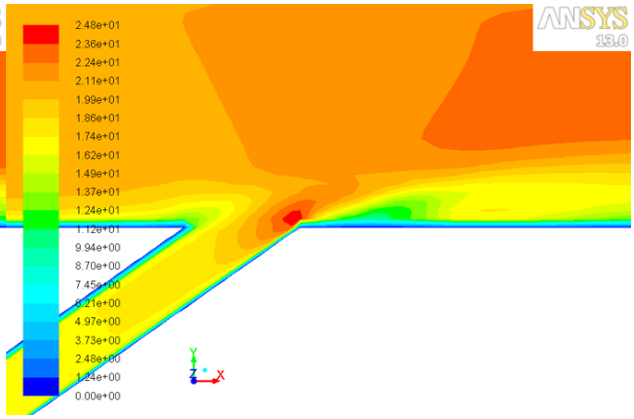

Fig. 85: Velocity Contours for $F_{D0.5}H_{035}$ M=1

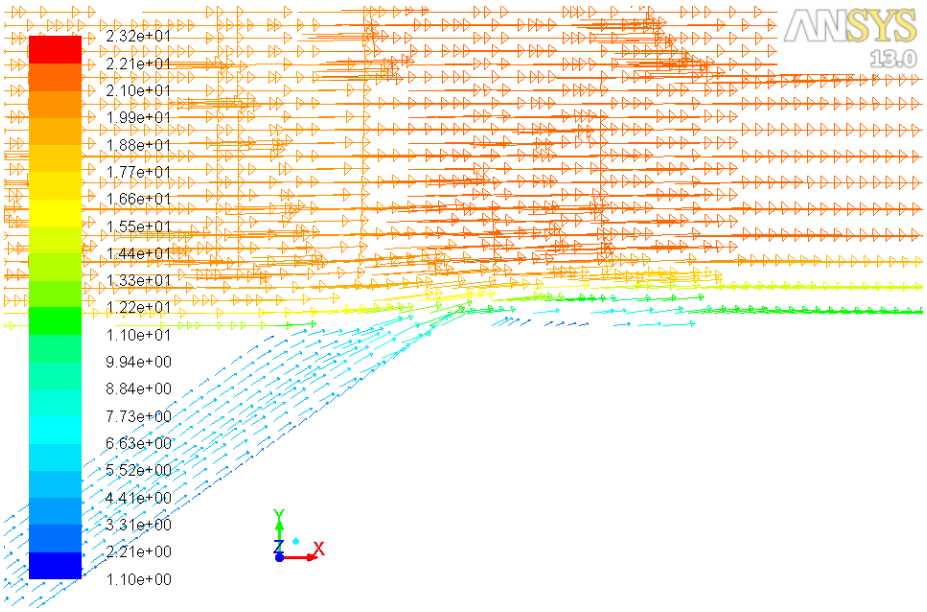

Fig. 86: Velocity Vectors for $F_{D0.5}H_{035}$ M=0.24

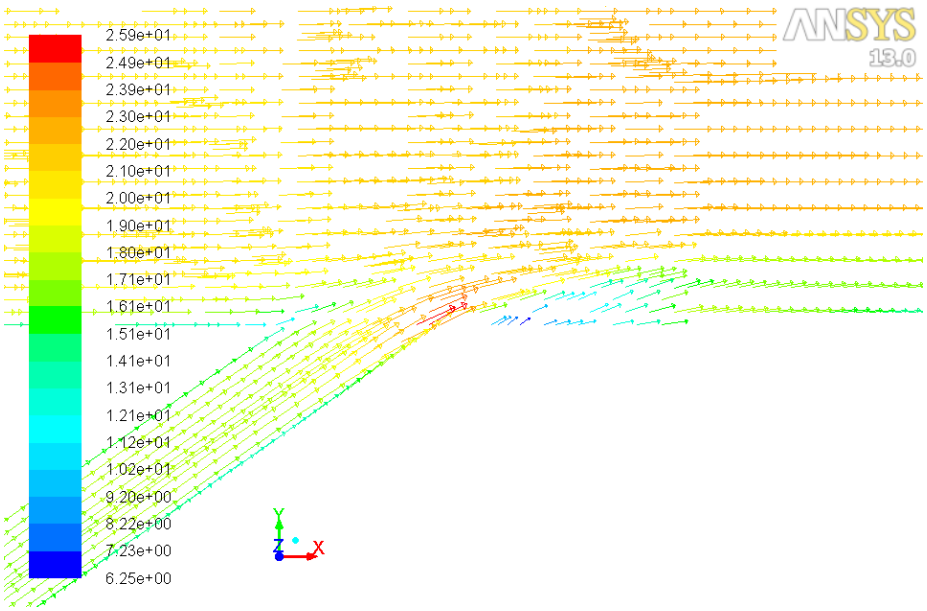

Fig. 87: Velocity Vectors for $F_{D0.5}H_{035}$ M=1

By comparing figures 86 and 87 above, it is seen that in both cases there is an area of lower velocity, and thus higher pressure, immediately after the injection site. By looking at the velocity vectors it is evident that this area is much smaller the in the lower blowing ratio case. This shows that in the low blowing ratio case the coolant reattaches back onto the surface much more quickly than in the high blowing ratio case. One can also see that the area of lower velocity, higher pressure, flow seems to end at the start of the flow aligned blockers. It is believed that the front of the flow aligned blockers create an area of stagnation, which is the cause of the low velocity flow. However, to be sure one must observer the three dimensional effects of this configuration. The next page illustrates the temperature contours of this configuration.

5.1.3 Temperature Contours

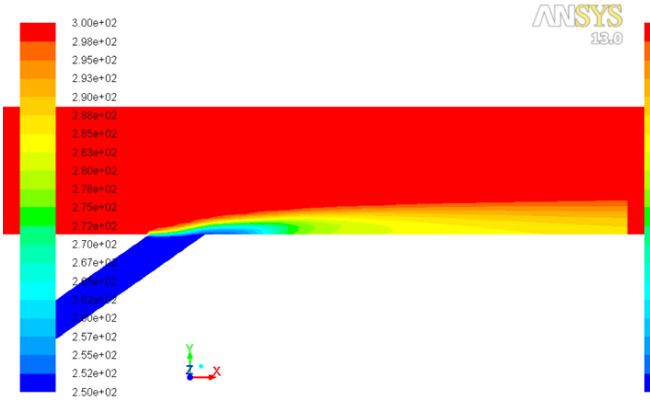

Fig. 88: Temperature Contours for $F_{D0.5}H_{\theta35}$ M=0.24

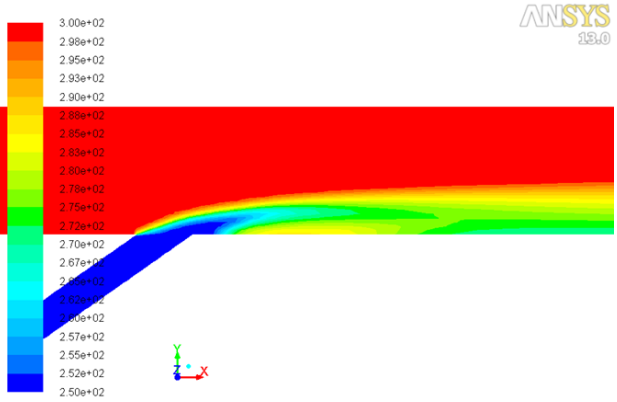

Fig. 89: Temperature Contours for $F_{D0.5}H_{\theta35}$ M=1

As shown in figure 88 the coolant acts very similar to the baseline case but produces slightly cooler surface temperatures. In the higher blowing ratio case there is a streak of higher temperature air located shortly after the injection site. This flow of warmer air slowly rises to the top, while at the same location cooler air above it falls to the surface. This two dimensional temperature contour actually represents a three dimensional phenomena. Warmer air trapped in front of the flow aligned blockers is pulled into the middle by kidney vortices, which is then circulated towards the top. At the same time, the coolant in the center, between the flow aligned blockers, is circulated around the outside and down towards the bottom.

5.1.4 Laterally Averaged Film Cooling Effectiveness

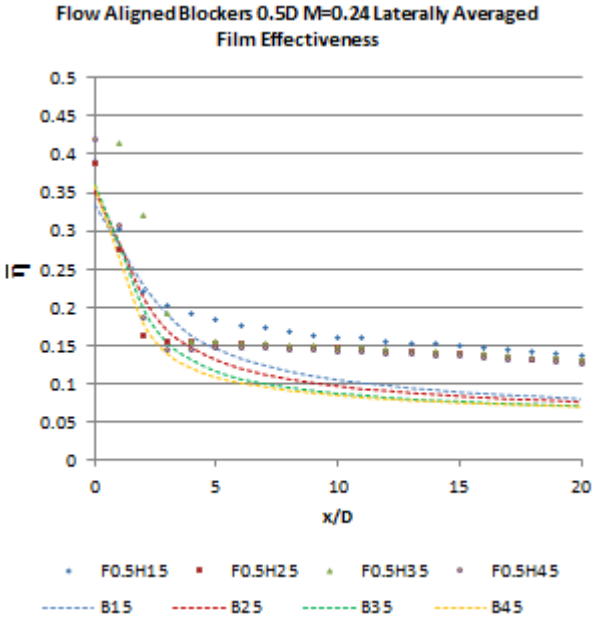

Fig. 90: Laterally Averaged Film Effectiveness for $F_{D0.5}H_{035}$ M=0.24

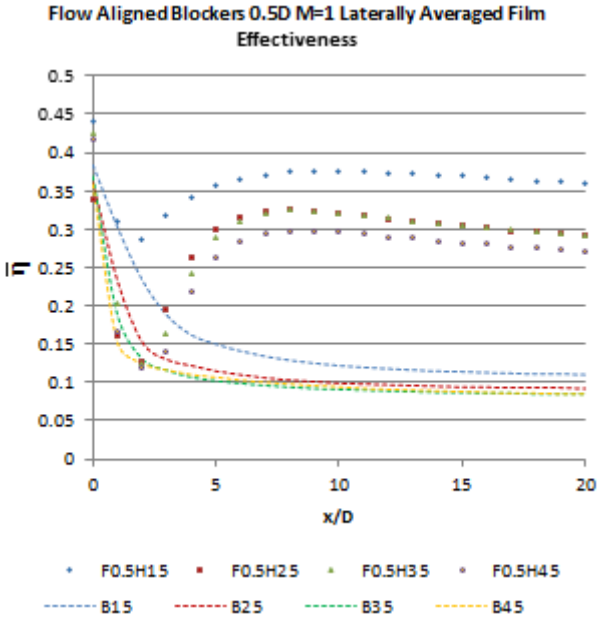

Fig. 91: Laterally Averaged Film Effectiveness for $F_{D0.5}H_{035}$ M=1

The laterally averaged film cooling effectiveness values mimic the centerline film cooling effectiveness values in both the low and high blowing ratio cases. Once again the 15° injection angle provides the best results due to the lower jet penetration in the higher blowing ratio case. The figures below show the typical surface temperature contours of this baseline configuration.

5.1.5 Surface Temperature Contours

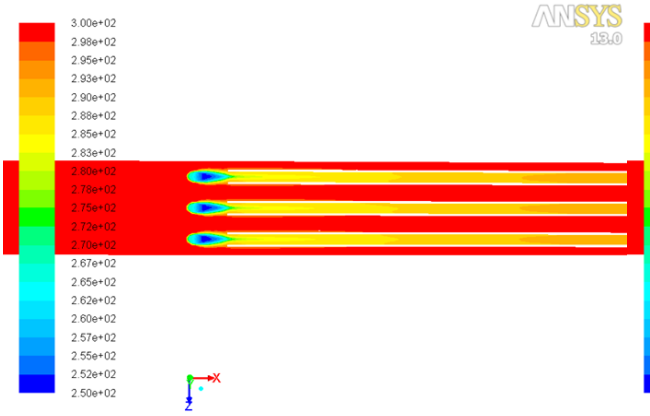

Fig. 92: Surface Temperature Contours for $F_{D0.5}H_{035}$ M=0.24

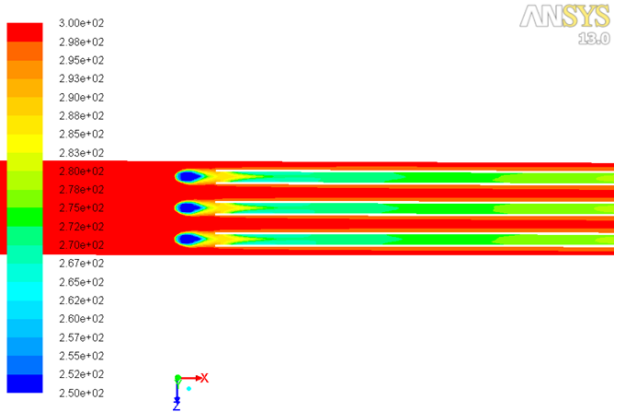

Fig. 93: Surface Temperature Contours for $F_{D0.5}H_{035}$ M=1

Figure 92 above illustrates both the pros and cons of flow aligned blocker. On one hand the coolant between the flow aligned blockers is protected from the hot mainstream flow, while on the other hand the flow outside of these blockers is unaffected by the coolant. Figure 93 shows drastic drop in surface temperature due to the low velocity area in front of the flow aligned blockers, as well as the from jet penetration in the high blowing ratio case. This is also visible but less apparent in the low blowing ratio case. The flow aligned blockers provide very good

protection of the coolant from the mainstream flow, which result in excellent low surface temperatures far downstream of the injection sites.

5.1.6 Kidney Vortices

The figures below illustrate the kidney vortices that occur due to the injection of the coolant into the mainstream flow.

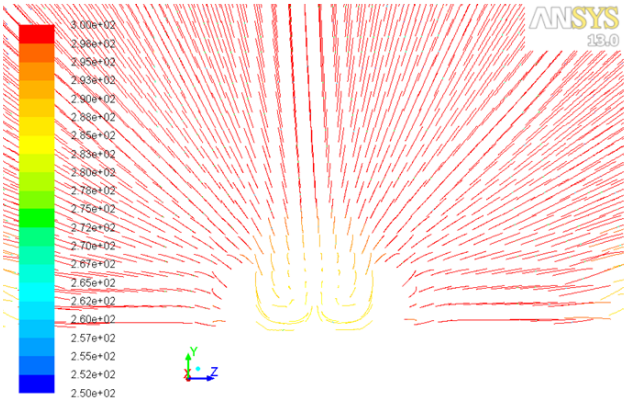

Fig. 94: Kidney Vortices for $F_{D0.5}H_{\theta 35}$ M=0.24

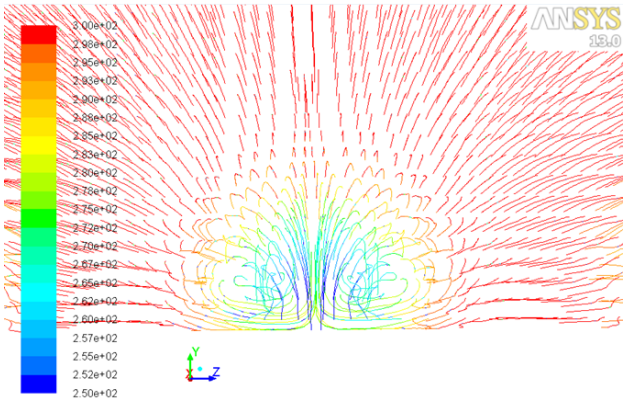

Fig. 95: Kidney Vortices for $F_{D0.5}H_{\theta 35}$ M=1

Figure 94 shows the kidney vortices trapped within the walls of the flow aligned blockers. The higher blowing ratio case injects more coolant into the flow, allowing the kidney vortices to recirculate much more cold air between the flow aligned blockers. The figures below show the temperature progression of this 0.5 D height flow aligned blocker configuration. It is clearly seen how the flow aligned blockers contain the kidney vortices by only allowing them to circulate coolant air.

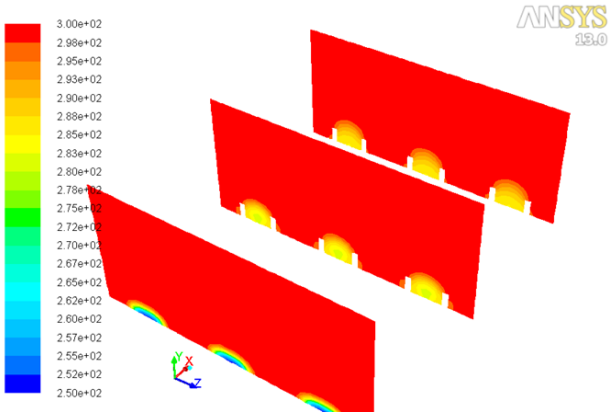

Fig. 96: Temperature Progression for $F_{D0.5}H_{\theta 35}$ M=0.24

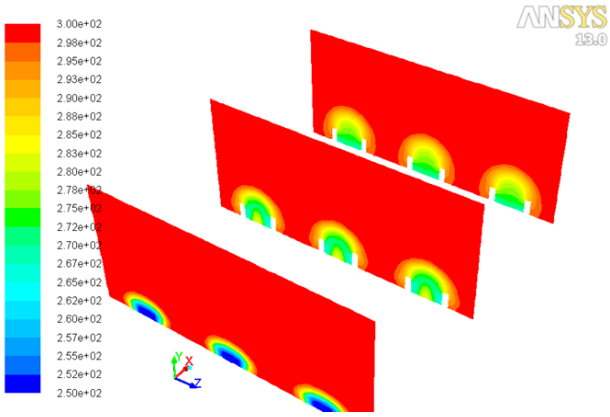

Fig. 97: Temperature Progression for $F_{D0.5}H_{\theta 35}$ M=1

5.2 Flow Aligned Blocker with 1D Height

5.2.1 Centerline Film Cooling Effectiveness

Please observe the centerline film cooling effectiveness results below for the ramp configurations.

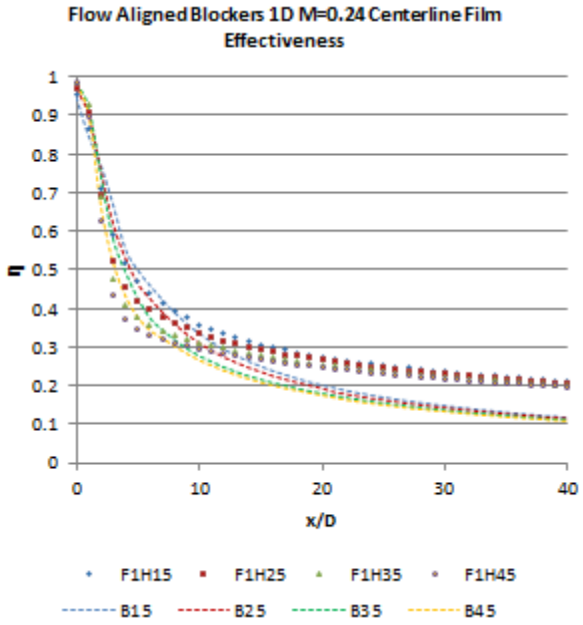

Fig. 98: Centerline Film Effectiveness for $F_{D1}H_{035}$ M=0.24

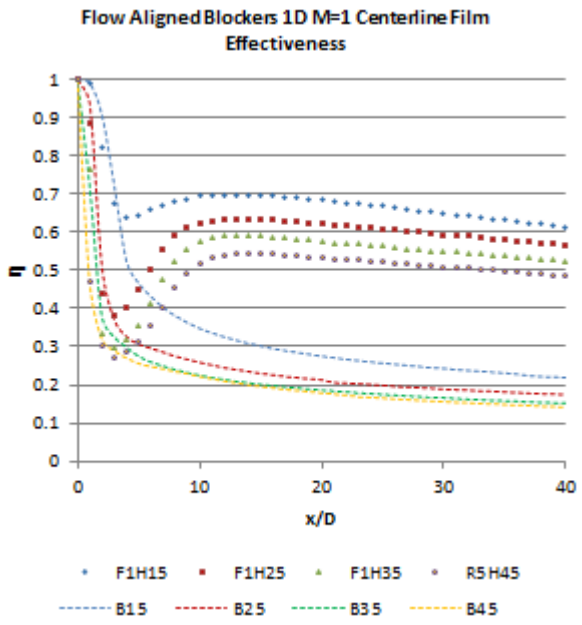

Fig. 99: Centerline Film Effectiveness for $F_{D1}H_{035}$ M=1

By looking at figure 98 one can see that the film cooling effectiveness values are very similar, but slightly higher, than those of the 0.5 D height flow aligned blocker configuration. The same trends are shown in both the low and higher blowing ratio cases.

5.2.2 Velocity Contours and Vectors

Please observe the velocity contours and vectors below.

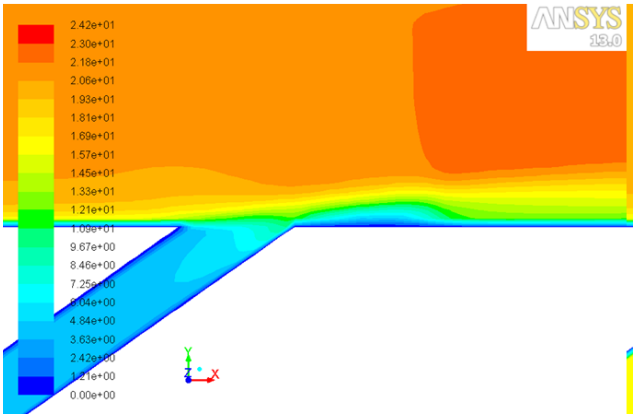

Fig. 100: Velocity Contours for $F_{D1}H_{035}$ M=0.24

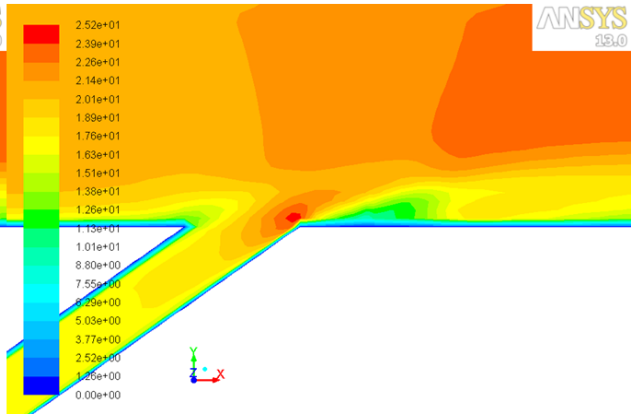

Fig. 101: Velocity Contours for $F_{D1}H_{035}$ M=1

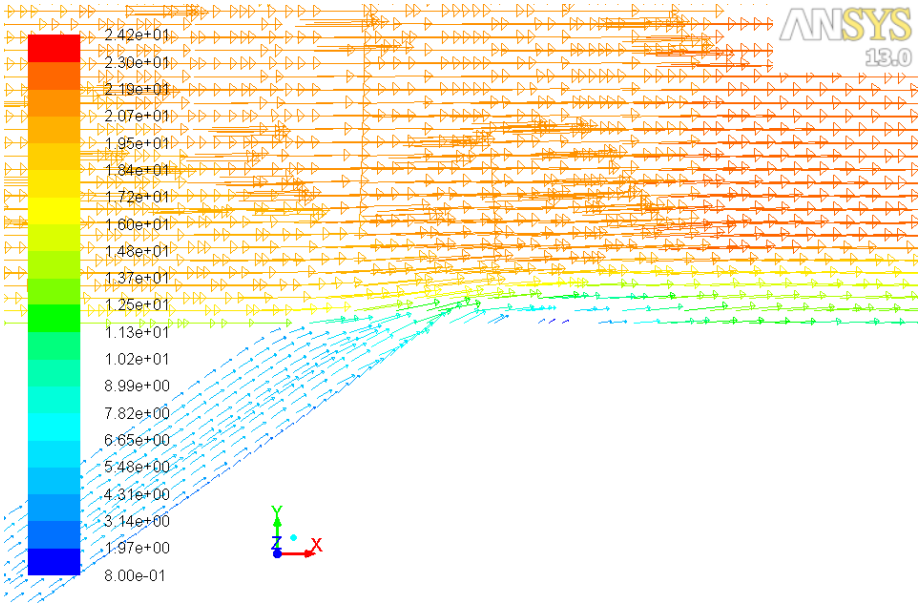

Fig. 102: Velocity Vectors for $F_{D1}H_{035}$ M=0.24

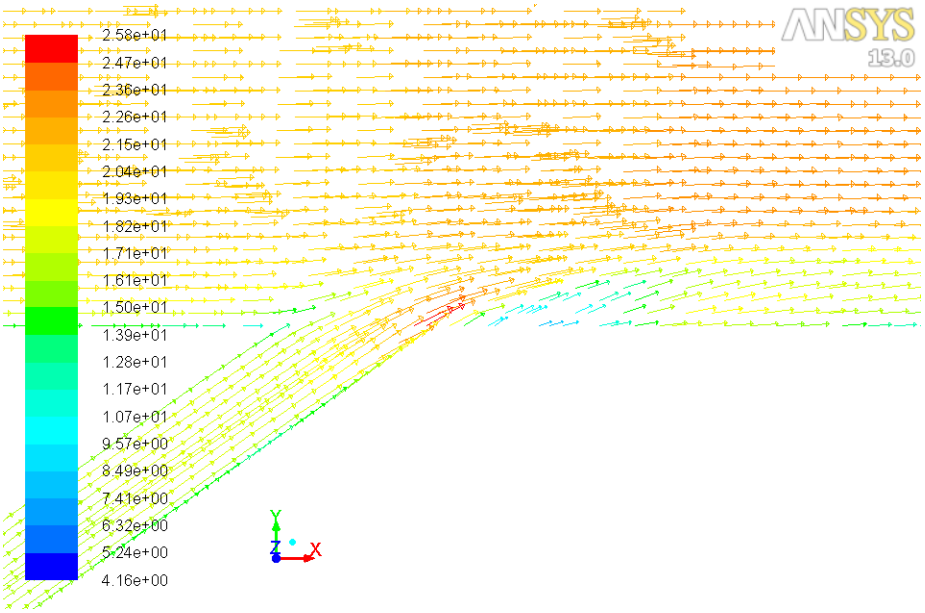

Fig. 103: Velocity Vectors for $F_{D1}H_{035}$ M=1

As seen with the 0.5 D height flow aligned blocker configuration, there are locations of low velocity, high pressure, flow in both the low and high blowing ratio cases. The velocity vectors and contours look very similar, with the main difference being that the low velocity flow areas are larger. The same phenomena of warmer air in front of the flow aligned blockers being pulled into the center occurs once again. Please refer to the 0.5 D height flow aligned blocker configuration for an explanation of the flow.

5.2.3 Temperature Contours

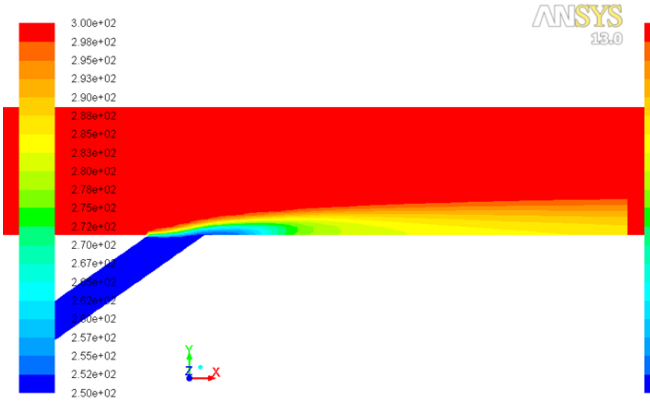

Fig. 104: Temperature Contours for $F_{D1}H_{035}$ M=0.24

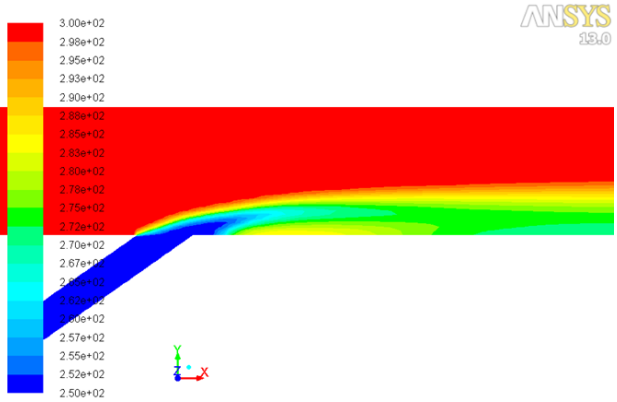

Fig. 105: Temperature Contours for $F_{D1}H_{035}$ M=1

The temperature contours depicted above are very similar to those of the 0.5 D height flow aligned blocker configuration.

5.2.4 Laterally Averaged Film Cooling Effectiveness

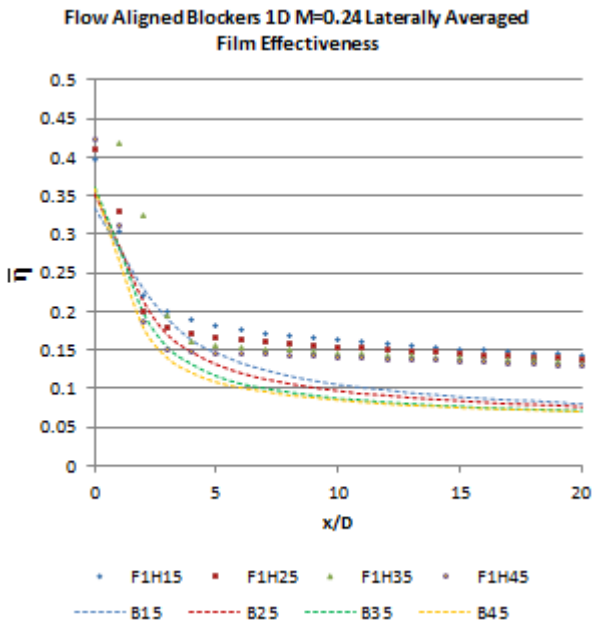

Fig. 106: Laterally Averaged Film Effectiveness for $F_{D1}H_{035}$ M=0.24

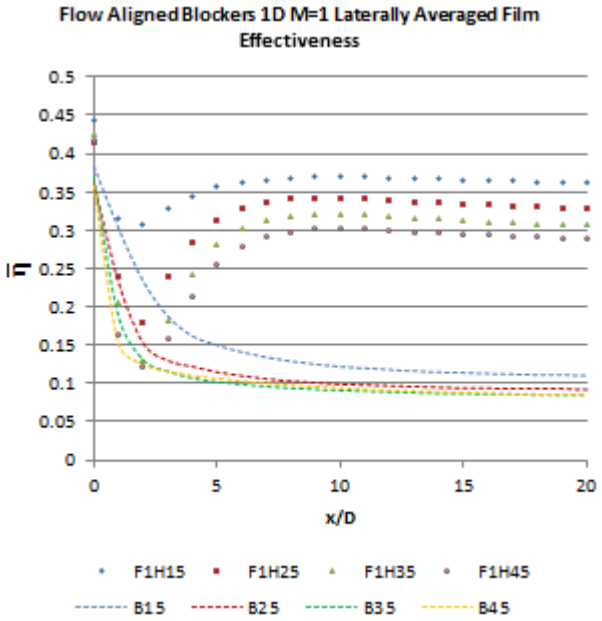

Fig. 107: Laterally Averaged Film Effectiveness for $F_{D1}H_{035}$ M=1

The laterally averaged film cooling effectiveness values mimic the centerline film cooling effectiveness values in both the low and high blowing ratio cases. Once again the 15° injection angle provides the best results, and increasing the injection angle lowers the laterally averaged film cooling effectiveness. The figures below show the typical surface temperature contours of this baseline configuration.

5.2.5 Surface Temperature Contours

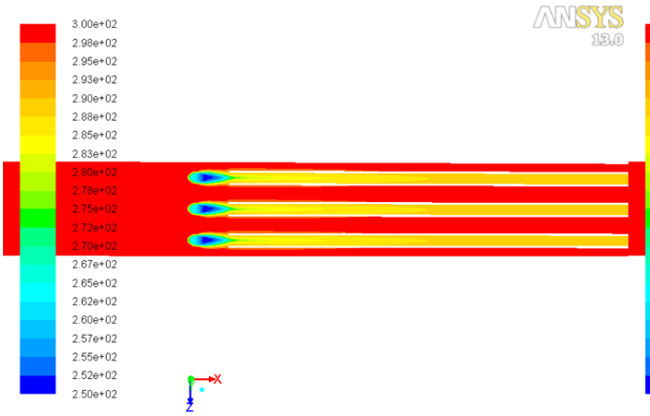

Fig. 108: Surface Temperature Contours for $F_{D1}H_{035}$ M=0.24

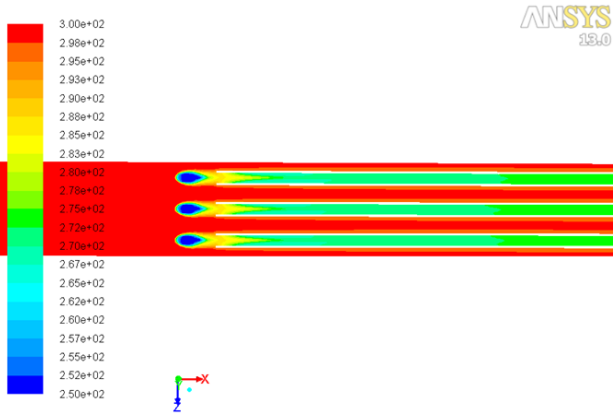

Fig. 109: Surface Temperature Contours for $F_{D1}H_{035}$ M=1

The temperature contours depicted above are very similar to those of the 0.5 D height flow aligned blocker configuration.

5.2.6 Kidney Vortices

The figures below illustrate the kidney vortices that occur due to the injection of the coolant into the mainstream flow.

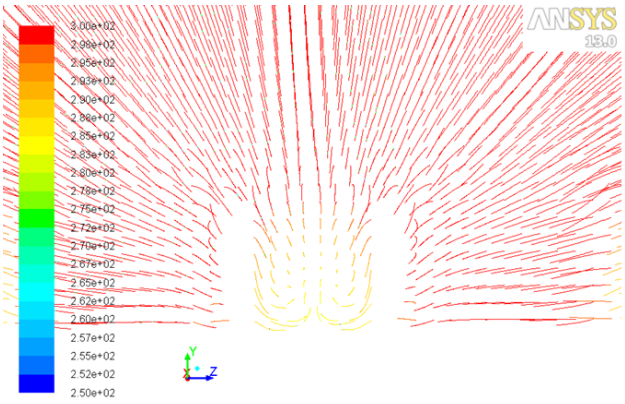

Fig. 110: Kidney Vortices for $F_{D1}H_{035}$ M=0.24

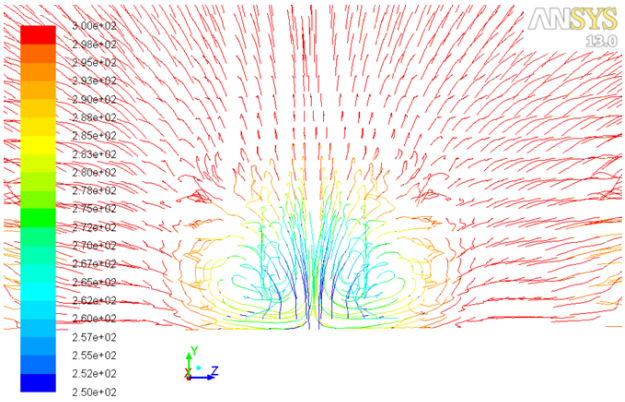

Fig. 111: Kidney Vortices for $F_{D1}H_{035}$ M=1

Figures 110 and 111 above show the kidney vortices trapped between the flow aligned blocker walls. When comparing these figures to those of the 0.5D height flow aligned blocker configuration, the results are very similar. However, the 1D height of this configuration is able to retain more of the coolant injected into the flow. The kidney shaved vortices are also more elongated and the top is more contained below the height of the flow aligned blockers. The temperature contours below show the greater containment of the kidney vortices downstream of the injected coolant.

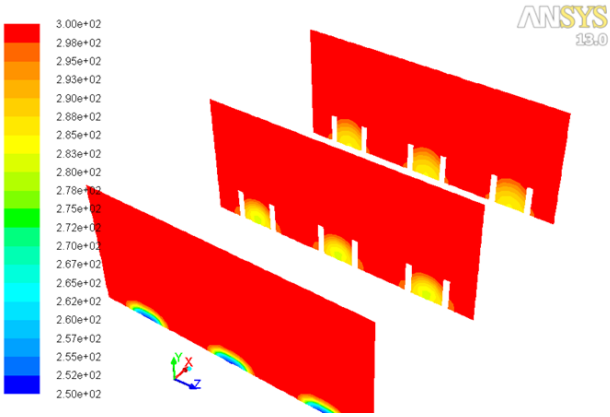

Fig. 112: Temperature Progression for $F_{D1}H_{035}$ M=0.24

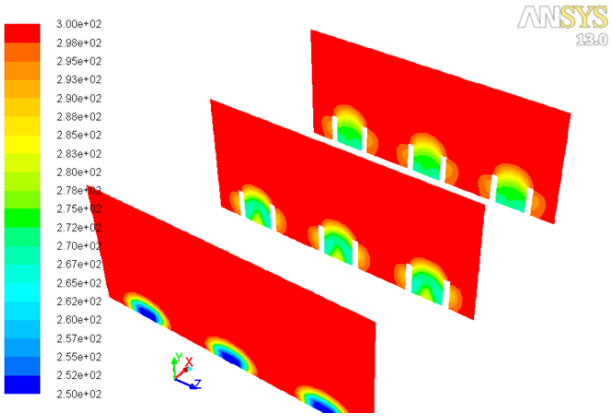

Fig. 113: Temperature Progression for $F_{D1}H_{035}$ M=1

5.3 Comparison of all Flow Aligned Blocker Configurations

The graph below shows the laterally averaged film cooling effectiveness performance gains and losses for the flow aligned blockers surface enhancements for x/D < 20.

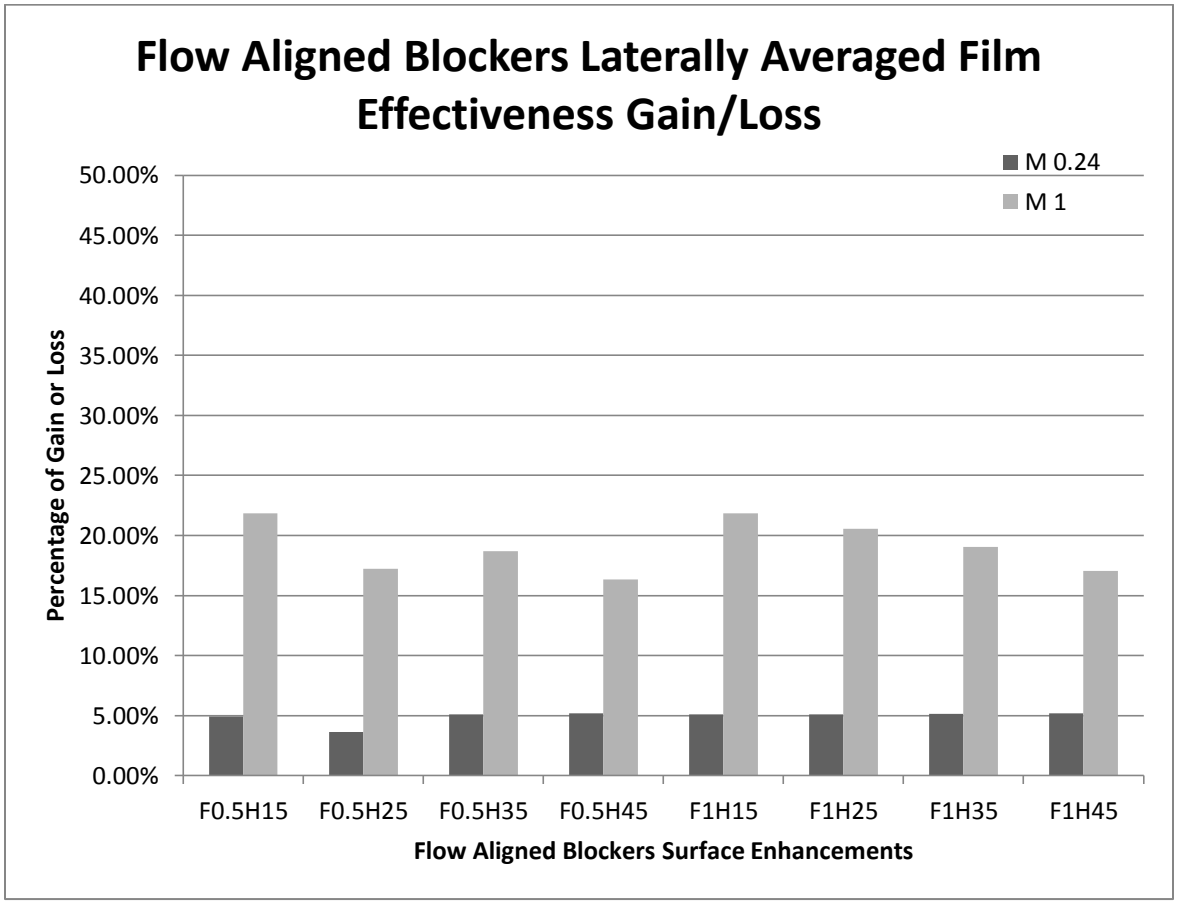

Fig. 114: Laterally Averaged Film Effectiveness Performance Gains or Losses for Flow Aligned Blockers

Looking at the results from the low blowing ratio for both the 0.5 D and 1 D height configurations, there appears to be a flat performance gain of 5%. Therefore the low blowing ratio case is unaffected by flow aligned blocker heights above 0.5 D. The high blowing ratio cases show major film cooling performance gains in both height configurations, ranging from 23% with the 15° injection angle lowering to 15% with the 45° injection angle. Although both height configurations performed very similarly, on average the 1 D height performed slightly better by approximately 1%.

Three conclusions can be drawn from this data. First one can see that the flow aligned blocker surface enhancement increases the film cooling performance in every instance. Secondly, higher blowing ratios produce significantly better results than both the baseline and lower blowing ratio configurations. Thirdly lower injection angles produce the best results at high blowing ratios.

Chapter 6: Comparative Study of Trench Surface Enhancements

6.1 Trench with 0.5D Depth

6.1.1 Centerline Film Cooling Effectiveness

Figures 115 and 116 show the centerline film cooling effectiveness results below for the ramp configurations.

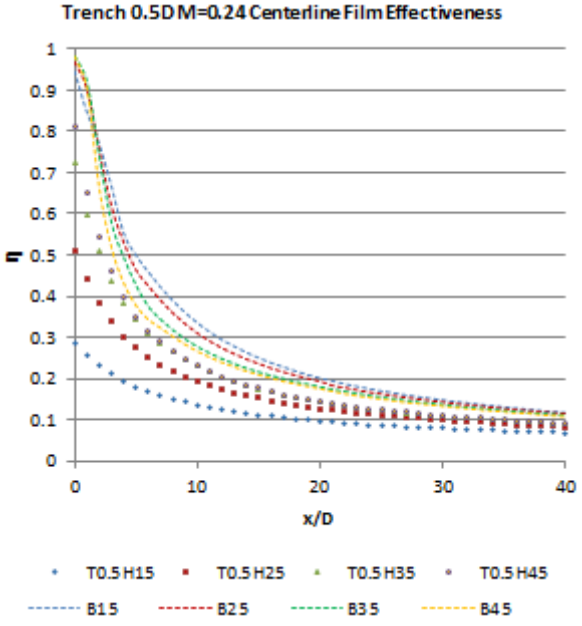

Fig. 115: Centerline Film Effectiveness for $T_{D0.5}H_{035}$ M=0.24

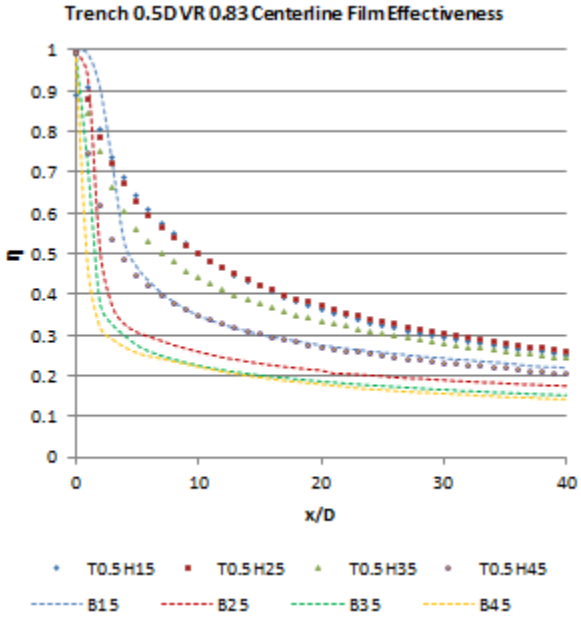

Fig. 116: Centerline Film Effectiveness for $T_{D0.5}H_{035}$ M=1

Figure 115 indicates that the trench decreases the centerline film cooling effectiveness for the low blowing ratio case. This is expected since the trench allows the coolant to expand in the lateral direction, as well as lose momentum and cannot combat the mainstream flow. It is supported by the fact that the higher injection angles provide better results, since they have more jet penetration.

Conversely figure 116 shows the higher blowing ratio produces an increase in the centerline film cooling effectiveness over the baseline configuration. Once again the higher injection angles produce the best results. Unlike with the baseline configuration, the injected coolant first hits the front wall of the trench, and spills over the edge. It is for this reason why there isn't as steep a drop in film cooling effectiveness since it does not face the problem of too much jet penetration into the mainstream. To better understand the characteristics of these graphs one must examine the velocity contours, velocity vectors, and temperature contours, in the following figures.

6.1.2 Velocity Contours and Vectors

Please observe the velocity contours and vectors below.

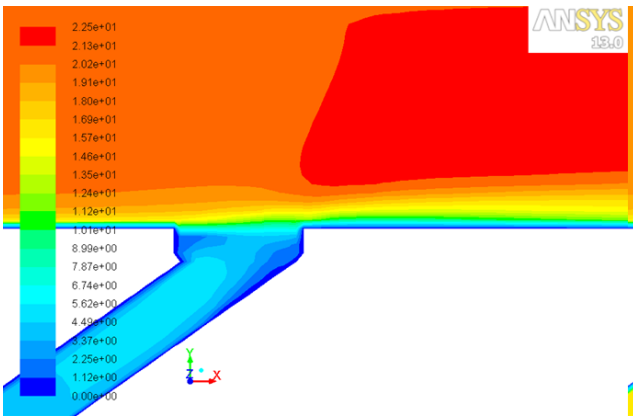

Fig. 117: Velocity Contours for $T_{D0.5}H_{035}$ M=0.24

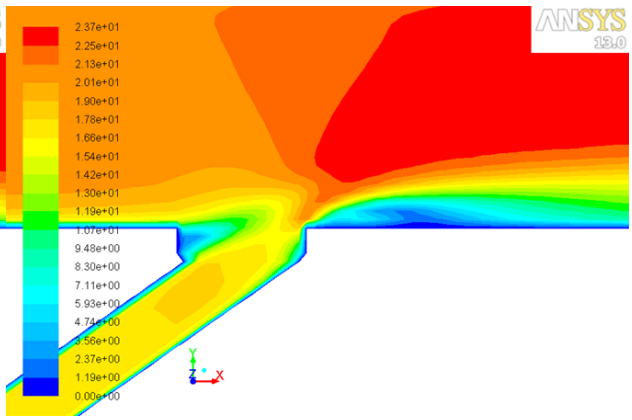

Fig. 118: Velocity Contours for $T_{D0.5}H_{035}$ M=1

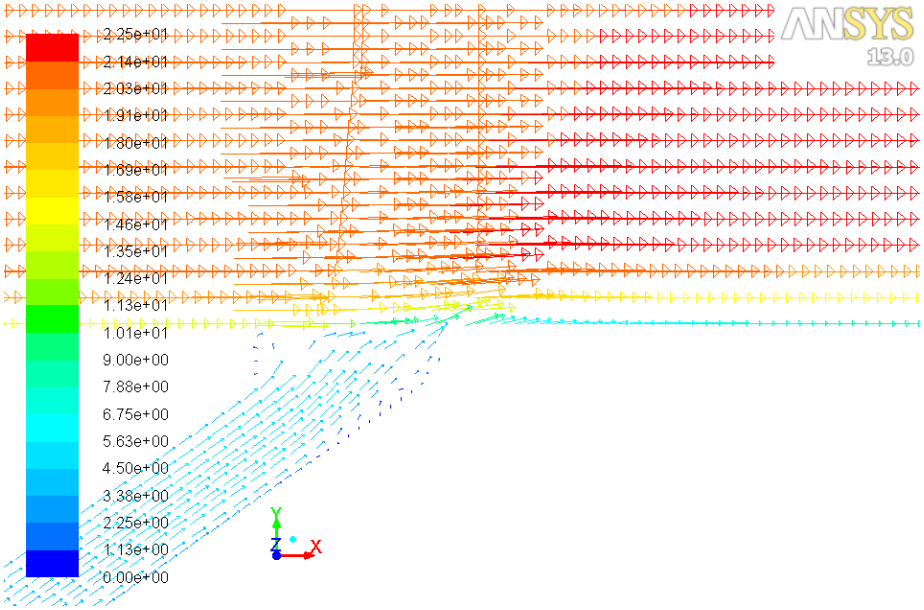

Fig. 119: Velocity Vectors for $T_{D0.5}H_{035}$ M=0.24

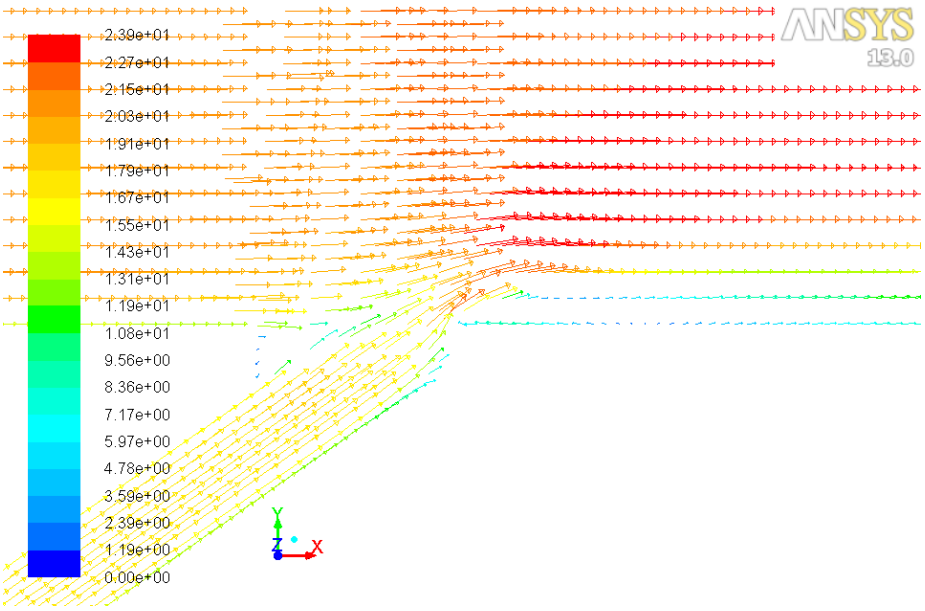

Fig. 120: Velocity Vectors for $T_{D0.5}H_{035}$ M=1

By examining figure 119, it is seen that in the low blowing ratio case the coolant does not have enough momentum to combat the high velocity of the mainstream flow, resulting in poor film cooling effectiveness. figure 120 shows the higher momentum coolant jet able to penetrate the mainstream slightly, and slide over the front edge of the trench. There is a small area of recirculation at the back of the trench, and also another minor region immediately in front of the trench.

6.1.3 Temperature Contours

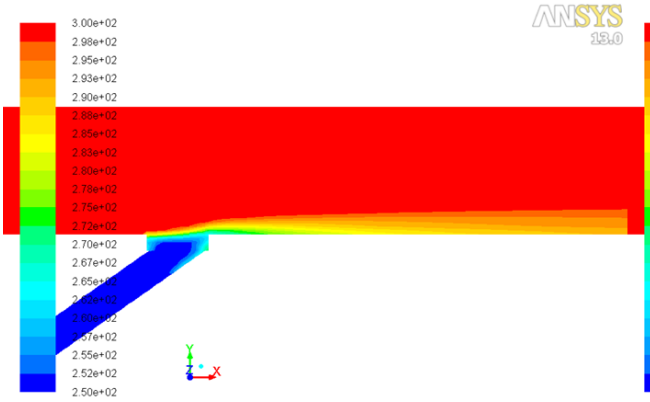

Fig. 121: Temperature Contours for $T_{D0.5}H_{\theta 35}$ M=0.24

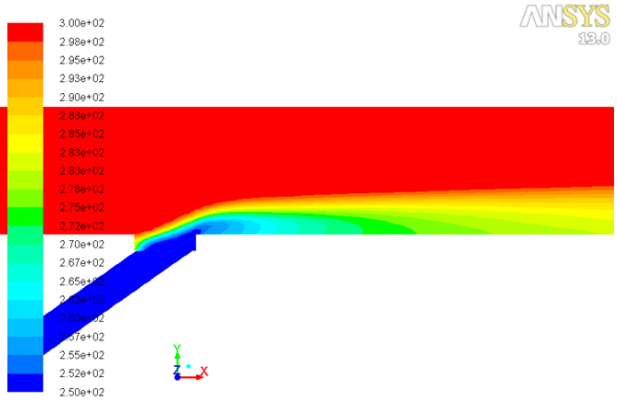

Fig. 122: Temperature Contours for $T_{D0.5}H_{\theta 35}$ M=1

By examining figure 121 above, it is seen that in the low blowing ratio case the coolant does not have enough momentum to combat the high velocity of the mainstream flow, resulting in poor film cooling effectiveness. Figure 122 shows the higher momentum coolant jet able to penetrate the mainstream slightly, and slide over the front edge of the trench. There is a small area of recirculation at the back of the trench, and also another minor region immediately in front of the trench.

6.1.4 Laterally Averaged Film Cooling Effectiveness

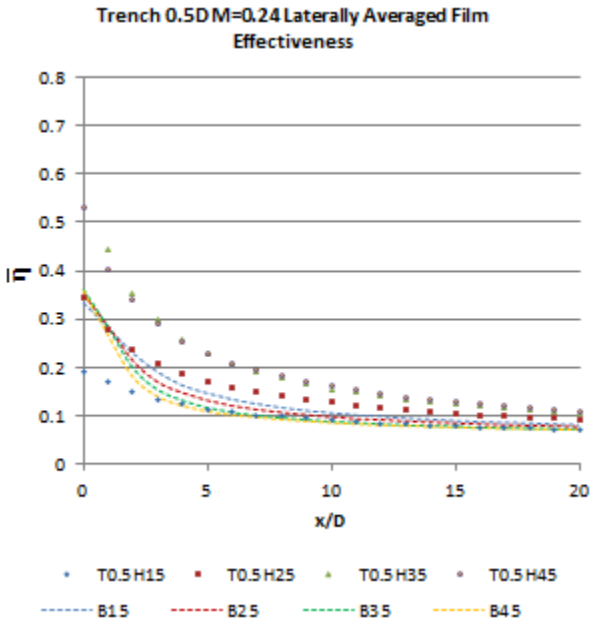

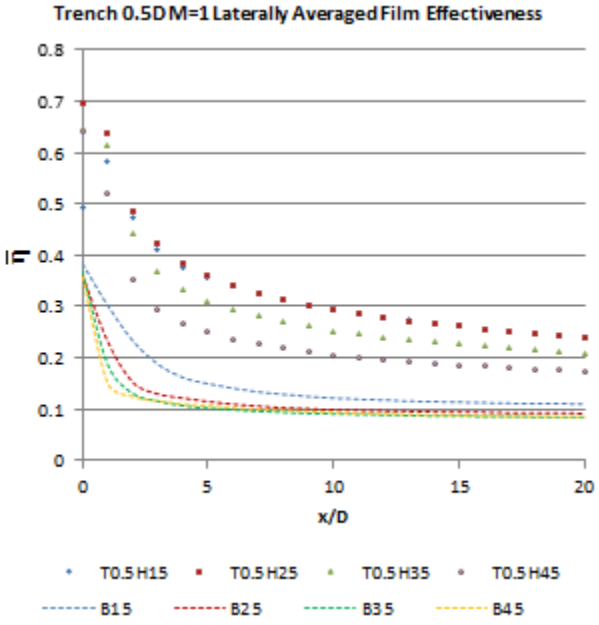

Fig. 123: Laterally Averaged Film Effectiveness for $T_{D0.5}H_{035}$ M=0.24 Fig. 124: Laterally Averaged Film Effectiveness for $T_{D0.5}H_{035}$ M=1

The laterally averaged film cooling effectiveness values mimic the centerline film cooling effectiveness values in both the low and high blowing ratio cases. The 15° injection angle provides the worst results in the low blowing ratio case as expected due to its lack of momentum, and increasing the injection angle increases the laterally averaged film cooling effectiveness. The higher blowing ratio case performs significantly better than the baseline configuration at all injection angles. The figures below show the surface temperature contours of this 0.5 D depth trench configuration.

6.1.5 Surface Temperature Contours

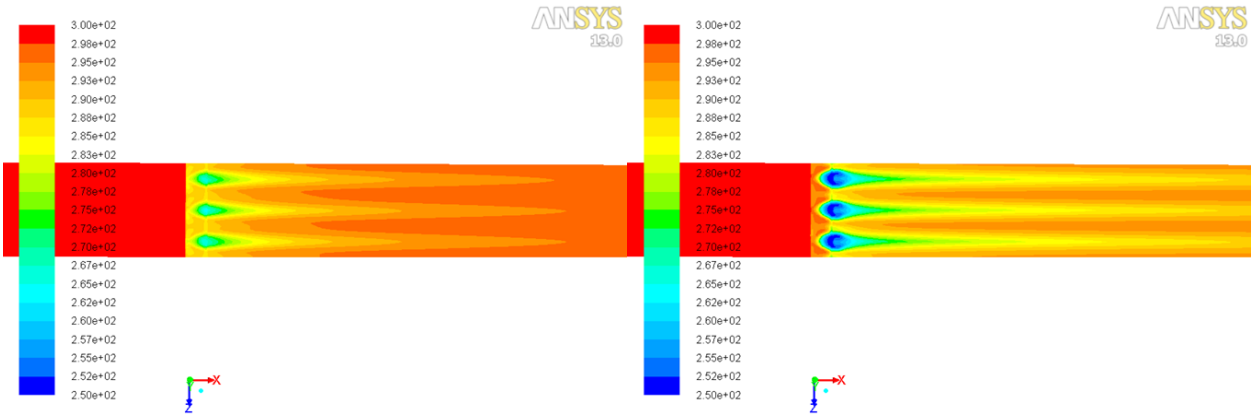

Fig. 125: Surface Temperature Contours for $T_{D0.5}H_{035}$ M=0.24 Fig. 126: Surface Temperature Contours for $T_{D0.5}H_{035}$ M=1

Figure 125 above illustrates the lateral spreading of the coolant, as well as the good cooling film attachment to the surface. It is important to note that these temperature contours may be misleading, since the coolant hole locations are not where they appear in the figures. The actual location of the

coolant holes fall between the two lighter bands, which signify the trench walls, slightly behind the areas of lowest temperature. Figure 126 shows the how the greater momentum allows the film to cool the surface further downstream of the injection site. It is apparent that although not as strong, kidney vortices still cause decay in the film cooling effectiveness downstream of the injection site.

6.1.6 Kidney Vortices

The figures below illustrate the kidney vortices that occur due to the injection of the coolant into the mainstream flow.

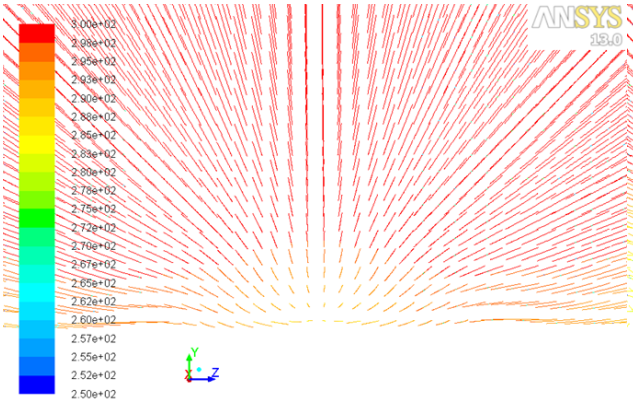

Fig. 127: Kidney Vortices for $T_{D0.5}H_{\theta 35}$ M=0.24

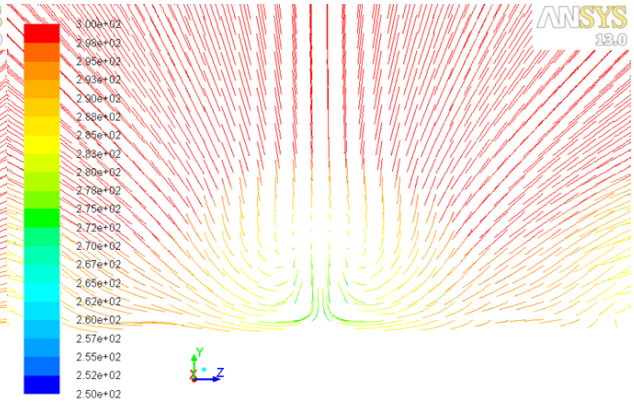

Fig. 128: Kidney Vortices for $T_{D0.5}H_{\theta 35}$ M=1

Figure 127 shows the lack of kidney vortex formation due to the low momentum of the injected coolant into the mainstream, as well as the lateral spreading cause by the trench. In the higher blowing ratio case the coolant has more momentum and creates kidney vortices that are not as strong as in previous configurations. Due to the lateral spreading these vortices pull surrounding air that is slightly cooler than the mainstream temperature. The temperature progression downstream of the injection site is shown the figures below.

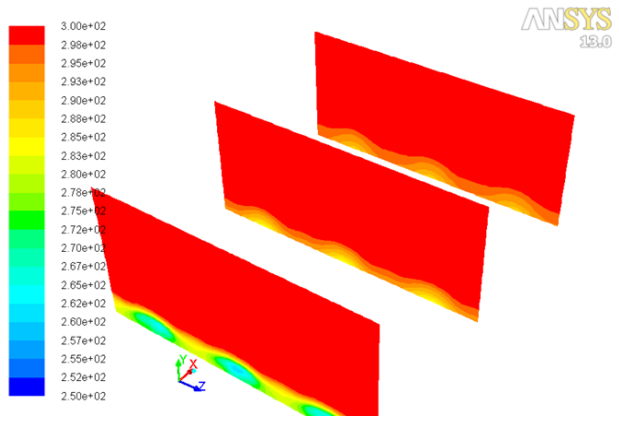

Fig. 129: Temperature Progression for $T_{D0.5}H_{\theta 35}$ M=0.24

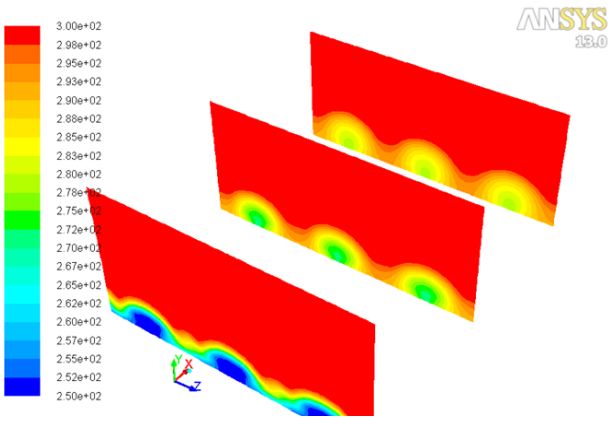

Fig. 130: Temperature Progression for $T_{D0.5}H_{\theta 35}$ M=1

6.2 Trench with 1D Depth

6.2.1 Centerline Film Cooling Effectiveness

Please observe the centerline Film Cooling Effectiveness results below for the ramp configurations.

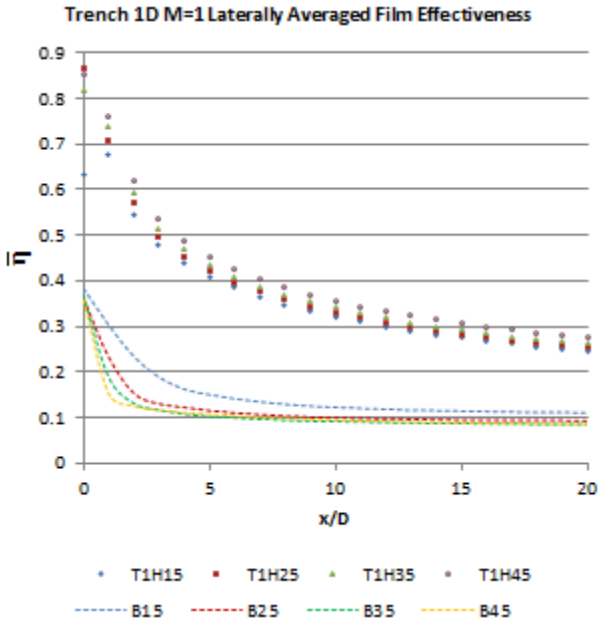

Fig. 131: Centerline Film Effectiveness for $T_{D1}H_{035}$ M=0.24

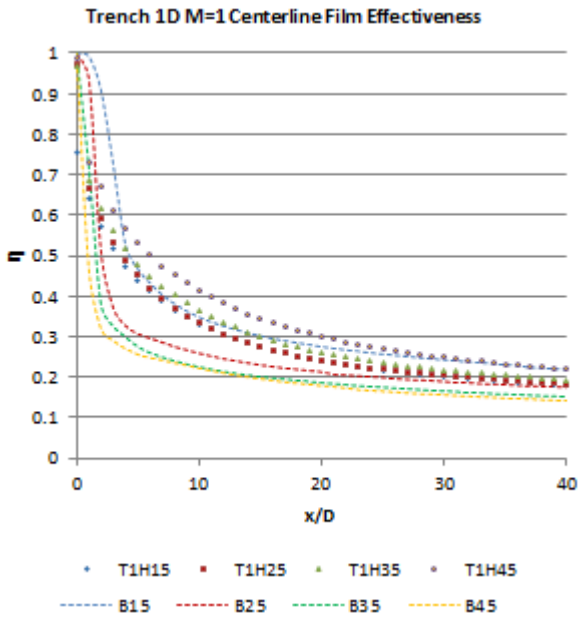

Fig. 132: Centerline Film Effectiveness for $T_{D1}H_{035}$ M=1

Figure 131 shows the trench decreases the centerline film cooling effectiveness for the low blowing ratio case. As seen in the previous configuration, this is expected since the deeper trench allows the coolant to expand in the lateral direction and the larger area decreases the momentum of the fluid. Increasing the injection angles increases performance slightly, but it remains far below the performance of the baseline configuration.

Figure 132 shows that all of the injection angles in this configuration perform better than their baseline counterparts except for the injection angle of 15°. Although the initial centerline film cooling effectiveness starts at a lower magnitude when compared with the baseline configuration, it does not show a dip as seen from jet penetration. As with the lower blowing ratio cases, increasing the injection angle increases the centerline film cooling effectiveness.

6.2.2 Velocity Contours and Vectors

Please observe the velocity contours and vectors below.

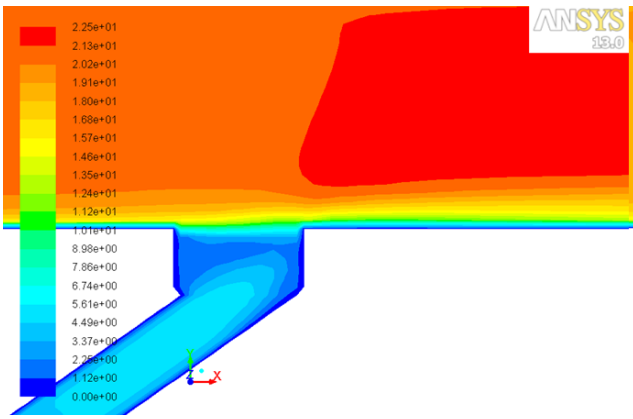

Fig. 133: Velocity Contours for $T_{D1}H_{035}$ M=0.24

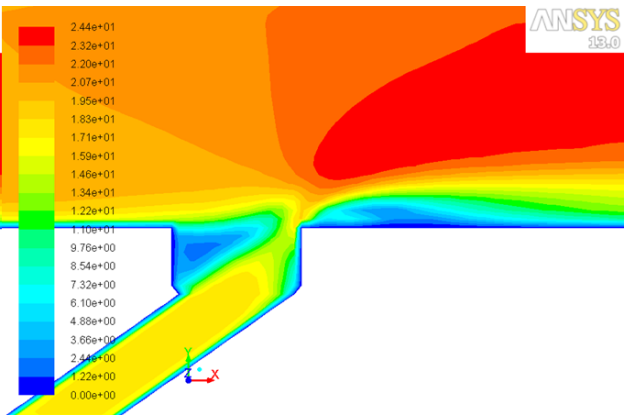

Fig. 134: Velocity Contours for $T_{D1}H_{035}$ M=1

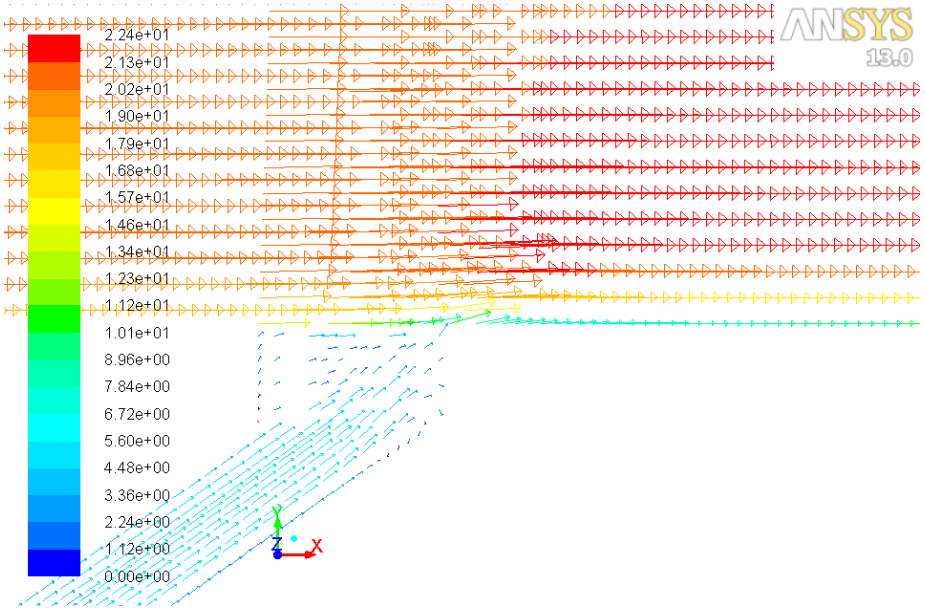

Fig. 135: Velocity Vectors for $T_{D1}H_{035}$ M=0.24

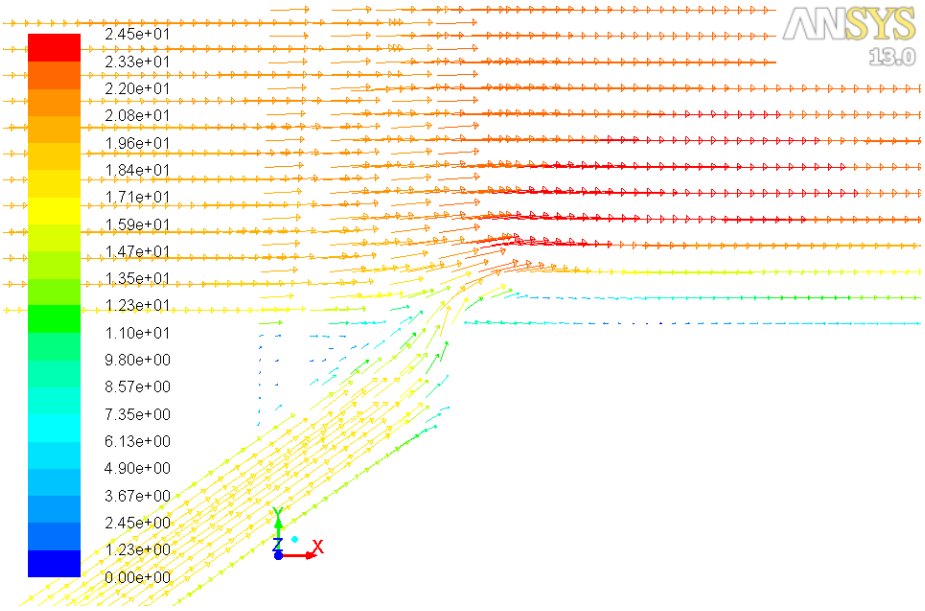

Fig. 136: Velocity Vectors for $T_{D1}H_{\theta 35}$ M=1

By examining figure 135, it is seen that in the low blowing ratio case the coolant does not have enough momentum to combat the high velocity of the mainstream flow, resulting in poor film cooling effectiveness. The deeper trench creates an area of very low velocity at the injection site. Figure 136 shows the higher momentum coolant jet that has enough momentum to overcome the mainstream flow and provide protection to the surface. The deeper trench in this configuration creates two larger areas of recirculation than as previously seen in the shallower trench configuration. By looking at these figures it is unclear to determine the exact effects this would have on the film cooling performance.

6.2.3 Temperature Contours

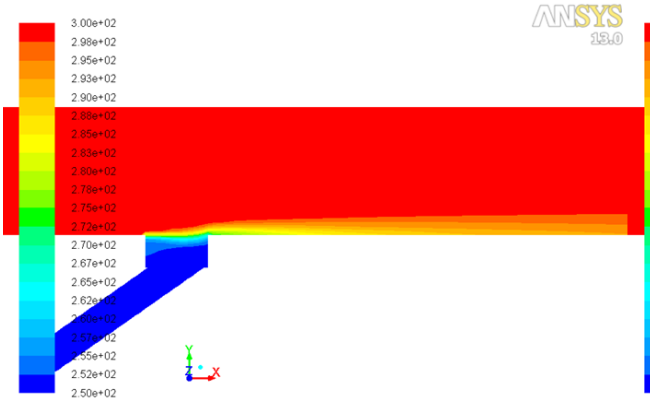

Fig. 137: Temperature Contours for $T_{D1}H_{\theta 35}$ M=0.24

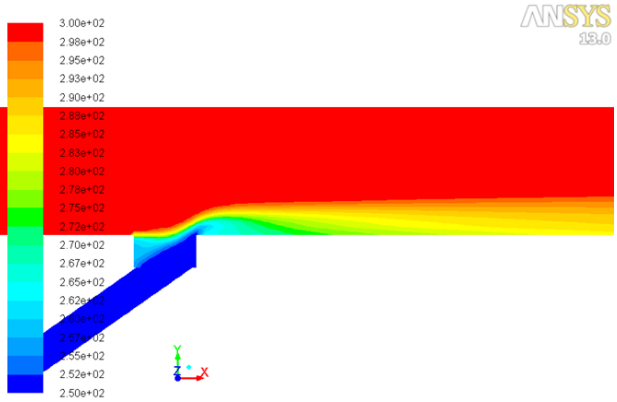

Fig. 138: Temperature Contours for $T_{D1}H_{\theta 35}$ M=1

By examining figure 137, it is seen that in the low blowing ratio case the coolant does not have enough momentum to combat the high velocity of the mainstream flow, resulting in poor surface temperatures. Figure 138 shows that even with the deeper trench the higher blowing ratio allow the coolant to provide better surface temperatures than the baseline configuration. The areas of recirculation seen on the previous page do not seem to negatively affect the film cooling performance.

6.2.4 Laterally Averaged Film Cooling Effectiveness

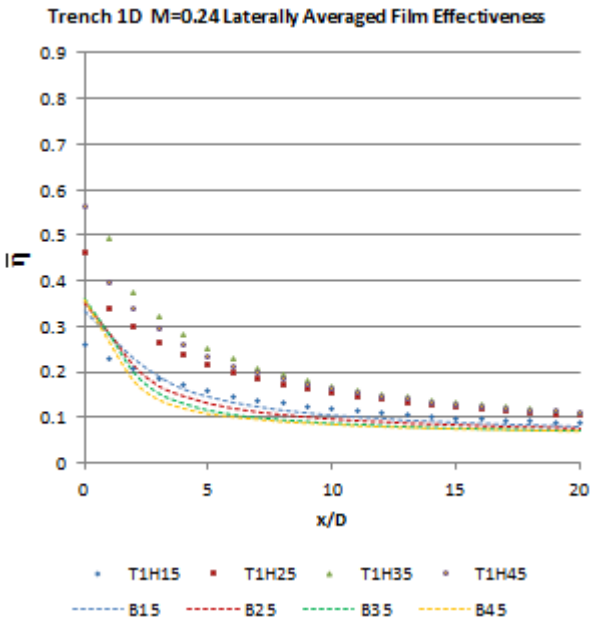

Fig. 139: Laterally Averaged Film Effectiveness for $T_{D1}H_{\theta 35}$ M=0.24

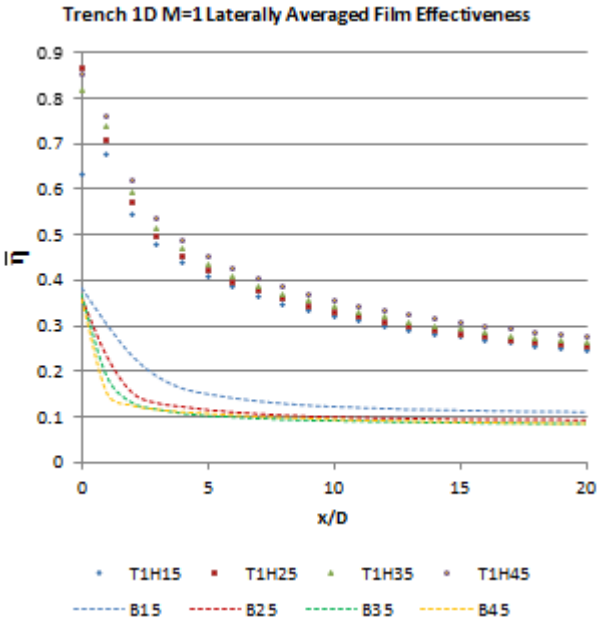

Fig. 140: Laterally Averaged Film Effectiveness for $T_{D1}H_{\theta 35}$ M=1

The laterally averaged film cooling effectiveness values are better than the baseline configuration and peak with the 35° injection angle for the low blowing ratio case. The higher blowing ratio tremendously increases these values, and minor gains are made through increasing the injection

angle. The figures below show the surface temperature contours, illustrating the increased performance due to the coolant's lateral spreading.

6.2.5 Surface Temperature Contours

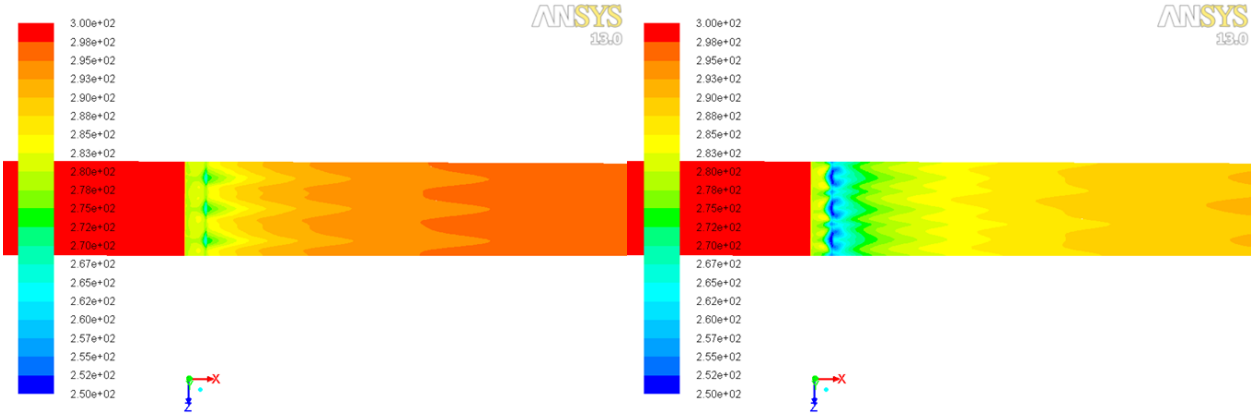

Fig. 141: Surface Temperature Contours for $T_{D1}H_{035}$ M=0.24

Fig. 142: Surface Temperature Contours for $T_{D1}H_{035}$ M=1

Figure 141 above illustrates the lateral spreading of the coolant which provides better surface protection when compared with the baseline configuration. Figure 142 shows how the increased blowing ratio takes full advantage of lateral spreading within the trench to create a better, more evenly cooled surface in the span wise direction of the flow. This lateral spreading creates weak kidney vortices which are displayed in the following figures.

6.2.6 Kidney Vortices

The figures below illustrate the kidney vortices that occur due to the injection of the coolant into the mainstream flow.

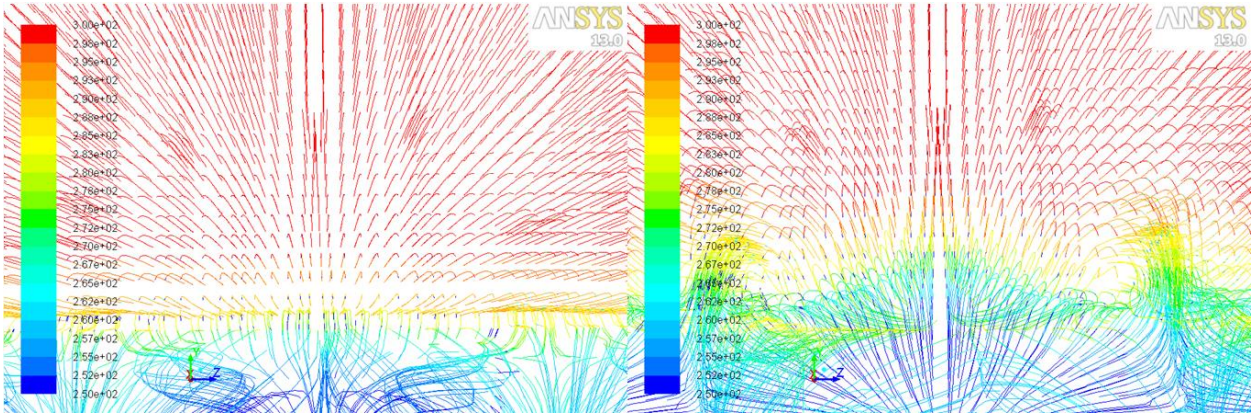

Fig. 143: Kidney Vortices for $T_{D1}H_{035}$ M=0.24

Fig. 144: Kidney Vortices for $T_{D1}H_{035}$ M=1

Figure 143 shows the lack of kidney vortex formation due to the low momentum of the injected coolant into the mainstream, as well as the lateral spreading cause by the trench. In the higher blowing ratio case the coolant has more momentum and spreads out further laterally. The vortices that are created when the coolant jets interact with the main flow pull warmer air down

towards the surface. Since the lateral spreading goes beyond the size of the vortices created, distinct peaks and valleys are observed in the temperature contour figures below.

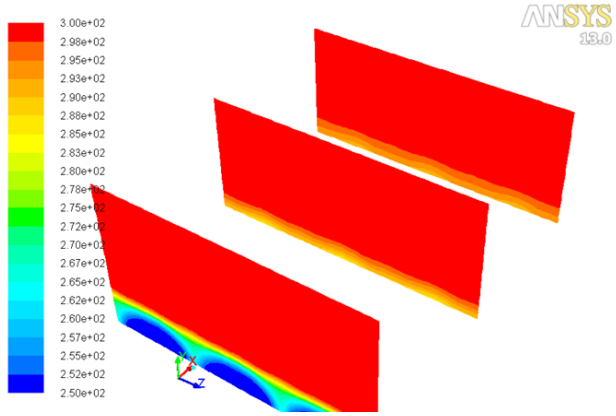

Fig. 145: Temperature Progression for $T_{D1}H_{035}$ M=0.24

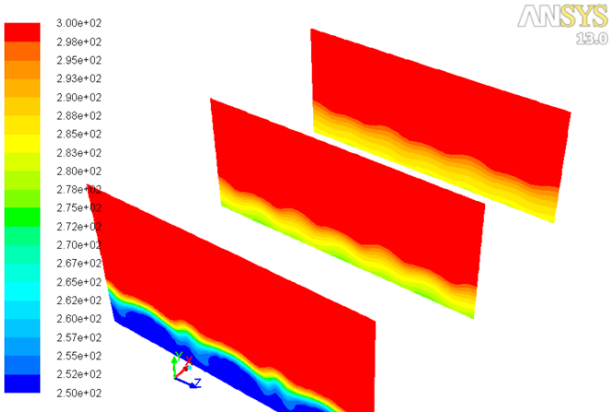

Fig. 146: Temperature Progression for $T_{D1}H_{035}$ M=1

Comparing the figures above to those of the shallower trench configuration, one can see that the increased laterally averaged film cooling effectiveness comes from the even spread of coolant in the lateral direction, as opposed to localized streams of protection along the length surface.

6.3 Comparison of all Trench Configurations

The graph below shows the laterally averaged film cooling effectiveness performance gains and losses for the flow aligned blockers surface enhancements while x/D < 20.

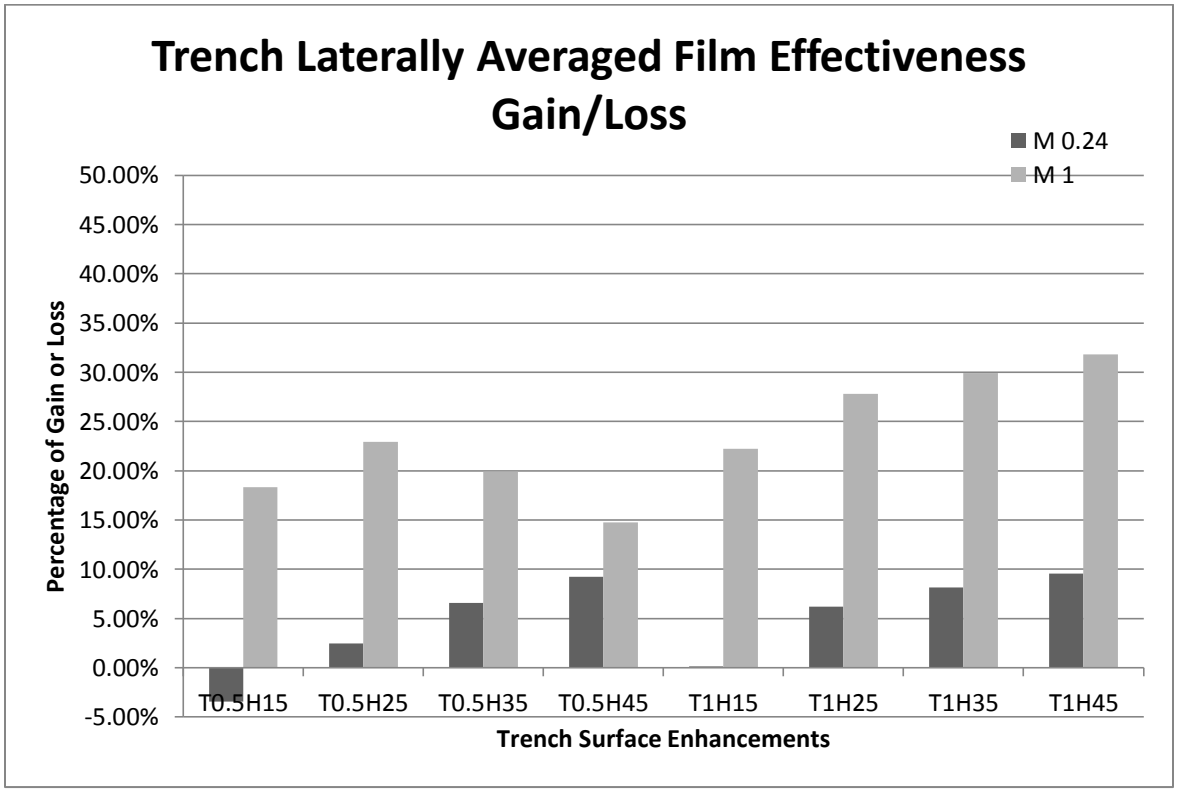

Fig. 147: Laterally Averaged Film Effectiveness Performance Gains or Losses for Flow Aligned Blockers

Observing the graph above, for the 0.5 D depth trench performance gains a realized when the injection angle was above 15°. At an injection angle of 25° a film cooling performance gain of 2.5% was achieved which rose to 9% at an injection angle of 45°. The higher blowing ratio case shows an increase in performance from 15° to 25° injection angle which then drops to the lowest performance gain at 45°. For this project the peak performance gain at the 25° injection angle was found to be 23%, however the data suggest that the true peak in performance may lie slightly above or below this injection angle. The 1 D trench depth configuration shows slightly better performance gains over shallower trench depth configuration. However, the higher blowing ratio case shows much higher and steady increase in film cooling performance with increasing injection angle. At the 15° injection angle the performance gain was found to be 22%, and this value rose to 32% at the 45° injection angle.

Numerous conclusions can be drawn from the data above. First, the trench surface enhancement prefers higher injection angles when using a low blowing ratio. Secondly, when using a high blowing ratio with the 0.5 D trench depth there is a special injection angle which provides the best results. This is contrary to many other configurations in which steady increase or decrease in

film cooling performance is observed with a steady change in injection angle. The 1 D depth trench configuration at the high velocity ratio shows diminishing performance gains with increasing injection angle, which indicates a peak shortly beyond 45°.

Chapter 7: Conclusion & Future Work

7.1 Summary

Numerical analysis has been carried out to find the film cooling performance of various surface enhancements in comparison to the standard coolant injection configuration. A comparative study of the effects of the blowing ratio has also been carried out for each surface enhancement configuration. In addition to calculating and discussing the centerline and laterally averaged film cooling effectiveness results, detailed analysis of the flow and temperature field of each configuration is also presented. In the end the laterally averaged film cooling effectiveness results were used to determine the best performing configurations.

7.2 Validation

In Chapter 2 the solution convergence as well as a grid convergence study was carried out in order to determine the best CFD setup. Numerous turbulence models were also considered, and the realizable k-ε model was selected. The centerline and laterally averaged film cooling values were then compared to an experimental study by Sinha et al [16]. It was concluded that a grid of 1 million elements was needed, and the CFD analysis was carried out using ANSYS Fluent 14 using the resources from the High Performance Computing Virtual Laboratory (HPCVL) in Queens University, Ontario, Canada.

7.3 Comparative Study of Surface Enhancements

In general the flow and temperature field findings from the results of this project matched those found by much literature reviewed. The ramp surface enhancements showed areas of recirculation behind the ramp which lowered the coolant jet's momentum. It also showed lateral spreading, as well as better jet attachment to the surface. The flow aligned blockers clearly illustrated the effects of separation between the coolant jet kidney vortices and the mainstream flow. The trench configuration showed both the hugging of the coolant to surface, allowing for better performance from higher blowing ratios, and the decreased performance far downstream. The kidney vortex formation and lack thereof due to lateral spreading as also well represented in the results.

Reviewing the laterally averaged film cooling effectiveness results trenches provide the best performance with a gain of 32% over the baseline at the high blowing ratio of 1. Flow aligned blockers and the ramp configurations both provided similar peak improvements of approximately 20% at the same blowing ratio. Although it would appear that trenches provide the best film cooling effectiveness is important to remember the model of the geometry used in this project, as well as the flow regimes due to the surface enhancements.

Flow aligned blockers provide excellent cooling performance far downstream, but showed a distinct drop in film cooling performance at the beginning of the flow aligned blockers. In theory this problem could easily be remedied by moving the flow aligned blockers to the injection location. Also, the flow aligned blocker surface enhancement lacks the lateral spreading as seen

with the ramp and trench configurations. The film cooling effectiveness values were averaged not only in the inter-hole region, but also in the uncooled region between adjacent flow aligned blockers. Therefore if the injection holes are spaced closely together, undoubtedly the flow aligned blockers would provide the best film cooling performance out of all of the configurations tested in this project.

7.4 Future Works

The aim of this project was to show a detailed account of the flow and temperature fields due to the addition of surface enhancements. As such, not all aspects affecting film cooling could be studied in its entirety due to the time constraints of this project.

As stated in the introduction the plenum and length to diameter ratio's effects on the flows were reduced to ensure a uniform coolant jet velocity profile which would highlight the changes in its flow only due to the surface enhancements. Therefore, it would be important to analyze different plenum and length to diameter configurations and see their effects on the surface enhancements' performance.

A wide variety of geometries was used in the various surface enhancement configurations to ensure a broad spectrum of results in order to best capture what each configuration best has to offer. By using the results of this experiment as benchmarks, optimization of these configurations can be carried out to find optimal heights, depths, blowing ratios, and injection angles of each respective configuration.

References

[1] J. Han, S. Dutta and S. V. Ekkad, Gas Turbine Heat Transfer and Cooling Technology, New York: Taylor & Francis, 2000.

[2] S. Volker, T. Samel, C. Heneka, H. Ladisch, A. Shulz and H.-J. Bauer, "Experimental and Numerical Investigation of Flow Field and Downstream Surface Temperatures of Cylindrical and Diffuser Shaped Film Cooling Holes," *Journal of Turbomachinery*, pp. 1-9, 2013.

[3] S. Baldauf, A. Schulz and S. Wittig, "High Resolution Measurements of Local Effectiveness by Discrete Hole Film Cooling," *ASME Journal of Turbomachinery,* pp. 758-765, 2001.

[4] D. L. Schmidt, B. Sen and D. Bogard, "Film Cooling With Compound Angle Holes; Adiabatic Effectiveness," *ASME Journal of Turbomachinery,* pp. 807-813, 1996.

[5] P. S. Chen, M. K. Chyu and T. I.-P. Shih, "Effects of upstream ramp on the performance of film cooling," *International Journal of Thermal Sciences,* pp. 1085-1094, 2011.

[6] D. Kercher, "A Film-Cooling CFD Bibliography: 1971-1996," *International Journal of Rotating Machinery,* pp. 61-72, 1998.

[7] B. A. Haven and M. Kurosaka, "Kidney and anti-kidney vortices in crossflow jets," *Journal of Fluid Mechanics,* pp. 27-64, 1997.

[8] S. Chen, "Film Cooling Enhancement with Surface Restructure," University of Pittsburgh, Pittsburgh, 2008.

[9] S. Na and T. I.-P. Shih, "Increasing Adiabatic Film-Cooling Effectiveness by Using an Upstream Ramp," *Journal of Heat Transfer,* pp. 464-471, 2007.

[10] Y. Lu and A. E. S. V. Dhungel, "Effect of Trench Width and Depth," *Journal of Turbomachinery,* vol. 131, pp. 1-13, 2009.

[11] B. S., S. P. Alavi Tabrizi and J. B. A., "Film cooling effectiveness from trenched shaped and compound," *Heat Mass Transfer,* vol. 44, pp. 989-998, 2008.

[12] T. I.-P. Shih, S. Na and M. K. Chyu, "Preventing Hot Gas Ingestion by Film-cooling Jets via Flow-aligned Blockers," in *ASME Turbo Expo 2006: Power for Land, Sea and Air*, Barcelona, 2006.

[13] S. D. Peterson and M. W. Plesniak, "Short-hole jet-in-crossflow velocity field and its relationship," *Experiments in Fluids,* pp. 889-898, 2002.

[14] L. El-Gabry, J. Heidmann and A. Ameri, "Penetration Characteristics of Film-Cooling Jets at High Blowing Ratio," *AIAA Journal,* pp. 1020-1024, 2010.

[15] W. Vickery and H. Iacovides, "Computation of Gas Turbine Blad Film Cooling," The University of Manchester, Manchester, 2012.

[16] A. K. Sinha, D. G. Bogard and M. E. Crawford, "Film-Cooling Effectiveness Downstream of a Single Row of Holes with Variable Density Ratio," *Journal of Turbomachinery,* pp. 442-449, 1991.